2 Digital Image Fundamentals

Those who wish to succeed must ask the right preliminary questions.

Aristotle

Preview

The purpose of this chapter is to introduce several concepts related to digital images and some of the notation used throughout the book. Section 2.1 briefly summarizes the mechanics of the human visual system, including image formation in the eye and its capabilities for brightness adaptation and discrimination. Section 2.2 discusses light, other components of the electromagnetic spectrum, and their imaging characteristics. Section 2.3 discusses imaging sensors and how they are used to generate digital images. Section 2.4 introduces the concepts of uniform image sampling and gray-level quantization. Additional topics discussed in that section include digital image representation, the effects of varying the number of samples and gray levels in an image, some important phenomena associated with sampling, and techniques for image zooming and shrinking. Section 2.5 deals with some basic relationships between pixels that are used throughout the book. Finally, Section 2.6 defines the conditions for linear operations. As noted in that section, linear operators play a central role in the development of image processing techniques.

Elements of Visual Perception

Although the digital image processing field is built on a foundation of mathematical and probabilistic formulations, human intuition and analysis play a central role in the choice of one technique versus another, and this choice often is

made based on subjective, visual judgments. Hence, developing a basic understanding of human visual perception as a first step in our journey through this book is appropriate. Given the complexity and breadth of this topic, we can only aspire to cover the most rudimentary aspects of human vision. In particular, our interest lies in the mechanics and parameters related to how images are formed in the eye. We are interested in learning the physical limitations of human vision in terms of factors that also are used in our work with digital images. Thus, factors such as how human and electronic imaging compare in terms of resolution and ability to adapt to changes in illumination are not only interesting, they also are important from a practical point of view.

Structure of the Human Eye

Figure 2.1 shows a simplified horizontal cross section of the human eye. The eye is nearly a sphere, with an average diameter of approximately 20 mm. Three membranes enclose the eye: the *cornea* and *sclera* outer cover; the *choroid*; and the *retina*. The cornea is a tough, transparent tissue that covers the anterior

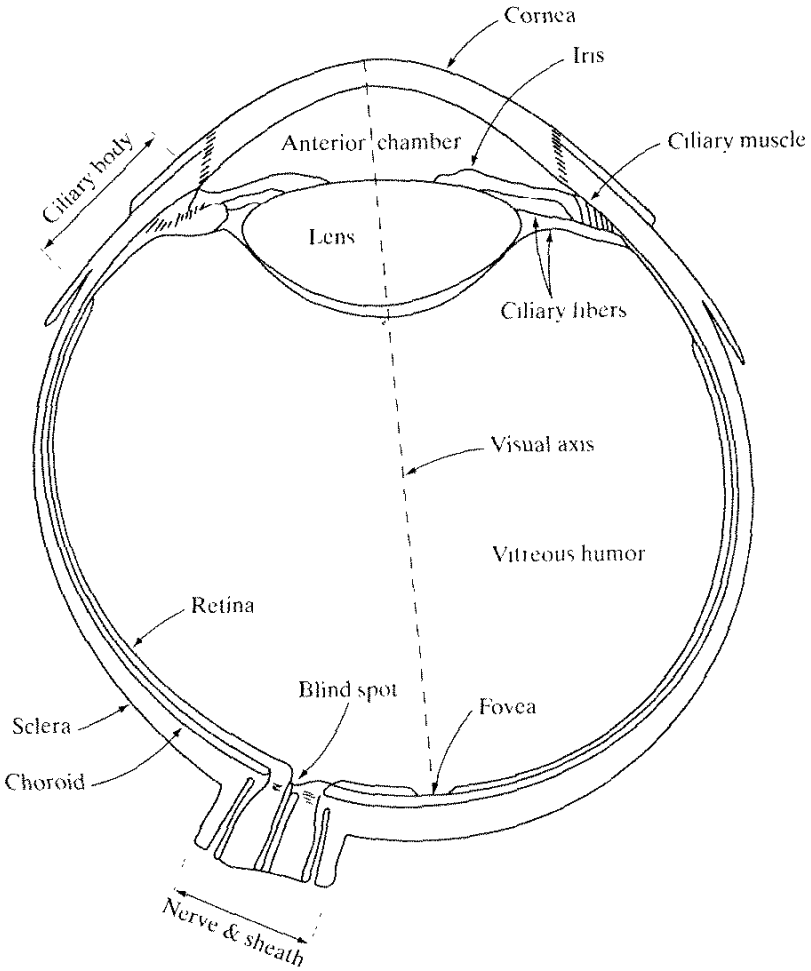

FIGURE 2.1 Simplified diagram of a cross section of the human eye.

surface of the eye. Continuous with the cornea, the sclera is an opaque membrane that encloses the remainder of the optic globe.

The choroid lies directly below the sclera. This membrane contains a network of blood vessels that serve as the major source of nutrition to the eye. Even superficial injury to the choroid, often not deemed serious, can lead to severe eye damage as a result of inflammation that restricts blood flow. The choroid coat is heavily pigmented and hence helps to reduce the amount of extraneous light entering the eye and the backscatter within the optical globe. At its anterior extreme, the choroid is divided into the *ciliary body* and the *iris diaphragm*. The latter contracts or expands to control the amount of light that enters the eye. The central opening of the iris (the *pupil*) varies in diameter from approximately 2 to 8 mm. The front of the iris contains the visible pigment of the eye, whereas the back contains a black pigment.

The *lens* is made up of concentric layers of fibrous cells and is suspended by fibers that attach to the ciliary body. It contains 60 to 70% water, about 6% fat, and more protein than any other tissue in the eye. The lens is colored by a slightly yellow pigmentation that increases with age. In extreme cases, excessive clouding of the lens, caused by the affliction commonly referred to as *cataracts*, can lead to poor color discrimination and loss of clear vision. The lens absorbs approximately 8% of the visible light spectrum, with relatively higher absorption at shorter wavelengths. Both infrared and ultraviolet light are absorbed appreciably by proteins within the lens structure and, in excessive amounts, can damage the eye.

The innermost membrane of the eye is the retina, which lines the inside of the wall's entire posterior portion. When the eye is properly focused, light from an object outside the eye is imaged on the retina. Pattern vision is afforded by the distribution of discrete light receptors over the surface of the retina. There are two classes of receptors: *cones* and *rods*. The cones in each eye number between 6 and 7 million. They are located primarily in the central portion of the retina, called the *fovea*, and are highly sensitive to color. Humans can resolve fine details with these cones largely because each one is connected to its own nerve end. Muscles controlling the eye rotate the eyeball until the image of an object of interest falls on the fovea. Cone vision is called *photopic* or bright-light vision.

The number of rods is much larger: Some 75 to 150 million are distributed over the retinal surface. The larger area of distribution and the fact that several rods are connected to a single nerve end reduce the amount of detail discernible by these receptors. Rods serve to give a general, overall picture of the field of view. They are not involved in color vision and are sensitive to low levels of illumination. For example, objects that appear brightly colored in daylight when seen by moonlight appear as colorless forms because only the rods are stimulated. This phenomenon is known as *scotopic* or dim-light vision.

Figure 2.2 shows the density of rods and cones for a cross section of the right eye passing through the region of emergence of the optic nerve from the eye. The absence of receptors in this area results in the so-called *blind spot* (see Fig. 2.1). Except for this region, the distribution of receptors is radially symmetric about the fovea. Receptor density is measured in degrees from the fovea (that is, in degrees off axis, as measured by the angle formed by the visual axis and a line passing through the center of the lens and intersecting the retina).

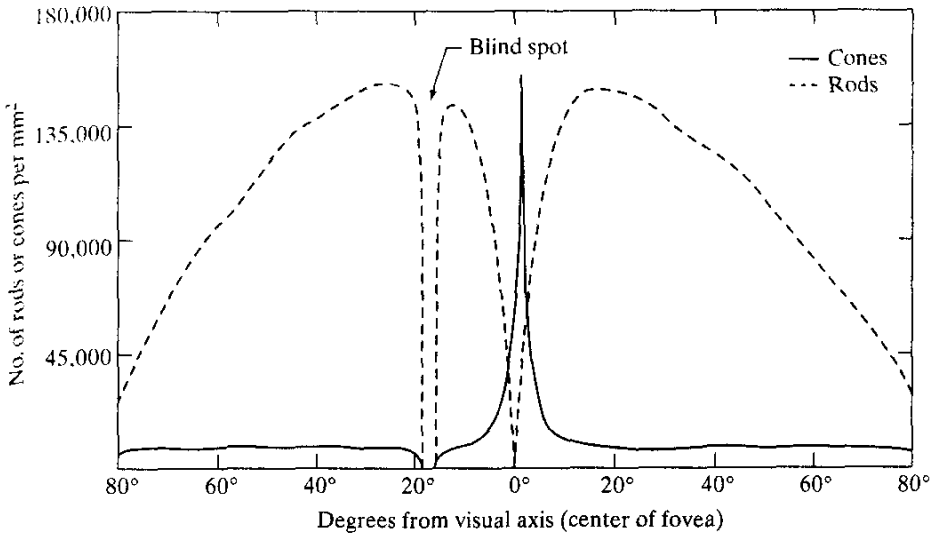

FIGURE 2.2 Distribution of rods and cones in the retina.

Note in Fig. 2.2 that cones are most dense in the center of the retina (in the center area of the fovea). Note also that rods increase in density from the center out to approximately 20° off axis and then decrease in density out to the extreme periphery of the retina.

The fovea itself is a circular indentation in the retina of about 1.5 mm in diameter. However, in terms of future discussions, talking about square or rectangular arrays of sensing elements is more useful. Thus, by taking some liberty in interpretation, we can view the fovea as a square sensor array of size 1.5 mm × 1.5 mm. The density of cones in that area of the retina is approximately 150,000 elements per mm^2. Based on these approximations, the number of cones in the region of highest acuity in the eye is about 337,000 elements. Just in terms of raw resolving power, a charge-coupled device (CCD) imaging chip of medium resolution can have this number of elements in a receptor array no larger than 5 mm × 5 mm. While the ability of humans to integrate intelligence and experience with vision makes this type of comparison dangerous. Keep in mind for future discussions that the basic ability of the eye to resolve detail is certainly within the realm of current electronic imaging sensors.

2.1.2 Image Formation in the Eye

The principal difference between the lens of the eye and an ordinary optical lens is that the former is flexible. As illustrated in Fig. 2.1, the radius of curvature of the anterior surface of the lens is greater than the radius of its posterior surface. The shape of the lens is controlled by tension in the fibers of the ciliary body. To focus on distant objects, the controlling muscles cause the lens to be relatively flattened. Similarly, these muscles allow the lens to become thicker in order to focus on objects near the eye.

The distance between the center of the lens and the retina (called the *focal length*) varies from approximately 17 mm to about 14 mm, as the refractive power of the lens increases from its minimum to its maximum. When the eye

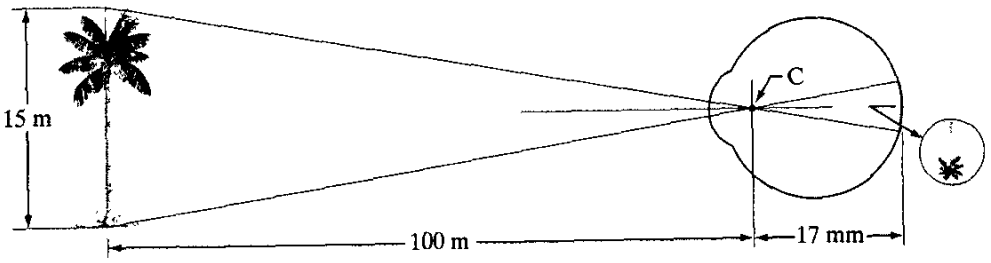

FIGURE 2.3 Graphical representation of the eye looking at a palm tree. Point C is the optical center of the lens.

focuses on an object farther away than about 3 m, the lens exhibits its lowest refractive power. When the eye focuses on a nearby object, the lens is most strongly refractive. This information makes it easy to calculate the size of the retinal image of any object. In Fig. 2.3, for example, the observer is looking at a tree 15 m high at a distance of 100 m. If h is the height in mm of that object in the retinal image, the geometry of Fig. 2.3 yields $15/100 = h/17$ or $h = 2.55$ mm. As indicated in Section 2.1.1, the retinal image is reflected primarily in the area of the fovea. Perception then takes place by the relative excitation of light receptors, which transform radiant energy into electrical impulses that are ultimately decoded by the brain.

2.1.3 Brightness Adaptation and Discrimination

Because digital images are displayed as a discrete set of intensities, the eye's ability to discriminate between different intensity levels is an important consideration in presenting image-processing results. The range of light intensity levels to which the human visual system can adapt is enormous—on the order of 10^{10}—from the scotopic threshold to the glare limit. Experimental evidence indicates that *subjective brightness* (intensity as *perceived* by the human visual system) is a logarithmic function of the light intensity incident on the eye. Figure 2.4, a plot of light intensity versus subjective brightness, illustrates this char-

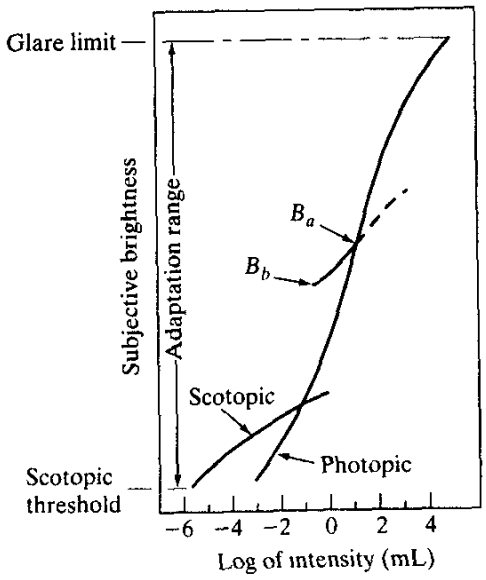

FIGURE 2.4 Range of subjective brightness sensations showing a particular adaptation level.

acteristic. The long solid curve represents the range of intensities to which the visual system can adapt. In photopic vision alone, the range is about 10^6. The transition from scotopic to photopic vision is gradual over the approximate range from 0.001 to 0.1 millilambert (−3 to −1 mL in the log scale), as the double branches of the adaptation curve in this range show.

The essential point in interpreting the impressive dynamic range depicted in Fig. 2.4 is that the visual system cannot operate over such a range *simultaneously*. Rather, it accomplishes this large variation by changes in its overall sensitivity, a phenomenon known as *brightness adaptation*. The total range of distinct intensity levels it can discriminate simultaneously is rather small when compared with the total adaptation range. For any given set of conditions, the current sensitivity level of the visual system is called the *brightness adaptation level*, which may correspond, for example, to brightness B_a in Fig. 2.4. The short intersecting curve represents the range of subjective brightness that the eye can perceive when adapted to this level. This range is rather restricted, having a level B_b at and below which all stimuli are perceived as indistinguishable blacks. The upper (dashed) portion of the curve is not actually restricted but, if extended too far, loses its meaning because much higher intensities would simply raise the adaptation level higher than B_a.

The ability of the eye to discriminate between *changes* in light intensity at any specific adaptation level is also of considerable interest. A classic experiment used to determine the capability of the human visual system for brightness discrimination consists of having a subject look at a flat, uniformly illuminated area large enough to occupy the entire field of view. This area typically is a diffuser, such as opaque glass, that is illuminated from behind by a light source whose intensity, I, can be varied. To this field is added an increment of illumination, ΔI, in the form of a short-duration flash that appears as a circle in the center of the uniformly illuminated field, as Fig. 2.5 shows.

If ΔI is not bright enough, the subject says "no," indicating no perceivable change. As ΔI gets stronger, the subject may give a positive response of "yes," indicating a perceived change. Finally, when ΔI is strong enough, the subject will give a response of "yes" all the time. The quantity $\Delta I_c/I$, where ΔI_c is the increment of illumination discriminable 50% of the time with background illumination I, is called the *Weber ratio*. A small value of $\Delta I_c/I$, means that a small percentage change in intensity is discriminable. This represents "good" brightness discrimination. Conversely, a large value of $\Delta I_c/I$, means that a large percentage change in intensity is required. This represents "poor" brightness discrimination.

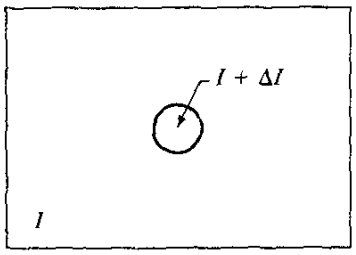

FIGURE 2.5 Basic experimental setup used to characterize brightness discrimination.

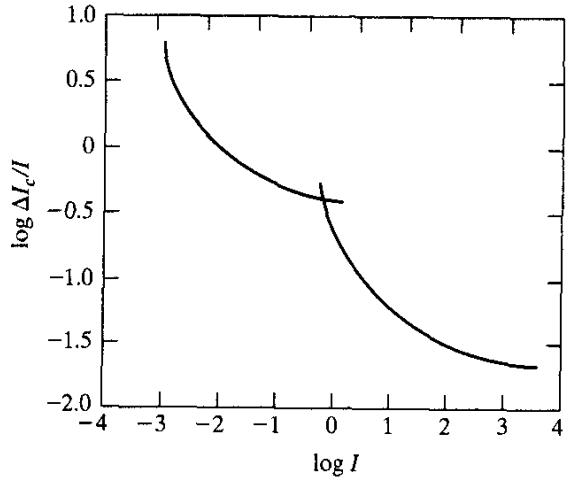

FIGURE 2.6
Typical Weber ratio as a function of intensity.

A plot of $\log \Delta I_c/I$, as a function of $\log I$ has the general shape shown in Fig. 2.6. This curve shows that brightness discrimination is poor (the Weber ratio is large) at low levels of illumination, and it improves significantly (the Weber ratio decreases) as background illumination increases. The two branches in the curve reflect the fact that at low levels of illumination vision is carried out by activity of the rods, whereas at high levels (showing better discrimination) vision is the function of cones.

If the background illumination is held constant and the intensity of the other source, instead of flashing, is now allowed to vary incrementally from never being perceived to always being perceived, the typical observer can discern a total of one to two dozen different intensity changes. Roughly, this result is related to the number of different intensities a person can see at any one point in a monochrome image. This result does not mean that an image can be represented by such a small number of intensity values because, as the eye roams about the image, the average background changes, thus allowing a *different* set of incremental changes to be detected at each new adaptation level. The net consequence is that the eye is capable of a much broader range of *overall* intensity discrimination. In fact, we show in Section 2.4.3 that the eye is capable of detecting objectionable contouring effects in monochrome images whose overall intensity is represented by fewer than approximately two dozen levels.

Two phenomena clearly demonstrate that perceived brightness is not a simple function of intensity. The first is based on the fact that the visual system tends to undershoot or overshoot around the boundary of regions of different intensities. Figure 2.7(a) shows a striking example of this phenomenon. Although the intensity of the stripes is constant, we actually perceive a brightness pattern that is strongly scalloped, especially near the boundaries [Fig. 2.7(b)]. These seemingly scalloped bands are called *Mach bands* after Ernst Mach, who first described the phenomenon in 1865.

The second phenomenon, called *simultaneous contrast*, is related to the fact that a region's perceived brightness does not depend simply on its intensity, as Fig. 2.8 demonstrates. All the center squares have exactly the same intensity.

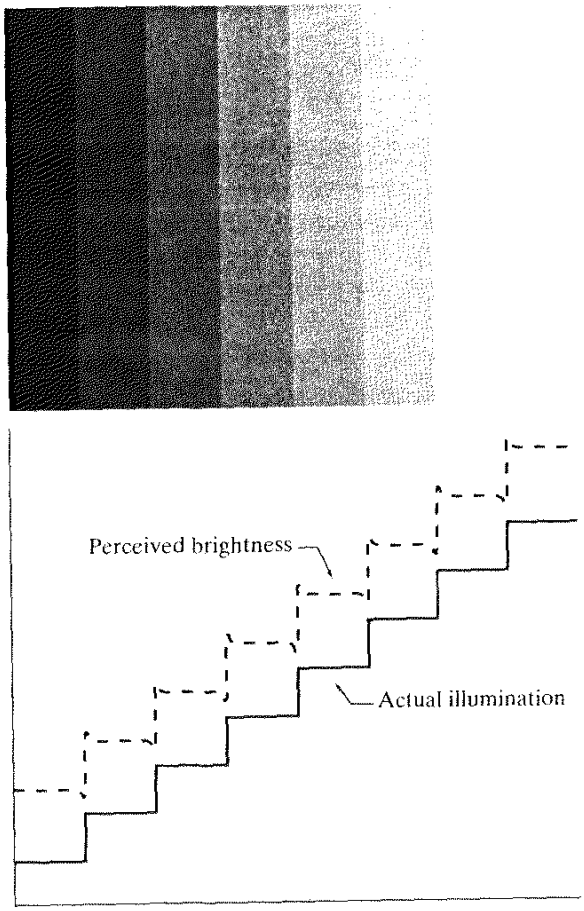

a
b

FIGURE 2.7
(a) An example showing that perceived brightness is not a simple function of intensity. The relative vertical positions between the two profiles in (b) have no special significance; they were chosen for clarity.

However, they appear to the eye to become darker as the background gets lighter. A more familiar example is a piece of paper that seems white when lying on a desk, but can appear totally black when used to shield the eyes while looking directly at a bright sky.

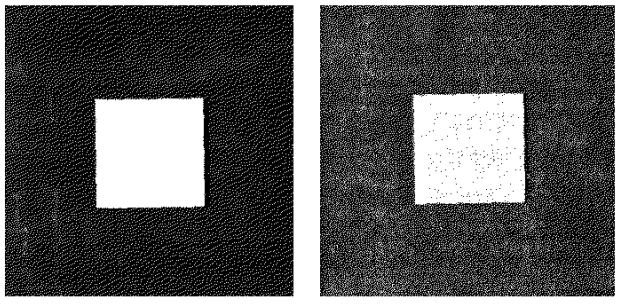

a b c

FIGURE 2.8 Examples of simultaneous contrast. All the inner squares have the same intensity, but they appear progressively darker as the background becomes lighter.

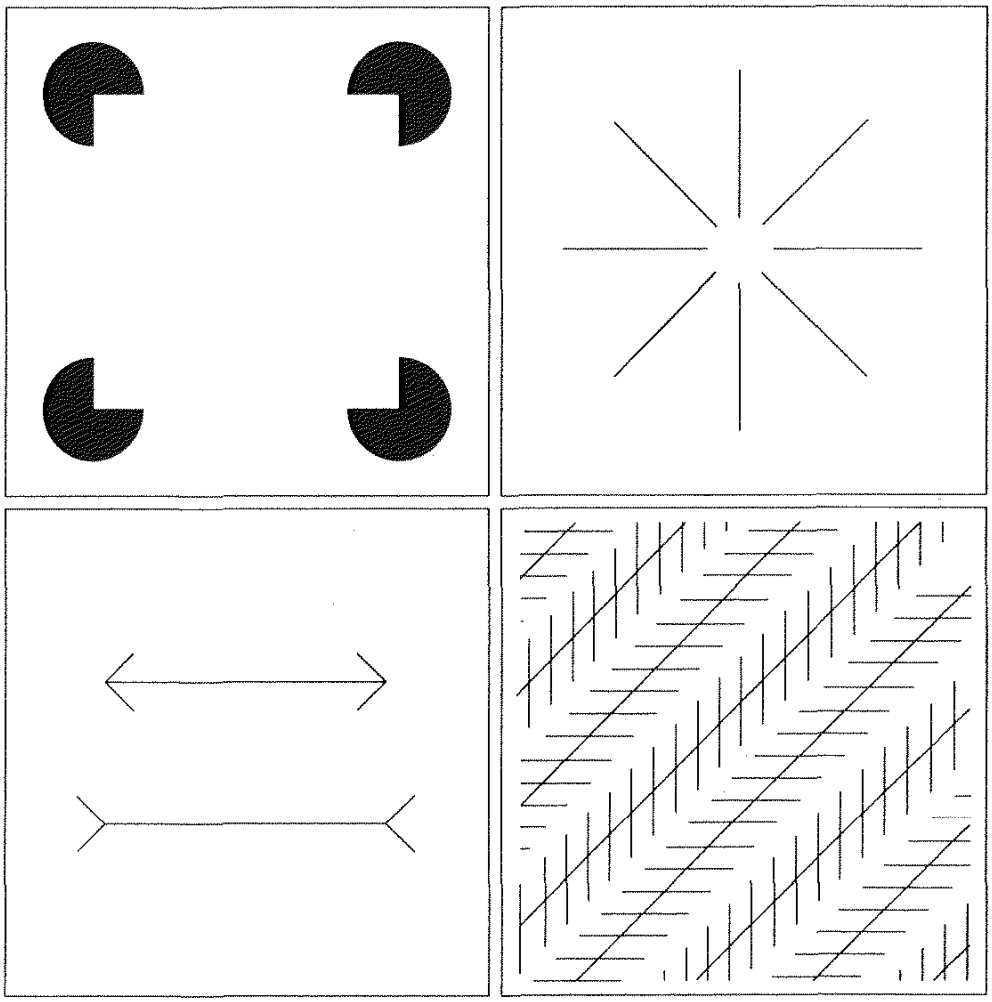

a b
c d

FIGURE 2.9 Some well-known optical illusions.

Other examples of human perception phenomena are optical illusions, in which the eye fills in nonexisting information or wrongly perceives geometrical properties of objects. Some examples are shown in Fig. 2.9. In Fig. 2.9(a), the outline of a square is seen clearly, in spite of the fact that no lines defining such a figure are part of the image. The same effect, this time with a circle, can be seen in Fig. 2.9(b); note how just a few lines are sufficient to give the illusion of a complete circle. The two horizontal line segments in Fig. 2.9(c) are of the same length, but one appears shorter than the other. Finally, all lines in Fig. 2.9(d) that are oriented at 45° are equidistant and parallel. Yet the crosshatching creates the illusion that those lines are far from being parallel. Optical illusions are a characteristic of the human visual system that is not fully understood.

Light and the Electromagnetic Spectrum

The electromagnetic spectrum was introduced in Section 1.3. We now consider this topic in more detail. In 1666, Sir Isaac Newton discovered that when a beam of sunlight is passed through a glass prism, the emerging beam of light is not

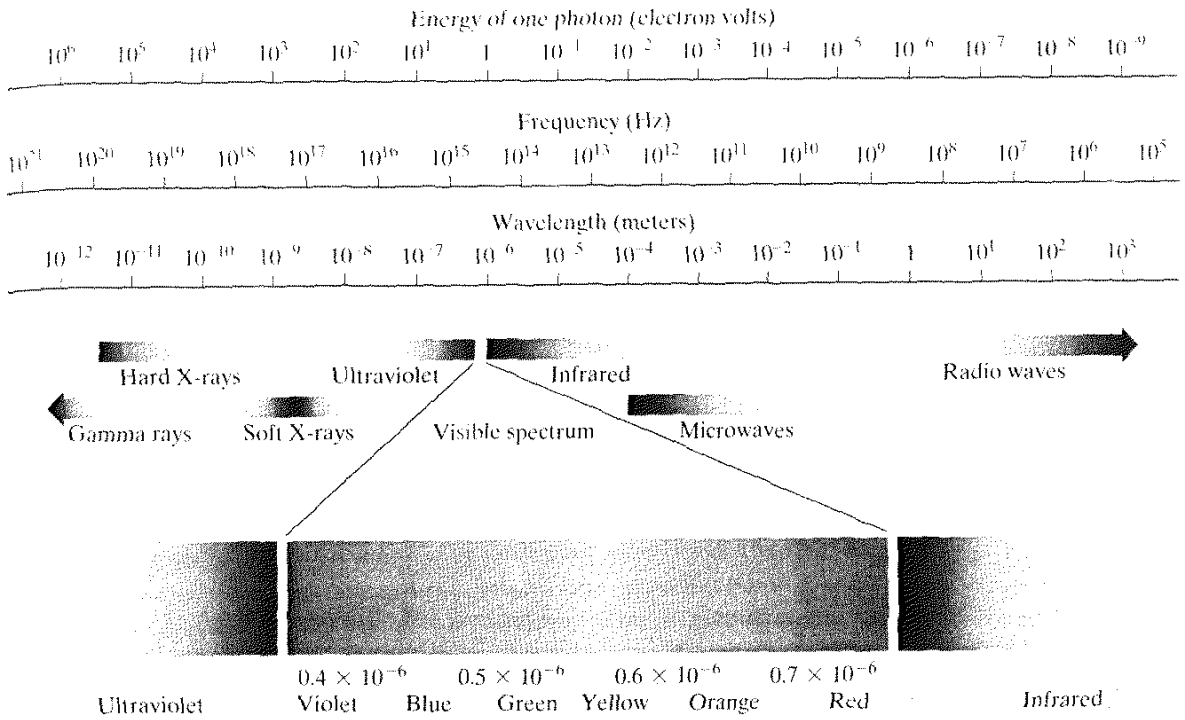

FIGURE 2.10 The electromagnetic spectrum. The visible spectrum is shown zoomed to facilitate explanation, but note that the visible spectrum is a rather narrow portion of the EM spectrum.

white but consists instead of a continuous spectrum of colors ranging from violet at one end to red at the other. As shown in Fig. 2.10, the range of colors we perceive in visible light represents a very small portion of the electromagnetic spectrum. On one end of the spectrum are radio waves with wavelengths billions of times longer than those of visible light. On the other end of the spectrum are gamma rays with wavelengths millions of times smaller than those of visible light. The electromagnetic spectrum can be expressed in terms of wavelength, frequency, or energy. Wavelength (λ) and frequency (ν) are related by the expression

$$\lambda = \frac{c}{\nu} \tag{2.2-1}$$

where c is the speed of light (2.998×10^{8} m/s). The energy of the various components of the electromagnetic spectrum is given by the expression

$$E = h\nu \tag{2.2-2}$$

where h is Planck's constant. The units of wavelength are meters, with the terms *microns* (denoted μm and equal to 10^{-6} m) and *nanometers* (10^{-9} m) being used just as frequently. Frequency is measured in Hertz (Hz), with one Hertz being equal to one cycle of a sinusoidal wave per second. A commonly used unit of energy is the electron-volt.

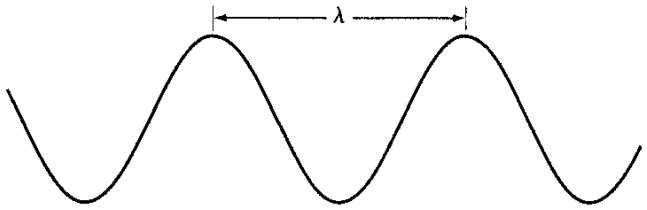

FIGURE 2.11 Graphical representation of one wavelength.

Electromagnetic waves can be visualized as propagating sinusoidal waves with wavelength λ (Fig. 2.11), or they can be thought of as a stream of massless particles, each traveling in a wavelike pattern and moving at the speed of light. Each massless particle contains a certain amount (or bundle) of energy. Each bundle of energy is called a *photon*. We see from Eq. (2.2-2) that energy is proportional to frequency, so the higher-frequency (shorter wavelength) electromagnetic phenomena carry more energy per photon. Thus, radio waves have photons with low energies, microwaves have more energy than radio waves, infrared still more, then visible, ultraviolet, X-rays, and finally gamma rays, the most energetic of all. This is the reason that gamma rays are so dangerous to living organisms.

Light is a particular type of electromagnetic radiation that can be seen and sensed by the human eye. The visible (color) spectrum is shown expanded in Fig. 2.10 for the purpose of discussion (we consider color in much more detail in Chapter 6). The visible band of the electromagnetic spectrum spans the range from approximately 0.43 μm (violet) to about 0.79 μm (red). For convenience, the color spectrum is divided into six broad regions: violet, blue, green, yellow, orange, and red. No color (or other component of the electromagnetic spectrum) ends abruptly, but rather each range blends smoothly into the next, as shown in Fig. 2.10.

The colors that humans perceive in an object are determined by the nature of the light *reflected* from the object. A body that reflects light and is relatively balanced in all visible wavelengths appears white to the observer. However, a body that favors reflectance in a limited range of the visible spectrum exhibits some shades of color. For example, green objects reflect light with wavelengths primarily in the 500 to 570 nm range while absorbing most of the energy at other wavelengths.

Light that is void of color is called *achromatic* or *monochromatic* light. The only attribute of such light is its *intensity*, or amount. The term *gray level* generally is used to describe monochromatic intensity because it ranges from black, to grays, and finally to white. Chromatic light spans the electromagnetic energy spectrum from approximately 0.43 to 0.79 μm, as noted previously. Three basic quantities are used to describe the quality of a chromatic light source: radiance; luminance; and brightness. *Radiance* is the total amount of energy that flows from the light source, and it is usually measured in watts (W). *Luminance*, measured in lumens (lm), gives a measure of the amount of energy an observer *perceives* from a light source. For example, light emitted from a source operating in the far infrared region of the spectrum could have significant energy (radiance), but an observer would hardly perceive it; its luminance would be almost zero. Finally, as discussed in Section 2.1, *brightness* is a subjective descriptor of light perception that is practically impossible to measure. It embod-

ies the achromatic notion of intensity and is one of the key factors in describing color sensation.

Continuing with the discussion of Fig. 2.10, we note that at the short-wavelength end of the electromagnetic spectrum, we have gamma rays and hard X-rays. As discussed in Section 1.3.1, gamma radiation is important for medical and astronomical imaging, and for imaging radiation in nuclear environments. Hard (high-energy) X-rays are used in industrial applications. Chest X-rays are in the high end (shorter wavelength) of the soft X-rays region and dental X-rays are in the lower energy end of that band. The soft X-ray band transitions into the far ultraviolet light region, which in turn blends with the visible spectrum at longer wavelengths. Moving still higher in wavelength, we encounter the infrared band, which radiates heat, a fact that makes it useful in imaging applications that rely on "heat signatures." The part of the infrared band close to the visible spectrum is called the *near-infrared* region. The opposite end of this band is called the *far-infrared* region. This latter region blends with the microwave band. This band is well known as the source of energy in microwave ovens, but it has many other uses, including communication and radar. Finally, the radio wave band encompasses television as well as AM and FM radio. In the higher energies, radio signals emanating from certain stellar bodies are useful in astronomical observations. Examples of images in most of the bands just discussed are given in Section 1.3.

In principle, if a sensor can be developed that is capable of detecting energy radiated by a band of the electromagnetic spectrum, we can image events of interest in that band. It is important to note, however, that the wavelength of an electromagnetic wave required to "see" an object must be of the same size as or smaller than the object. For example, a water molecule has a diameter on the order of 10^{-10} m. Thus, to study molecules, we would need a source capable of emitting in the far ultraviolet or soft X-ray region. This limitation, along with the physical properties of the sensor material, establishes the fundamental limits on the capability of imaging sensors, such as visible, infrared, and other sensors in use today.

Although imaging is based predominantly on energy radiated by electromagnetic waves, this is not the only method for image generation. For example, as discussed in Section 1.3.7, sound reflected from objects can be used to form ultrasonic images. Other major sources of digital images are electron beams for electron microscopy and synthetic images used in graphics and visualization.

Image Sensing and Acquisition

The types of images in which we are interested are generated by the combination of an "illumination" source and the reflection or absorption of energy from that source by the elements of the "scene" being imaged. We enclose *illumination* and *scene* in quotes to emphasize the fact that they are considerably more general than the familiar situation in which a visible light source illuminates a common everyday 3-D (three-dimensional) scene. For example, the illumination may originate from a source of electromagnetic energy such as radar, infrared,

or X-ray energy. But, as noted earlier, it could originate from less traditional sources, such as ultrasound or even a computer-generated illumination pattern. Similarly, the scene elements could be familiar objects, but they can just as easily be molecules, buried rock formations, or a human brain. We could even image a source, such as acquiring images of the sun. Depending on the nature of the source, illumination energy is reflected from, or transmitted through, objects. An example in the first category is light reflected from a planar surface. An example in the second category is when X-rays pass through a patient's body for the purpose of generating a diagnostic X-ray film. In some applications, the reflected or transmitted energy is focused onto a photoconverter (e.g., a phosphor screen), which converts the energy into visible light. Electron microscopy and some applications of gamma imaging use this approach.

Figure 2.12 shows the three principal sensor arrangements used to transform illumination energy into digital images. The idea is simple: Incoming energy is

a
b
c

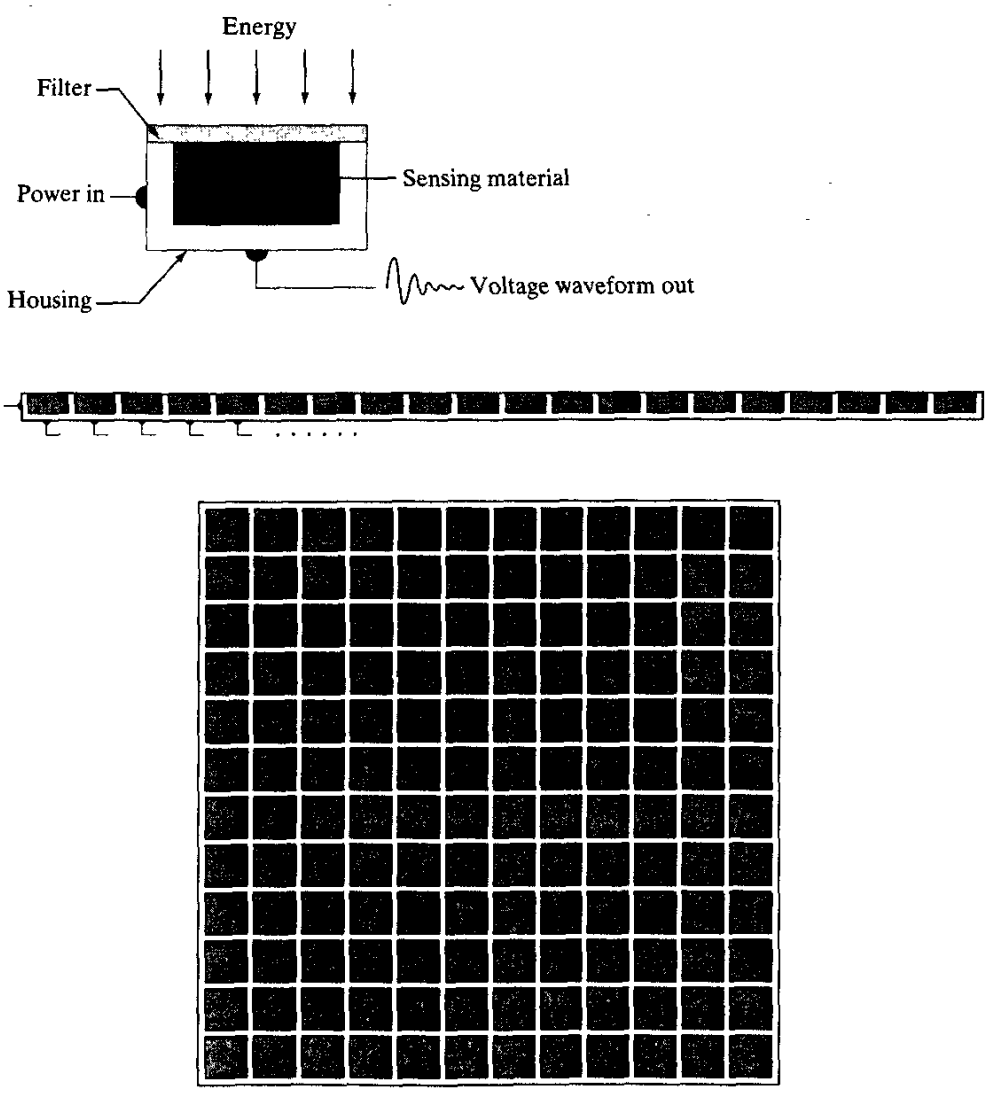

FIGURE 2.12
(a) Single imaging sensor.
(b) Line sensor.
(c) Array sensor.

2.3.2 Image Acquisition Using Sensor Strips

A geometry that is used much more frequently than single sensors consists of an in-line arrangement of sensors in the form of a sensor strip, as Fig. 2.12(b) shows. The strip provides imaging elements in one direction. Motion perpendicular to the strip provides imaging in the other direction, as shown in Fig. 2.14(a). This is the type of arrangement used in most flat bed scanners. Sensing devices with 4000 or more in-line sensors are possible. In-line sensors are used routinely in airborne imaging applications, in which the imaging system is mounted on an aircraft that flies at a constant altitude and speed over the geographical area to be imaged. One-dimensional imaging sensor strips that respond to various bands of the electromagnetic spectrum are mounted perpendicular to the direction of flight. The imaging strip gives one line of an image at a time, and the motion of the strip completes the other dimension of a two-dimensional image. Lenses or other focusing schemes are used to project the area to be scanned onto the sensors.

Sensor strips mounted in a ring configuration are used in medical and industrial imaging to obtain cross-sectional ("slice") images of 3-D objects, as Fig. 2.14(b) shows. A rotating X-ray source provides illumination and the por-

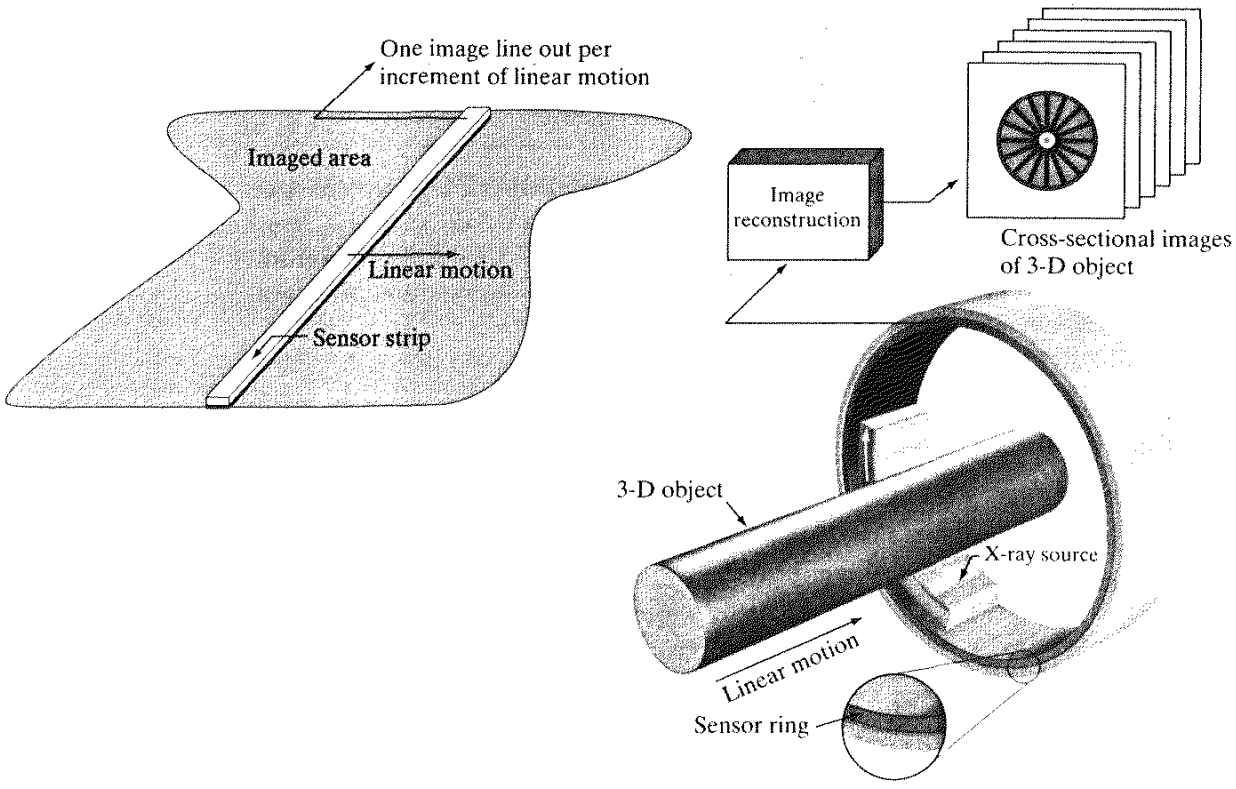

a b

FIGURE 2.14 (a) Image acquisition using a linear sensor strip. (b) Image acquisition using a circular sensor strip.

tion of the sensors opposite the source collect the X-ray energy that pass through the object (the sensors obviously have to be sensitive to X-ray energy). This is the basis for medical and industrial computerized axial tomography (CAT) imaging as indicated in Sections 1.2 and 1.3.2. It is important to note that the output of the sensors must be processed by reconstruction algorithms whose objective is to transform the sensed data into meaningful cross-sectional images. In other words, images are not obtained directly from the sensors by motion alone; they require extensive processing. A 3-D digital volume consisting of stacked images is generated as the object is moved in a direction perpendicular to the sensor ring. Other modalities of imaging based on the CAT principle include magnetic resonance imaging (MRI) and positron emission tomography (PET). The illumination sources, sensors, and types of images are different, but conceptually they are very similar to the basic imaging approach shown in Fig. 2.14(b).

2.3.3 Image Acquisition Using Sensor Arrays

Figure 2.12(c) shows individual sensors arranged in the form of a 2-D array. Numerous electromagnetic and some ultrasonic sensing devices frequently are arranged in an array format. This is also the predominant arrangement found in digital cameras. A typical sensor for these cameras is a CCD array, which can be manufactured with a broad range of sensing properties and can be packaged in rugged arrays of 4000×4000 elements or more. CCD sensors are used widely in digital cameras and other light sensing instruments. The response of each sensor is proportional to the integral of the light energy projected onto the surface of the sensor, a property that is used in astronomical and other applications requiring low noise images. Noise reduction is achieved by letting the sensor integrate the input light signal over minutes or even hours (we discuss noise reduction by integration in Chapter 3). Since the sensor array shown in Fig. 2.15(c) is two dimensional, its key advantage is that a complete image can be obtained by focusing the energy pattern onto the surface of the array. Motion obviously is not necessary, as is the case with the sensor arrangements discussed in the preceding two sections.

The principal manner in which array sensors are used is shown in Fig. 2.15. This figure shows the energy from an illumination source being reflected from a scene element, but, as mentioned at the beginning of this section, the energy also could be transmitted through the scene elements. The first function performed by the imaging system shown in Fig. 2.15(c) is to collect the incoming energy and focus it onto an image plane. If the illumination is light, the front end of the imaging system is a lens, which projects the viewed scene onto the lens focal plane, as Fig. 2.15(d) shows. The sensor array, which is coincident with the focal plane, produces outputs proportional to the integral of the light received at each sensor. Digital and analog circuitry sweep these outputs and convert them to a video signal, which is then digitized by another section of the imaging system. The output is a digital image, as shown diagrammatically in Fig. 2.15(e). Conversion of an image into digital form is the topic of Section 2.4.

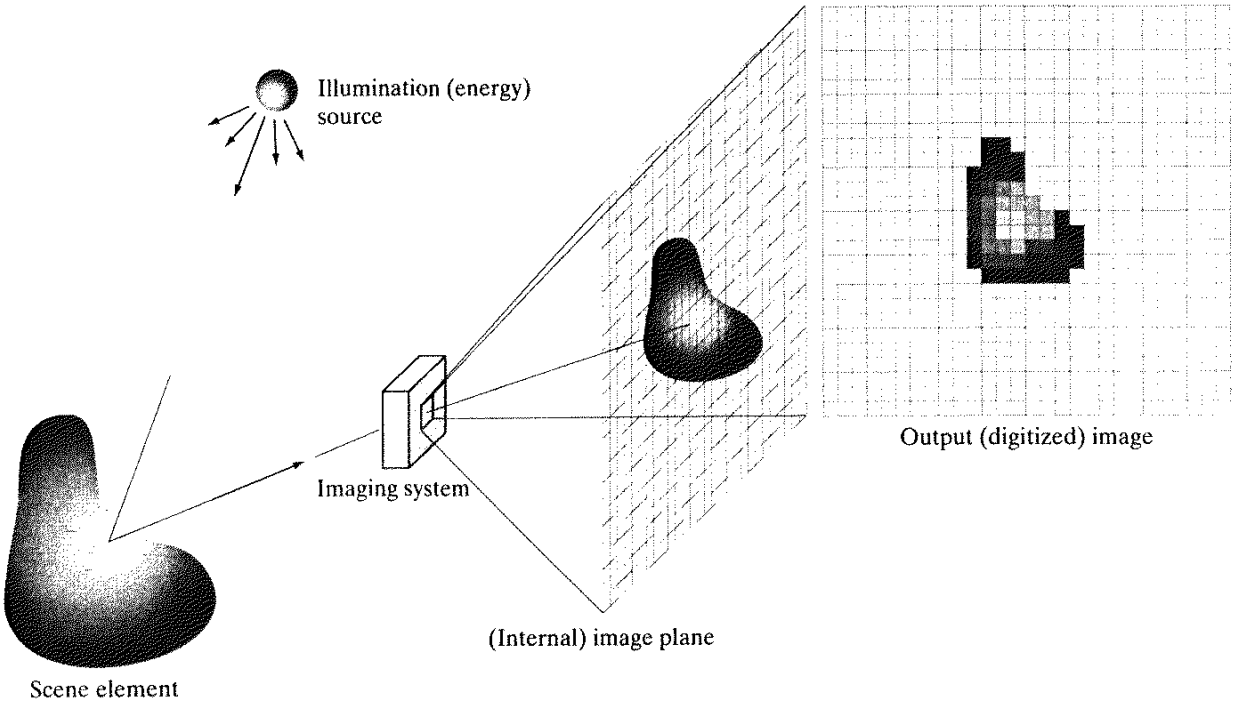

a
b c d e

FIGURE 2.15 An example of the digital image acquisition process. (a) Energy ("illumination") source. (b) An element of a scene. (c) Imaging system. (d) Projection of the scene onto the image plane. (e) Digitized image.

2.3.4 A Simple Image Formation Model

As introduced in Section 1.1, we shall denote images by two-dimensional functions of the form $f(x, y)$. The value or amplitude of f at spatial coordinates (x, y) is a positive scalar quantity whose physical meaning is determined by the source of the image. Most of the images in which we are interested in this book are monochromatic images, whose values are said to span the gray scale, as discussed in Section 2.2. When an image is generated from a physical process, its values are proportional to energy radiated by a physical source (e.g., electromagnetic waves). As a consequence, $f(x, y)$ must be nonzero and finite; that is,

$$0 < f(x, y) < \infty. \tag{2.3-1}$$

The function $f(x, y)$ may be characterized by two components: (1) the amount of source illumination incident on the scene being viewed, and (2) the amount of illumination reflected by the objects in the scene. Appropriately, these are called the *illumination* and *reflectance* components and are denoted by $i(x, y)$ and $r(x, y)$, respectively. The two functions combine as a product to form $f(x, y)$:

2.4 Image Sampling and Quantization

From the discussion in the preceding section, we see that there are numerous ways to acquire images, but our objective in all is the same: to generate digital images from sensed data. The output of most sensors is a continuous voltage waveform whose amplitude and spatial behavior are related to the physical phenomenon being sensed. To create a digital image, we need to convert the continuous sensed data into digital form. This involves two processes: *sampling* and *quantization*.

2.4.1 Basic Concepts in Sampling and Quantization

The basic idea behind sampling and quantization is illustrated in Fig. 2.16. Figure 2.16(a) shows a continuous image, $f(x, y)$, that we want to convert to digital form. An image may be continuous with respect to the x- and y-coordinates, and also in amplitude. To convert it to digital form, we have to sample the function in both coordinates and in amplitude. Digitizing the coordinate values is called *sampling*. Digitizing the amplitude values is called *quantization*.

The one-dimensional function shown in Fig. 2.16(b) is a plot of amplitude (gray level) values of the continuous image along the line segment AB in Fig. 2.16(a). The random variations are due to image noise. To sample this function, we take equally spaced samples along line AB, as shown in Fig. 2.16(c). The location of each sample is given by a vertical tick mark in the bottom part of the figure. The samples are shown as small white squares superimposed on the function. The set of these discrete locations gives the sampled function. However, the values of the samples still span (vertically) a continuous range of gray-level values. In order to form a digital function, the gray-level values also must be converted (*quantized*) into discrete quantities. The right side of Fig. 2.16(c) shows the gray-level scale divided into eight discrete levels, ranging from black to white. The vertical tick marks indicate the specific value assigned to each of the eight gray levels. The continuous gray levels are quantized simply by assigning one of the eight discrete gray levels to each sample. The assignment is made depending on the vertical proximity of a sample to a vertical tick mark. The digital samples resulting from both sampling and quantization are shown in Fig. 2.16(d). Starting at the top of the image and carrying out this procedure line by line produces a two-dimensional digital image.

Sampling in the manner just described assumes that we have a continuous image in both coordinate directions as well as in amplitude. In practice, the method of sampling is determined by the sensor arrangement used to generate the image. When an image is generated by a single sensing element combined with mechanical motion, as in Fig. 2.13, the output of the sensor is quantized in the manner described above. However, sampling is accomplished by selecting the number of individual mechanical increments at which we activate the sensor to collect data. Mechanical motion can be made very exact so, in principle, there is almost no limit as to how fine we can sample an image. However, practical limits are established by imperfections in the optics used to focus on the

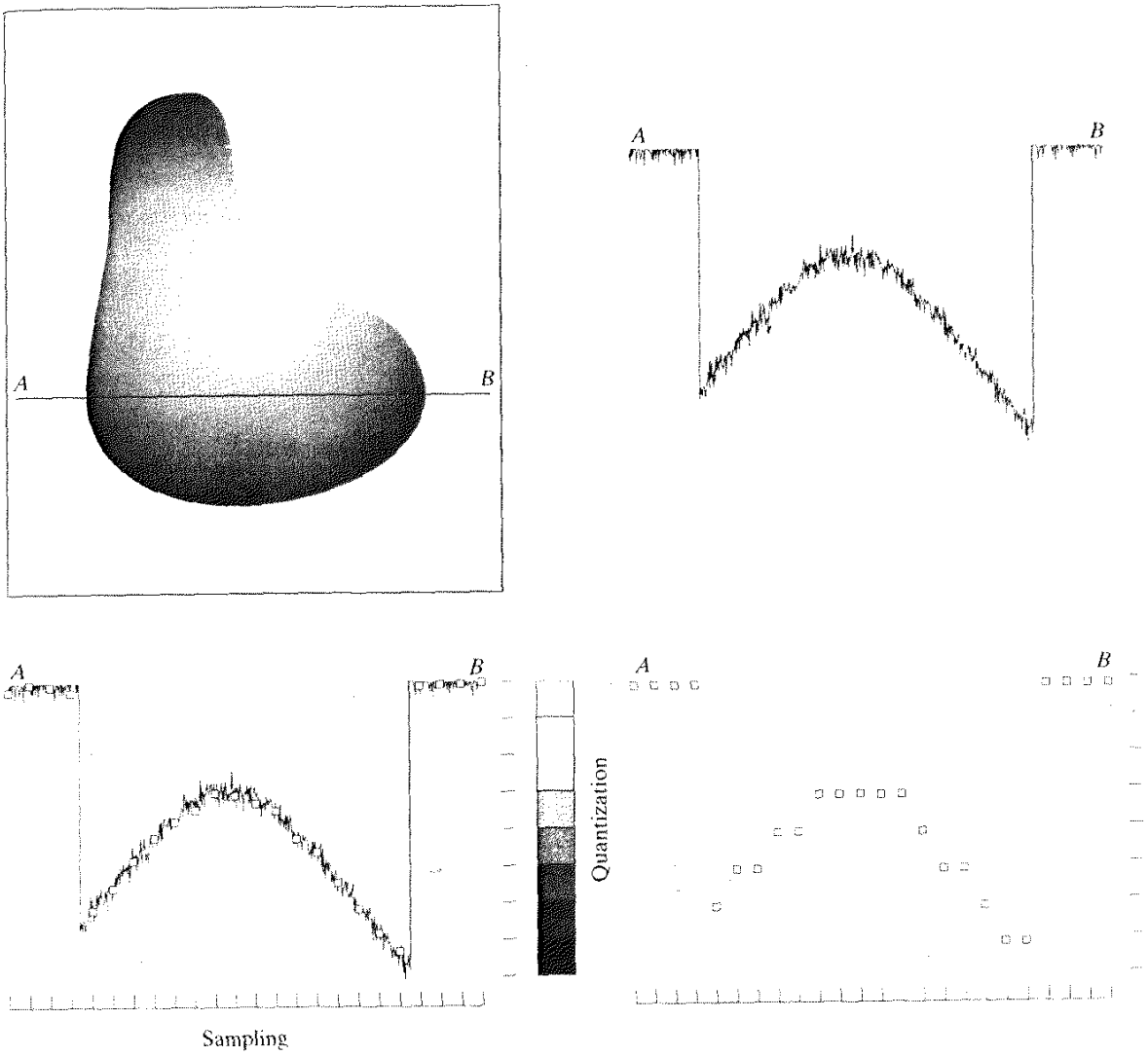

a b
c d

FIGURE 2.16 Generating a digital image. (a) Continuous image. (b) A scan line from A to B in the continuous image, used to illustrate the concepts of sampling and quantization. (c) Sampling and quantization. (d) Digital scan line.

sensor an illumination spot that is inconsistent with the fine resolution achievable with mechanical displacements.

When a sensing strip is used for image acquisition, the number of sensors in the strip establishes the sampling limitations in one image direction. Mechanical motion in the other direction can be controlled more accurately, but it makes little sense to try to achieve sampling density in one direction that exceeds the

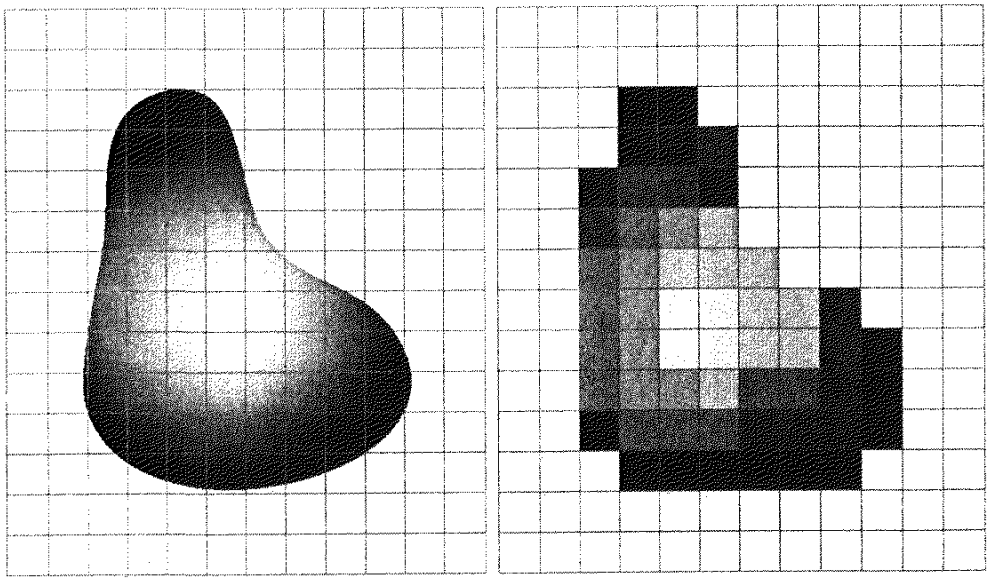

a b

FIGURE 2.17 (a) Continuos image projected onto a sensor array. (b) Result of image sampling and quantization.

sampling limits established by the number of sensors in the other. Quantization of the sensor outputs completes the process of generating a digital image.

When a sensing array is used for image acquisition, there is no motion and the number of sensors in the array establishes the limits of sampling in both directions. Quantization of the sensor outputs is as before. Figure 2.17 illustrates this concept. Figure 2.17(a) shows a continuous image projected onto the plane of an array sensor. Figure 2.17(b) shows the image after sampling and quantization. Clearly, the quality of a digital image is determined to a large degree by the number of samples and discrete gray levels used in sampling and quantization. However, as shown in Section 2.4.3, image content is an important consideration in choosing these parameters.

2.4.2 Representing Digital Images

The result of sampling and quantization is a matrix of real numbers. We will use two principal ways in this book to represent digital images. Assume that an image $f(x, y)$ is sampled so that the resulting digital image has M rows and N columns. The values of the coordinates (x, y) now become *discrete* quantities. For notational clarity and convenience, we shall use integer values for these discrete coordinates. Thus, the values of the coordinates at the origin are $(x, y) = (0, 0)$. The next coordinate values along the first row of the image are represented as $(x, y) = (0, 1)$. It is important to keep in mind that the notation $(0, 1)$ is used to signify the second sample along the first row. It does *not* mean that these are the actual values of physical coordinates when the image was sampled. Figure 2.18 shows the coordinate convention used throughout this book.

As a very rough rule of thumb, and assuming powers of 2 for convenience, images of size 256 × 256 pixels and 64 gray levels are about the smallest images that can be expected to be reasonably free of objectionable sampling checkerboards and false contouring.

The results in Examples 2.2 and 2.3 illustrate the effects produced on image quality by varying N and k independently. However, these results only partially answer the question of how varying N and k affect images because we have not considered yet any relationships that might exist between these two parameters. An early study by Huang [1965] attempted to quantify experimentally the effects on image quality produced by varying N and k simultaneously. The experiment consisted of a set of subjective tests. Images similar to those shown in Fig. 2.22 were used. The woman's face is representative of an image with relatively little detail; the picture of the cameraman contains an intermediate amount of detail; and the crowd picture contains, by comparison, a large amount of detail.

Sets of these three types of images were generated by varying N and k, and observers were then asked to rank them according to their subjective quality. Results were summarized in the form of so-called *isopreference curves* in the Nk-plane (Fig. 2.23 shows average isopreference curves representative of curves corresponding to the images shown in Fig. 2.22). Each point in the Nk-plane represents an image having values of N and k equal to the coordinates of that point. Points lying on an isopreference curve correspond to images of equal subjective quality. It was found in the course of the experiments that the isopreference curves tended to shift right and upward, but their shapes in each of the three image categories were similar to those shown in Fig. 2.23. This is not unexpected, since a shift up and right in the curves simply means larger values for N and k, which implies better picture quality.

The key point of interest in the context of the present discussion is that isopreference curves tend to become more vertical as the detail in the image increases. This result suggests that for images with a large amount of detail only

a b c

FIGURE 2.22 (a) Image with a low level of detail. (b) Image with a medium level of detail. (c) Image with a relatively large amount of detail. (Image (b) courtesy of the Massachusetts Institute of Technology.)

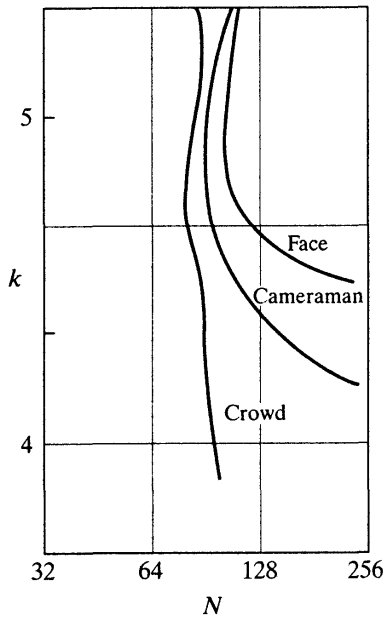

FIGURE 2.23 Representative isopreference curves for the three types of images in Fig. 2.22.

a few gray levels may be needed. For example, the isopreference curve in Fig. 2.23 corresponding to the crowd is nearly vertical. This indicates that, for a fixed value of N, the perceived quality for this type of image is nearly independent of the number of gray levels used (for the range of gray levels shown in Fig. 2.23). It is also of interest to note that perceived quality in the other two image categories remained the same in some intervals in which the spatial resolution was increased, but the number of gray levels actually decreased. The most likely reason for this result is that a decrease in k tends to increase the apparent contrast of an image, a visual effect that humans often perceive as improved quality in an image.

2.4.4 Aliasing and Moiré Patterns

As discussed in more detail in Chapter 4, functions whose area under the curve is finite can be represented in terms of sines and cosines of various frequencies. The sine/cosine component with the highest frequency determines the highest "frequency content" of the function. Suppose that this highest frequency is finite and that the function is of unlimited duration (these functions are called *band-limited functions*). Then, the Shannon sampling theorem [Bracewell (1995)] tells us that, if the function is sampled at a rate equal to or greater than twice its highest frequency, it is possible to recover completely the original function from its samples. If the function is *undersampled*, then a phenomenon called *aliasing* corrupts the sampled image. The corruption is in the form of additional frequency components being introduced into the sampled function. These are called *aliased frequencies*. Note that the *sampling rate* in images is the number of samples taken (in both spatial directions) per unit distance.

As it turns out, except for a special case discussed in the following paragraph, it is impossible to satisfy the sampling theorem in practice. We can only work with sampled data that are finite in duration. We can model the process of convert-

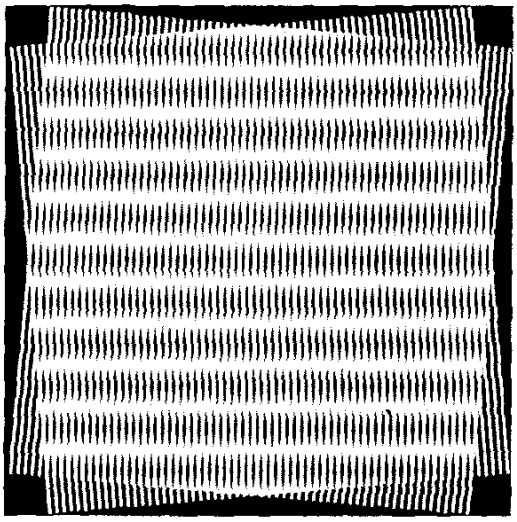

FIGURE 2.24 Illustration of the Moiré pattern effect.

ing a function of unlimited duration into a function of finite duration simply by multiplying the unlimited function by a "gating function" that is valued 1 for some interval and 0 elsewhere. Unfortunately, this function itself has frequency components that extend to infinity. Thus, the very act of limiting the duration of a band-limited function causes it to cease being band limited, which causes it to violate the key condition of the sampling theorem. The principal approach for reducing the aliasing effects on an image is to reduce its high-frequency components by blurring the image (we discuss blurring in detail in Chapter 4) *prior* to sampling. However, aliasing is always present in a sampled image. The effect of aliased frequencies can be seen under the right conditions in the form of so-called *Moiré patterns*[†], as discussed next.

There is one special case of significant importance in which a function of infinite duration can be sampled over a finite interval without violating the sampling theorem. When a function is periodic, it may be sampled at a rate equal to or exceeding twice its highest frequency, and it is possible to recover the function from its samples *provided* that the sampling captures *exactly* an integer number of periods of the function. This special case allows us to illustrate vividly the Moiré effect. Figure 2.24 shows two identical periodic patterns of equally spaced vertical bars, rotated in opposite directions and then superimposed on each other by multiplying the two images. A Moiré pattern, caused by a break-up of the periodicity, is seen in Fig. 2.24 as a 2-D sinusoidal (aliased) waveform (which looks like a corrugated tin roof) running in a vertical direction. A similar pattern can appear when images are digitized (e.g., scanned) from a printed page, which consists of periodic ink dots.

[†]The word *Moiré* appears to have originated with weavers and comes from the word *mohair*, a cloth made from Angora goat hairs.

2.4.5 Zooming and Shrinking Digital Images

We conclude the treatment of sampling and quantization with a brief discussion on how to zoom and shrink a digital image. This topic is related to image sampling and quantization because zooming may be viewed as oversampling, while shrinking may be viewed as undersampling. The key difference between these two operations and sampling and quantizing an original continuous image is that zooming and shrinking are applied to a *digital* image.

Zooming requires two steps: the creation of new pixel locations, and the assignment of gray levels to those new locations. Let us start with a simple example. Suppose that we have an image of size 500 × 500 pixels and we want to enlarge it 1.5 times to 750 × 750 pixels. Conceptually, one of the easiest ways to visualize zooming is laying an imaginary 750 × 750 grid over the original image. Obviously, the spacing in the grid would be less than one pixel because we are fitting it over a smaller image. In order to perform gray-level assignment for any point in the overlay, we look for the closest pixel in the original image and assign its gray level to the new pixel in the grid. When we are done with all points in the overlay grid, we simply expand it to the original specified size to obtain the zoomed image. This method of gray-level assignment is called *nearest neighbor interpolation*. (Pixel neighborhoods are discussed in the next section.)

Pixel replication, the method used to generate Figs. 2.20(b) through (f), is a special case of nearest neighbor interpolation. Pixel replication is applicable when we want to increase the size of an image an integer number of times. For instance, to double the size of an image, we can duplicate each column. This doubles the image size in the horizontal direction. Then, we duplicate each row of the enlarged image to double the size in the vertical direction. The same procedure is used to enlarge the image by any integer number of times (triple, quadruple, and so on). Duplication is just done the required number of times to achieve the desired size. The gray-level assignment of each pixel is predetermined by the fact that new locations are exact duplicates of old locations.

Although nearest neighbor interpolation is fast, it has the undesirable feature that it produces a checkerboard effect that is particularly objectionable at high factors of magnification. Figures 2.20(e) and (f) are good examples of this. A slightly more sophisticated way of accomplishing gray-level assignments is *bilinear interpolation* using the four nearest neighbors of a point. Let (x', y') denote the coordinates of a point in the zoomed image (think of it as a point on the grid described previously), and let $v(x', y')$ denote the gray level assigned to it. For bilinear interpolation, the assigned gray level is given by

$$v(x', y') = ax' + by' + cx'y' + d \tag{2.4-6}$$

where the four coefficients are determined from the four equations in four unknowns that can be written using the four nearest neighbors of point (x', y').

Image shrinking is done in a similar manner as just described for zooming. The equivalent process of pixel replication is row-column deletion. For example, to shrink an image by one-half, we delete every other row and column. We can use the zooming grid analogy to visualize the concept of shrinking by a noninteger factor, except

that we now *expand* the grid to fit over the original image, do gray-level nearest neighbor or bilinear interpolation, and then shrink the grid back to its original specified size. To reduce possible aliasing effects, it is a good idea to blur an image slightly before shrinking it. Blurring of digital images is discussed in Chapters 3 and 4.

It is possible to use more neighbors for interpolation. Using more neighbors implies fitting the points with a more complex surface, which generally gives smoother results. This is an exceptionally important consideration in image generation for 3-D graphics [Watt (1993)] and in medical image processing [Lehmann et al. (1999)], but the extra computational burden seldom is justifiable for general-purpose digital image zooming and shrinking, where bilinear interpolation generally is the method of choice.

EXAMPLE 2.4: Image zooming using bilinear interpolation.

Figures 2.20(d) through (f) are shown again in the top row of Fig. 2.25. As noted earlier, these images were zoomed from 128 × 128, 64 × 64, and 32 × 32 to 1024 × 1024 pixels using nearest neighbor interpolation. The equivalent results using bilinear interpolation are shown in the second row of Fig. 2.25. The improvements in overall appearance are clear, especially in the 128 × 128 and

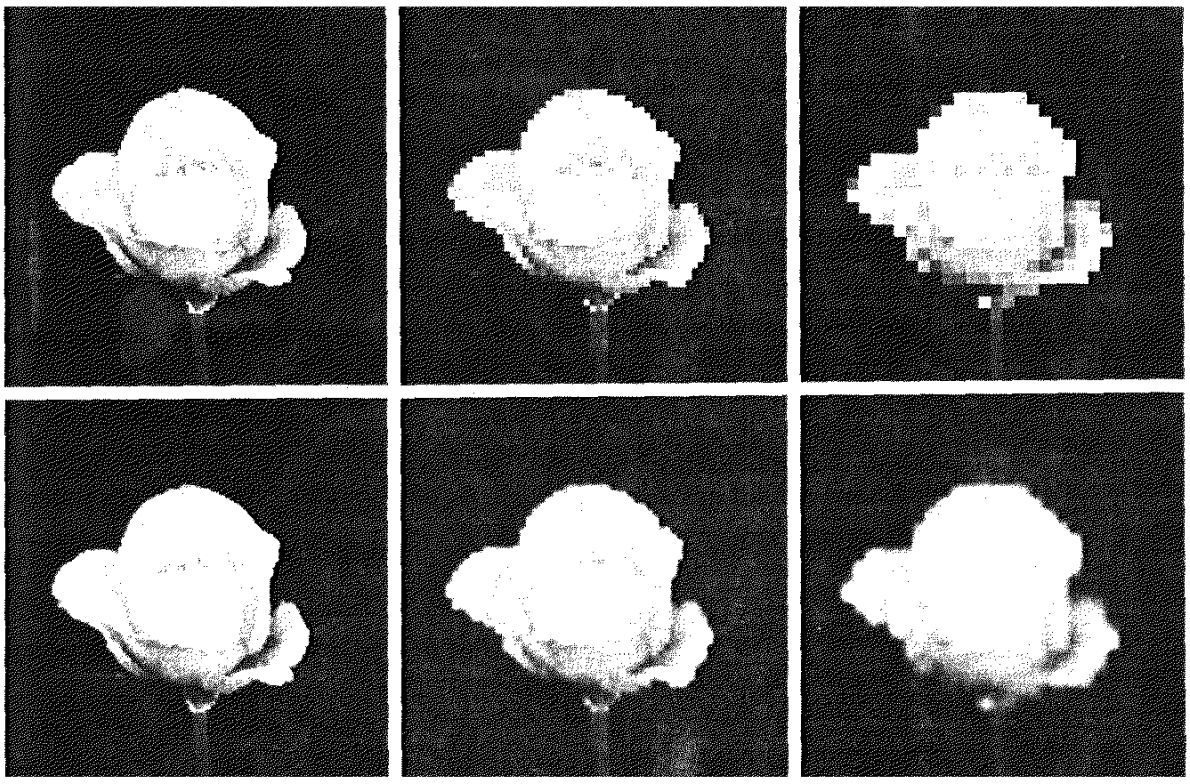

a b c
d e f

FIGURE 2.25 Top row: images zoomed from 128 × 128, 64 × 64, and 32 × 32 pixels to 1024 × 1024 pixels, using nearest neighbor gray-level interpolation. Bottom row: same sequence, but using bilinear interpolation.

64 × 64 cases. The 32 × 32 to 1024 × 1024 image is blurry, but keep in mind that this image was zoomed by a factor of 32. In spite of this, the result of bilinear interpolation shown in Fig. 2.25(f) is a reasonably good rendition of the original image shape, something that is lost in Fig. 2.25(c).

2.5 Some Basic Relationships Between Pixels

In this section, we consider several important relationships between pixels in a digital image. As mentioned before, an image is denoted by $f(x, y)$. When referring in this section to a particular pixel, we use lowercase letters, such as p and q.

2.5.1 Neighbors of a Pixel

A pixel p at coordinates (x, y) has four *horizontal* and *vertical* neighbors whose coordinates are given by

$$(x + 1, y), (x - 1, y), (x, y + 1), (x, y - 1)$$

This set of pixels, called the 4-*neighbors* of p, is denoted by $N_4(p)$. Each pixel is a unit distance from (x, y), and some of the neighbors of p lie outside the digital image if (x, y) is on the border of the image.

The four *diagonal* neighbors of p have coordinates

$$(x + 1, y + 1), (x + 1, y - 1), (x - 1, y + 1), (x - 1, y - 1)$$

and are denoted by $N_D(p)$. These points, together with the 4-neighbors, are called the 8-*neighbors* of p, denoted by $N_8(p)$. As before, some of the points in $N_D(p)$ and $N_8(p)$ fall outside the image if (x, y) is on the border of the image.

2.5.2 Adjacency, Connectivity, Regions, and Boundaries

Connectivity between pixels is a fundamental concept that simplifies the definition of numerous digital image concepts, such as regions and boundaries. To establish if two pixels are connected, it must be determined if they are neighbors and if their gray levels satisfy a specified criterion of similarity (say, if their gray levels are equal). For instance, in a binary image with values 0 and 1, two pixels may be 4-neighbors, but they are said to be connected only if they have the same value.

Let V be the set of gray-level values used to define adjacency. In a binary image, $V = \{1\}$ if we are referring to adjacency of pixels with value 1. In a gray-scale image, the idea is the same, but set V typically contains more elements. For example, in the adjacency of pixels with a range of possible gray-level values 0 to 255, set V could be any subset of these 256 values. We consider three types of adjacency:

(a) 4-*adjacency* Two pixels p and q with values from V are 4-adjacent if q is in the set $N_4(p)$.

(b) 8-*adjacency* Two pixels p and q with values from V are 8-adjacent if q is in the set $N_8(p)$.

(c) *m-adjacency* (mixed adjacency). Two pixels p and q with values from V are m-adjacent if

(i) q is in $N_4(p)$, *or*

(ii) q is in $N_D(p)$ *and* the set $N_4(p) \cap N_4(q)$ has no pixels whose values are from V.

Mixed adjacency is a modification of 8-adjacency. It is introduced to eliminate the ambiguities that often arise when 8-adjacency is used. For example, consider the pixel arrangement shown in Fig. 2.26(a) for $V = \{1\}$. The three pixels at the top of Fig. 2.26(b) show multiple (ambiguous) 8-adjacency, as indicated by the dashed lines. This ambiguity is removed by using m-adjacency, as shown in Fig. 2.26(c). Two image subsets S_1 and S_2 are adjacent if some pixel in S_1 is adjacent to some pixel in S_2. It is understood here and in the following definitions that *adjacent* means 4-, 8-, or m-adjacent.

A (*digital*) *path* (or *curve*) from pixel p with coordinates (x, y) to pixel q with coordinates (s, t) is a sequence of distinct pixels with coordinates

$$(x_0, y_0), (x_1, y_1), \ldots, (x_n, y_n)$$

where $(x_0, y_0) = (x, y)$, $(x_n, y_n) = (s, t)$, and pixels (x_i, y_i) and (x_{i-1}, y_{i-1}) are adjacent for $1 \leq i \leq n$. In this case, n is the *length* of the path. If $(x_0, y_0) = (x_n, y_n)$, the path is a *closed* path. We can define 4-, 8-, or m-paths depending on the type of adjacency specified. For example, the paths shown in Fig. 2.26(b) between the northeast and southeast points are 8-paths, and the path in Fig. 2.26(c) is an m-path. Note the absence of ambiguity in the m-path.

Let S represent a subset of pixels in an image. Two pixels p and q are said to be *connected* in S if there exists a path between them consisting entirely of pixels in S. For any pixel p in S, the *set* of pixels that are connected to it in S is called a *connected component* of S. If it only has one connected component, then set S is called a *connected set*.

Let R be a subset of pixels in an image. We call R a *region* of the image if R is a connected set. The *boundary* (also called *border* or *contour*) of a region R is the set of pixels in the region that have one or more neighbors that are not in R. If R happens to be an entire image (which we recall is a rectangular set of pixels), then its boundary is defined as the set of pixels in the first and last rows and columns of the image. This extra definition is required because an image has no neighbors beyond its border. Normally, when we refer to a region, we are

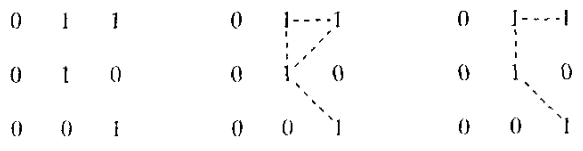

a b c

FIGURE 2.26 (a) Arrangement of pixels; (b) pixels that are 8-adjacent (shown dashed) to the center pixel; (c) m-adjacency.

referring to a subset of an image, and any pixels in the boundary of the region that happen to coincide with the border of the image are included implicitly as part of the region boundary.

The concept of an *edge* is found frequently in discussions dealing with regions and boundaries. There is a key difference between these concepts, however. The boundary of a finite region forms a closed path (Problem 2.14) and is thus a "global" concept. As discussed in detail in Chapter 10, edges are formed from pixels with derivative values that exceed a preset threshold. Thus, the idea of an edge is a "local" concept that is based on a measure of gray-level discontinuity at a point. It is possible to link edge points into edge segments, and sometimes these segments are linked in such a way that correspond to boundaries, but this is not always the case. The one exception in which edges and boundaries correspond is in binary images. Depending on the type of connectivity and edge operators used (we discuss these in Chapter 10), the edge extracted from a binary region will be the same as the region boundary. This is intuitive. Conceptually, until we arrive at Chapter 10, it is helpful to think of edges as intensity discontinuities and boundaries as closed paths.

2.5.3 Distance Measures

For pixels p, q, and z, with coordinates (x, y), (s, t), and (v, w), respectively, D is a *distance function* or *metric* if

(a) $D(p, q) \geq 0 \quad (D(p, q) = 0 \quad \text{iff} \quad p = q)$,
(b) $D(p, q) = D(q, p)$, and
(c) $D(p, z) \leq D(p, q) + D(q, z)$.

The *Euclidean distance* between p and q is defined as

$$D_e(p, q) = [(x - s)^2 + (y - t)^2]^{\frac{1}{2}}. \tag{2.5-1}$$

For this distance measure, the pixels having a distance less than or equal to some value r from (x, y) are the points contained in a disk of radius r centered at (x, y).

The D_4 *distance* (also called *city-block distance*) between p and q is defined as

$$D_4(p, q) = |x - s| + |y - t|. \tag{2.5-2}$$

In this case, the pixels having a D_4 distance from (x, y) less than or equal to some value r form a diamond centered at (x, y). For example, the pixels with D_4 distance ≤ 2 from (x, y) (the center point) form the following contours of constant distance:

$$\begin{array}{ccccc} & & 2 & & \\ & 2 & 1 & 2 & \\ 2 & 1 & 0 & 1 & 2 \\ & 2 & 1 & 2 & \\ & & 2 & & \end{array}$$

The pixels with $D_4 = 1$ are the 4-neighbors of (x, y).

The D_8 *distance* (also called *chessboard distance*) between p and q is defined as

$$D_8(p, q) = \max(|x - s|, |y - t|). \tag{2.5-3}$$

In this case, the pixels with D_8 distance from (x, y) less than or equal to some value r form a square centered at (x, y). For example, the pixels with D_8 distance ≤ 2 from (x, y) (the center point) form the following contours of constant distance:

$$\begin{matrix} 2 & 2 & 2 & 2 & 2 \\ 2 & 1 & 1 & 1 & 2 \\ 2 & 1 & 0 & 1 & 2 \\ 2 & 1 & 1 & 1 & 2 \\ 2 & 2 & 2 & 2 & 2 \end{matrix}$$

The pixels with $D_8 = 1$ are the 8-neighbors of (x, y).

Note that the D_4 and D_8 distances between p and q are independent of any paths that might exist between the points because these distances involve only the coordinates of the points. If we elect to consider m-adjacency, however, the D_m distance between two points is defined as the shortest m-path between the points. In this case, the distance between two pixels will depend on the values of the pixels along the path, as well as the values of their neighbors. For instance, consider the following arrangement of pixels and assume that p, p_2, and p_4 have value 1 and that p_1 and p_3 can have a value of 0 or 1:

$$\begin{matrix} & p_3 & p_4 \\ p_1 & p_2 & \\ p & & \end{matrix}$$

Suppose that we consider adjacency of pixels valued 1 (i.e., $V = \{1\}$). If p_1 and p_3 are 0, the length of the shortest m-path (the D_m distance) between p and p_4 is 2. If p_1 is 1, then p_2 and p will no longer be m-adjacent (see the definition of m-adjacency) and the length of the shortest m-path becomes 3 (the path goes through the points $pp_1p_2p_4$). Similar comments apply if p_3 is 1 (and p_1 is 0); in this case, the length of the shortest m-path also is 3. Finally, if both p_1 and p_3 are 1 the length of the shortest m-path between p and p_4 is 4. In this case, the path goes through the sequence of points $pp_1p_2p_3p_4$.

Image Operations on a Pixel Basis

Numerous references are made in the following chapters to operations between images, such as dividing one image by another. In Eq. (2.4-2), images were represented in the form of matrices. As we know, matrix division is not defined. However, when we refer to an operation like "dividing one image by another," we mean specifically that the division is carried out between *corresponding* pixels in the two images. Thus, for example, if f and g are images, the first element of the image formed by "dividing" f by g is simply the first pixel in f divided by the first pixel in g; of course, the assumption is that none of the pixels in g have value 0. Other arithmetic and logic operations are similarly defined between corresponding pixels in the images involved.

2.6 Linear and Nonlinear Operations

Let H be an operator whose input and output are images. H is said to be a *linear* operator if, for any two images f and g and any two scalars a and b,

$$H(af + bg) = aH(f) + bH(g). \tag{2.6-1}$$

In other words, the result of applying a linear operator to the sum of two images (that have been multiplied by the constants shown) is identical to applying the operator to the images individually, multiplying the results by the appropriate constants, and then adding those results. For example, an operator whose function is to compute the sum of K images is a linear operator. An operator that computes the absolute value of the difference of two images is not. An operator that fails the test of Eq. (2.6-1) is by definition *nonlinear*.

Linear operations are exceptionally important in image processing because they are based on a significant body of well-understood theoretical and practical results. Although nonlinear operations sometimes offer better performance, they are not always predictable, and for the most part are not well understood theoretically.

Summary

The material in this chapter is primarily background information for subsequent discussions. Our treatment of the human visual system, although brief, provides a basic idea of the capabilities of the eye in perceiving pictorial information. The discussion of light and the electromagnetic spectrum is fundamental in understanding the origin of the many images we use in this book. Similarly, the image model developed in Section 2.3.4 is used in the Chapter 4 as the basis for an image enhancement technique called *homomorphic filtering*, and again in Chapter 10 to explain the effect of illumination on the shape of image histograms.

The sampling ideas introduced in Section 2.4 are the foundation for many of the digitizing phenomena likely to be encountered in practice. These ideas can be expanded further once a basic understanding of frequency content is mastered. A detailed discussion of the frequency domain is given in Chapter 4. The concepts of sampling and aliasing effects also are of importance in the context of image acquisition.

The concepts introduced in Section 2.5 are the basic building blocks for processing techniques based on pixel neighborhoods. As shown in the following chapter and in Chapter 5, neighborhood processing methods are at the core of many image enhancement and restoration procedures. When applicable, neighborhood processing is favored in commercial applications of image processing due to their operational speed and simplicity of implementation in hardware and/or firmware. Finally, the concept of a linear operator and the theoretical and conceptual power associated with it will be used extensively in the following three chapters.

References and Further Reading

Additional reading for the material in Section 2.1 regarding the structure of the human eye may be found in Atchison and Smith [2000], and Oyster [1999]. For additional reading on visual perception, see Regan [2000] and Gordon [1997]. The book by Hubel [1988] and the now classic book by Cornsweet [1970] also are of interest. Born and Wolf [1999]

is a basic reference that discusses light in terms of electromagnetic theory. Electromagnetic energy propagation is covered in some detail by Felsen and Marcuvitz [1994].

The area of image sensing is quite broad and very fast moving. An excellent source of information on optical and other imaging sensors is the International Society for Optical Engineering (SPIE). The following are representative publications by the SPIE in this area: Blouke et al. [2001], Hoover and Doty [1996], and Freeman [1987].

The image model presented in Section 2.3.4 is from Oppenheim, Schafer, and Stockham [1968]. A reference for the illumination and reflectance values used in that section is the *IES Lighting Handbook* [2000]. For additional reading on image sampling and some of its effects, such as aliasing, see Bracewell [1995]. The early experiments mentioned in Section 2.4.3 on perceived image quality as a function of sampling and quatization were reported by Huang [1965]. The issue of reducing the number of samples and gray levels in an image while minimizing the ensuing degradation is still of current interest, as exemplified by Papamarkos and Atsalakis [2000]. For further reading on image shrinking and zooming, see Sid-Ahmed [1995], Unser et al. [1995], Umbaugh [1998], and Lehmann et al. [1999]. For further reading on the topics covered in Section 2.5, see Rosenfeld and Kak [1982], Marchand-Maillet and Sharaiha [2000], and Ritter and Wilson [2001]. Additional reading on linear systems in the context of image processing may be found in Castleman [1996].

Problems

★ **2.1** Using the background information provided in Section 2.1, and thinking purely in geometric terms, estimate the diameter of the smallest printed dot that the eye can discern if the page on which the dot is printed is 0.2 m away from the eyes. Assume for simplicity that the visual system ceases to detect the dot when the image of the dot on the fovea becomes smaller than the diameter of one receptor (cone) in that area of the retina. Assume further that the fovea can be modeled as a square array of dimensions 1.5 mm × 1.5 mm, and that the cones and spaces between the cones are distributed uniformly throughout this array.

2.2 When you enter a dark theater on a bright day, it takes an appreciable interval of time before you can see well enough to find an empty seat. Which of the visual processes explained in Section 2.1 is at play in this situation?

★ **2.3** Although it is not shown in Fig. 2.10, alternating current certainly is part of the electromagnetic spectrum. Commercial alternating current in the United States has a frequency of 60 Hz. What is the wavelength in kilometers of this component of the spectrum?

2.4 You are hired to design the front end of an imaging system for studying the boundary shapes of cells, bacteria, viruses, and protein. The front end consists, in this case, of the illumination source(s) and corresponding imaging camera(s). The diameters of circles required to enclose individual specimens in each of these categories are 50, 1, 0.1, and 0.01 μm, respectively.

(a) Can you solve the imaging aspects of this problem with a single sensor and camera? If your answer is yes, specify the illumination wavelength band and the type of camera needed. Identify the camera as being a color camera, far-infrared camera, or whatever appropriate name corresponds to the illumination source.

(b) If your answer in (a) is no, what type of illumination sources and corre-

See inside front cover

Detailed solutions to the problems marked with a star can be found in the book web site. The site also contains suggested projects based on the material in this chapter.

and cameras as requested in part (a). Use the *minimum* number of illumination sources and cameras needed to solve the problem.

2.5 A CCD camera chip of dimensions 7 × 7 mm, and having 1024 × 1024 elements, is focused on a square, flat area, located 0.5 m away. How many line pairs per mm will this camera be able to resolve? The camera is equipped with a 35-mm lens. (*Hint:* Model the imaging process as in Fig. 2.3, with the focal length of the camera lens substituting for the focal length of the eye.)

★2.6 An automobile manufacturer is automating the placement of certain components on the bumpers of a limited-edition line of sports cars. The components are color coordinated, so the robots need to know the color of each car in order to select the appropriate bumper component. Models come in only four colors: blue, green, red, and white. You are hired to propose a solution based on imaging. How would you solve the problem of automatically determining the color of each car, keeping in mind that *cost* is the most important consideration in your choice of components?

2.7 Suppose that a flat area with center at (x_0, y_0) is illuminated by a light source with intensity distribution

$$i(x, y) = Ke^{-[(x-x_0)^2+(y-y_0)^2]}.$$

Assume for simplicity that the reflectance of the area is constant and equal to 1.0, and let $K = 255$. If the resulting image is digitized with k bits of intensity resolution, and the eye can detect an abrupt change of eight shades of intensity between adjacent pixels, what value of k will cause visible false contouring?

2.8 Sketch the image in Problem 2.7 for $k = 2$.

★2.9 A common measure of transmission for digital data is the *baud rate*, defined as the number of bits transmitted per second. Generally, transmission is accomplished in packets consisting of a start bit, a byte (8 bits) of information, and a stop bit. Using these facts, answer the following:

(a) How many minutes would it take to transmit a 1024 × 1024 image with 256 gray levels using a 56K baud modem?

(b) What would the time be at 750K baud, a representative speed of a phone DSL (digital subscriber line) connection?

2.10 High-definition television (HDTV) generates images with a resolution of 1125 horizontal TV lines interlaced (where every other line is painted on the tube face in each of two fields, each field being 1/60th of a second in duration). The width-to-height aspect ratio of the images is 16:9. The fact that the horizontal lines are distinct fixes the vertical resolution of the images. A company has designed an image capture system that generates digital images from HDTV images. The resolution of each TV (horizontal) line in their system is in proportion to vertical resolution, with the proportion being the width-to-height ratio of the images. Each pixel in the color image has 24 bits of intensity resolution, 8 bits each of a red, a green, and a blue image. These three "primary" images form a color image. How many bits would it take to store a 2-hour HDTV program?

★2.11 Consider the two image subsets, S_1 and S_2, shown in the following figure. For $V = \{1\}$, determine whether these two subsets are (a) 4-adjacent, (b) 8-adjacent, or (c) m-adjacent.

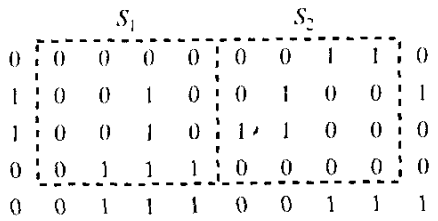

★**2.12** Develop an algorithm for converting a one-pixel-thick 8-path to a 4-path.

2.13 Develop an algorithm for converting a one-pixel-thick m-path to a 4-path.

2.14 Show that the boundary of the region, as defined in Section 2.5.2, is a closed path.

★**2.15** Consider the image segment shown.

(a) Let $V = \{0, 1\}$ and compute the lengths of the shortest 4-, 8-, and m-path between p and q. If a particular path does not exist between these two points, explain why.

(b) Repeat for $V = \{1, 2\}$.

$$\begin{matrix} 3 & 1 & 2 & 1\,(q) \\ 2 & 2 & 0 & 2 \\ 1 & 2 & 1 & 1 \\ (p)\,1 & 0 & 1 & 2 \end{matrix}$$

★**2.16** **(a)** Give the condition(s) under which the D_4 distance between two points p and q is equal to the shortest 4-path between these points.

(b) Is this path unique?

2.17 Repeat Problem 2.16 for the D_8 distance.

★**2.18** In the following chapter, we will deal with operators whose function is to compute the sum of pixel values in a small subimage area, S. Show that these are linear operators.

2.19 The median, ζ, of a set of numbers is such that half the values in the set are below ζ and the other half are above it. For example, the median of the set of values $\{2, 3, 8, 20, 21, 25, 31\}$ is 20. Show that an operator that computes the median of a subimage area, S, is nonlinear.

2.20 A plant produces a line of translucent miniature polymer squares. Stringent quality requirements dictate 100% visual inspection, and the plant manager finds the use of human inspectors increasingly expensive. Inspection is semiautomated. At each inspection station, a robotic mechanism places each polymer square over a light located under an optical system that produces a magnified image of the square. The image completely fills a viewing screen measuring 80 × 80 mm. Defects appear as dark circular blobs, and the inspector's job is to look at the screen and reject any sample that has one or more such dark blobs with a diameter of 0.8 mm or larger, as measured on the scale of the screen. The manager believes that, if she can find a way to automate the process completely, she will increase profits by 50%. She also believes that success in this project will aid her climb up the corporate ladder. After much investigation, the manager decides that the way to solve the problem is to view each inspection screen with a CCD TV camera and feed the output of the

camera into an image processing system capable of detecting the blobs, measuring their diameter, and activating the accept/reject buttons previously operated by an inspector. She is able to find a system that can do the job, as long as the smallest defect occupies an area of at least 2×2 pixels in the digital image. The manager hires you to help her specify the camera and lens system, but requires that you use off-the-shelf components. For the lenses, assume that this constraint means any integer multiple of 25 mm or 35 mm, up to 200 mm. For the cameras, it means resolutions of 512×512, 1024×1024, or 2048×2048 pixels. The *individual* imaging elements in these cameras are squares measuring 8×8 μm, and the spaces between imaging elements are 2 μm. For this application, the cameras cost much more than the lenses, so the problem should be solved with the lowest-resolution camera possible, based on the choice of lenses. As a consultant, you are to provide a written recommendation, showing in reasonable detail the analysis that led to your conclusion. Use the same imaging geometry suggested in Problem 2.5.

3 Image Enhancement in the Spatial Domain

It makes all the difference whether one sees darkness through the light or brightness through the shadows.

David Lindsay

Preview

The principal objective of enhancement is to process an image so that the result is more suitable than the original image for a specific application. The word *specific* is important, because it establishes at the outset that the techniques discussed in this chapter are very much problem oriented. Thus, for example, a method that is quite useful for enhancing X-ray images may not necessarily be the best approach for enhancing pictures of Mars transmitted by a space probe. Regardless of the method used, however, image enhancement is one of the most interesting and visually appealing areas of image processing.

Image enhancement approaches fall into two broad categories: spatial domain methods and frequency domain methods. The term *spatial domain* refers to the image plane itself, and approaches in this category are based on direct manipulation of pixels in an image. *Frequency domain* processing techniques are based on modifying the Fourier transform of an image. Spatial methods are covered in this chapter, and frequency domain enhancement is discussed in Chapter 4. Enhancement techniques based on various combinations of methods from these two categories are not unusual. We note also that many of the fundamental techniques introduced in this chapter in the context of enhancement are used in subsequent chapters for a variety of other image processing applications.

There is no general theory of image enhancement. When an image is processed for visual interpretation, the viewer is the ultimate judge of how well

a particular method works. Visual evaluation of image quality is a highly subjective process, thus making the definition of a "good image" an elusive standard by which to compare algorithm performance. When the problem is one of processing images for machine perception, the evaluation task is somewhat easier. For example, in dealing with a character recognition application, and leaving aside other issues such as computational requirements, the best image processing method would be the one yielding the best machine recognition results. However, even in situations when a clear-cut criterion of performance can be imposed on the problem, a certain amount of trial and error usually is required before a particular image enhancement approach is selected.

3.1 Background

As indicated previously, the term *spatial domain* refers to the aggregate of pixels composing an image. Spatial domain methods are procedures that operate directly on these pixels. Spatial domain processes will be denoted by the expression

$$g(x, y) = T[f(x, y)] \tag{3.1-1}$$

where $f(x, y)$ is the input image, $g(x, y)$ is the processed image, and T is an operator on f, defined over some neighborhood of (x, y). In addition, T can operate on a *set* of input images, such as performing the pixel-by-pixel sum of K images for noise reduction, as discussed in Section 3.4.2.

The principal approach in defining a neighborhood about a point (x, y) is to use a square or rectangular subimage area centered at (x, y), as Fig. 3.1 shows. The center of the subimage is moved from pixel to pixel starting, say, at the top left corner. The operator T is applied at each location (x, y) to yield the output, g, at that location. The process utilizes only the pixels in the area of the image spanned by the neighborhood. Although other neighborhood shapes, such as ap-

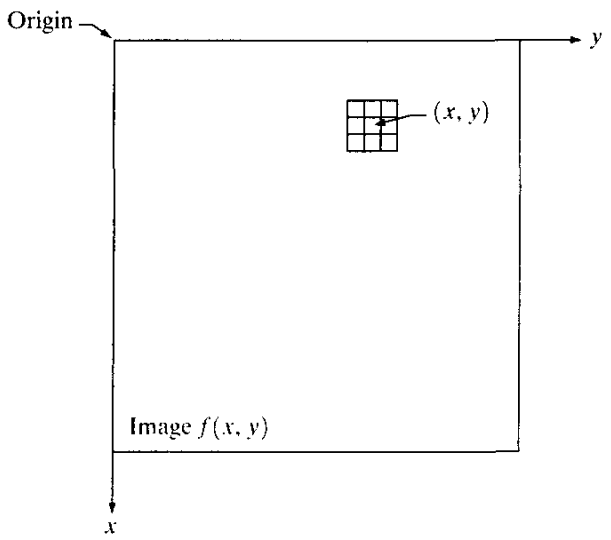

FIGURE 3.1 A 3×3 neighborhood about a point (x, y) in an image.

proximations to a circle, sometimes are used, square and rectangular arrays are by far the most predominant because of their ease of implementation.

The simplest form of T is when the neighborhood is of size 1×1 (that is, a single pixel). In this case, g depends only on the value of f at (x, y), and T becomes a *gray-level* (also called an *intensity* or *mapping*) *transformation function* of the form

$$s = T(r) \tag{3.1-2}$$

where, for simplicity in notation, r and s are variables denoting, respectively, the gray level of $f(x, y)$ and $g(x, y)$ at any point (x, y). For example, if $T(r)$ has the form shown in Fig. 3.2(a), the effect of this transformation would be to produce an image of higher contrast than the original by darkening the levels below m and brightening the levels above m in the original image. In this technique, known as *contrast stretching*, the values of r below m are compressed by the transformation function into a narrow range of s, toward black. The opposite effect takes place for values of r above m. In the limiting case shown in Fig. 3.2(b), $T(r)$ produces a two-level (binary) image. A mapping of this form is called a *thresholding* function. Some fairly simple, yet powerful, processing approaches can be formulated with gray-level transformations. Because enhancement at any point in an image depends only on the gray level at that point, techniques in this category often are referred to as *point processing*.

Larger neighborhoods allow considerably more flexibility. The general approach is to use a function of the values of f in a predefined neighborhood of (x, y) to determine the value of g at (x, y). One of the principal approaches in this formulation is based on the use of so-called *masks* (also referred to as *filters, kernels, templates*, or *windows*). Basically, a mask is a small (say, 3×3) 2-D array, such as the one shown in Fig. 3.1, in which the values of the mask coefficients determine the nature of the process, such as image sharpening. Enhancement techniques based on this type of approach often are referred to as *mask processing* or *filtering*. These concepts are discussed in Section 3.5.

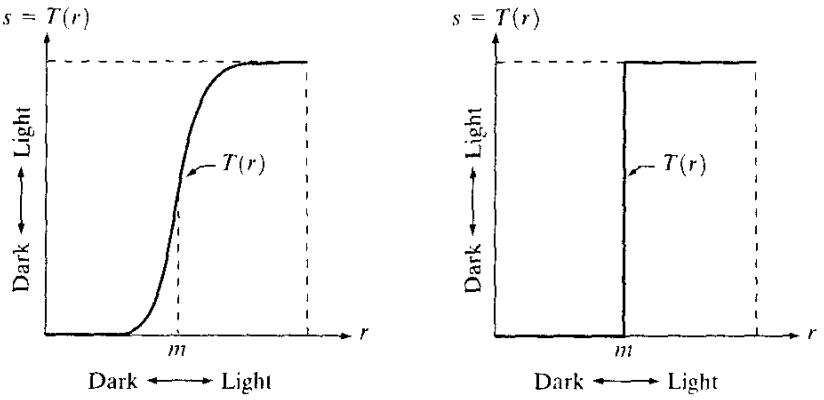

a b

FIGURE 3.2 Gray-level transformation functions for contrast enhancement.

Some Basic Gray Level Transformations

We begin the study of image enhancement techniques by discussing gray-level transformation functions. These are among the simplest of all image enhancement techniques. The values of pixels, before and after processing, will be denoted by r and s, respectively. As indicated in the previous section, these values are related by an expression of the form $s = T(r)$, where T is a transformation that maps a pixel value r into a pixel value s. Since we are dealing with digital quantities, values of the transformation function typically are stored in a one-dimensional array and the mappings from r to s are implemented via table lookups. For an 8-bit environment, a lookup table containing the values of T will have 256 entries.

As an introduction to gray-level transformations, consider Fig. 3.3, which shows three basic types of functions used frequently for image enhancement: linear (negative and identity transformations), logarithmic (log and inverse-log transformations), and power-law (nth power and nth root transformations). The identity function is the trivial case in which output intensities are identical to input intensities. It is included in the graph only for completeness.

3.2.1 Image Negatives

The negative of an image with gray levels in the range $[0, L-1]$ is obtained by using the negative transformation shown in Fig. 3.3, which is given by the expression

$$s = L - 1 - r. \tag{3.2-1}$$

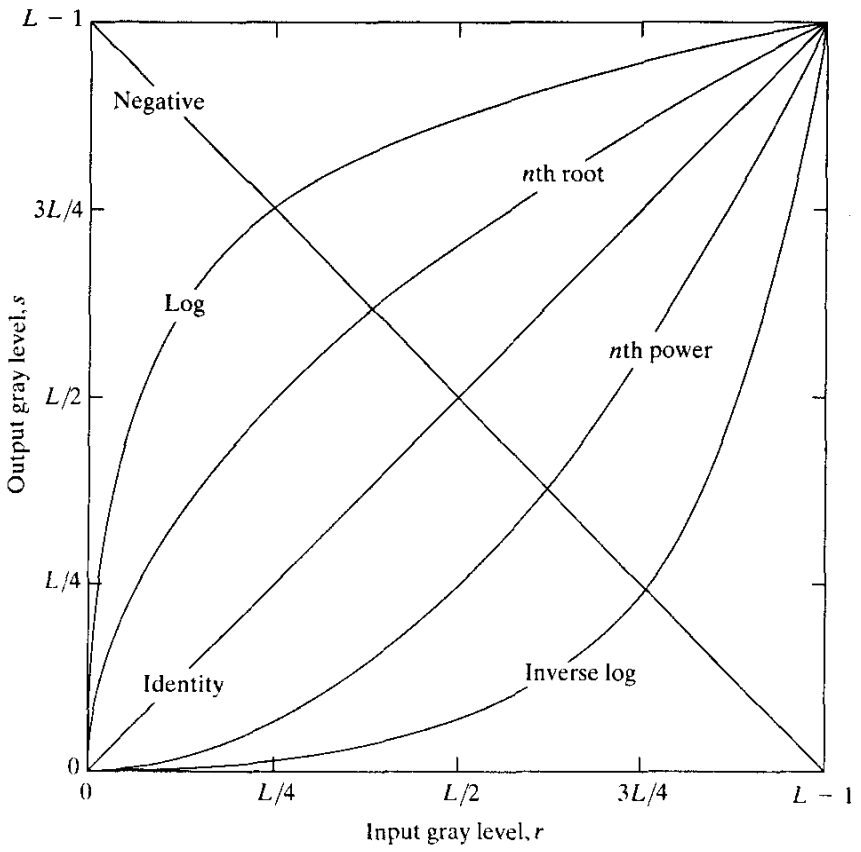

FIGURE 3.3 Some basic gray-level transformation functions used for image enhancement.

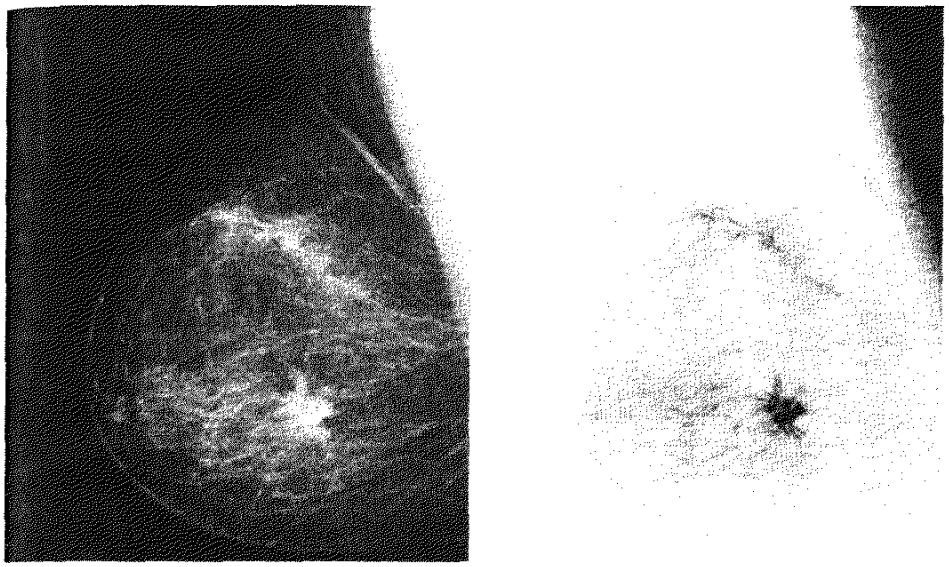

a b

FIGURE 3.4 (a) Original digital mammogram. (b) Negative image obtained using the negative transformation in Eq. (3.2-1). (Courtesy of G.E. Medical Systems.)

Reversing the intensity levels of an image in this manner produces the equivalent of a photographic negative. This type of processing is particularly suited for enhancing white or gray detail embedded in dark regions of an image, especially when the black areas are dominant in size. An example is shown in Fig. 3.4. The original image is a digital mammogram showing a small lesion. In spite of the fact that the visual content is the same in both images, note how much easier it is to analyze the breast tissue in the negative image in this particular case.

3.2.2 Log Transformations

The general form of the log transformation shown in Fig. 3.3 is

$$s = c \log(1 + r) \tag{3.2-2}$$

where c is a constant, and it is assumed that $r \geq 0$. The shape of the log curve in Fig. 3.3 shows that this transformation maps a narrow range of low gray-level values in the input image into a wider range of output levels. The opposite is true of higher values of input levels. We would use a transformation of this type to expand the values of dark pixels in an image while compressing the higher-level values. The opposite is true of the inverse log transformation.

Any curve having the general shape of the log functions shown in Fig. 3.3 would accomplish this spreading/compressing of gray levels in an image. In fact, the power-law transformations discussed in the next section are much more versatile for this purpose than the log transformation. However, the log function has the important characteristic that it compresses the dynamic range of images with large variations in pixel values. A classic illustration of an application in which pixel values have a large dynamic range is the Fourier spectrum, which will be discussed in Chapter 4. At the moment, we are concerned only with the image characteristics of spectra. It is not unusual to encounter spectrum values

a b

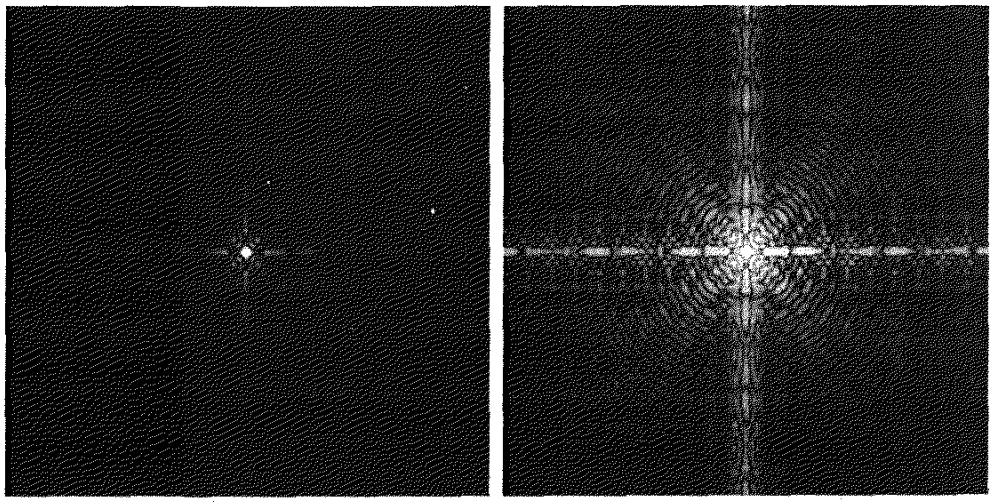

FIGURE 3.5
(a) Fourier spectrum.
(b) Result of applying the log transformation given in Eq. (3.2-2) with $c = 1$.

that range from 0 to 10^6 or higher. While processing numbers such as these presents no problems for a computer, image display systems generally will not be able to reproduce faithfully such a wide range of intensity values. The net effect is that a significant degree of detail will be lost in the display of a typical Fourier spectrum.

As an illustration of log transformations, Fig. 3.5(a) shows a Fourier spectrum with values in the range 0 to 1.5×10^6. When these values are scaled linearly for display in an 8-bit system, the brightest pixels will dominate the display, at the expense of lower (and just as important) values of the spectrum. The effect of this dominance is illustrated vividly by the relatively small area of the image in Fig. 3.5(a) that is not perceived as black. If, instead of displaying the values in this manner, we first apply Eq. (3.2-2) (with $c = 1$ in this case) to the spectrum values, then the range of values of the result become 0 to 6.2, a more manageable number. Figure 3.5(b) shows the result of scaling this new range linearly and displaying the spectrum in the same 8-bit display. The wealth of detail visible in this image as compared to a straight display of the spectrum is evident from these pictures. Most of the Fourier spectra seen in image processing publications have been scaled in just this manner.

3.2.3 Power-Law Transformations

Power-law transformations have the basic form

$$s = cr^{\gamma} \tag{3.2-3}$$

where c and γ are positive constants. Sometimes Eq. (3.2-3) is written as $s = c(r + \varepsilon)^{\gamma}$ to account for an offset (that is, a measurable output when the input is zero). However, offsets typically are an issue of display calibration and as a result they are normally ignored in Eq. (3.2-3). Plots of s versus r for various values of γ are shown in Fig. 3.6. As in the case of the log transformation, power-law curves with fractional values of γ map a narrow range of dark input values into a wider range of output values, with the opposite being true for high-

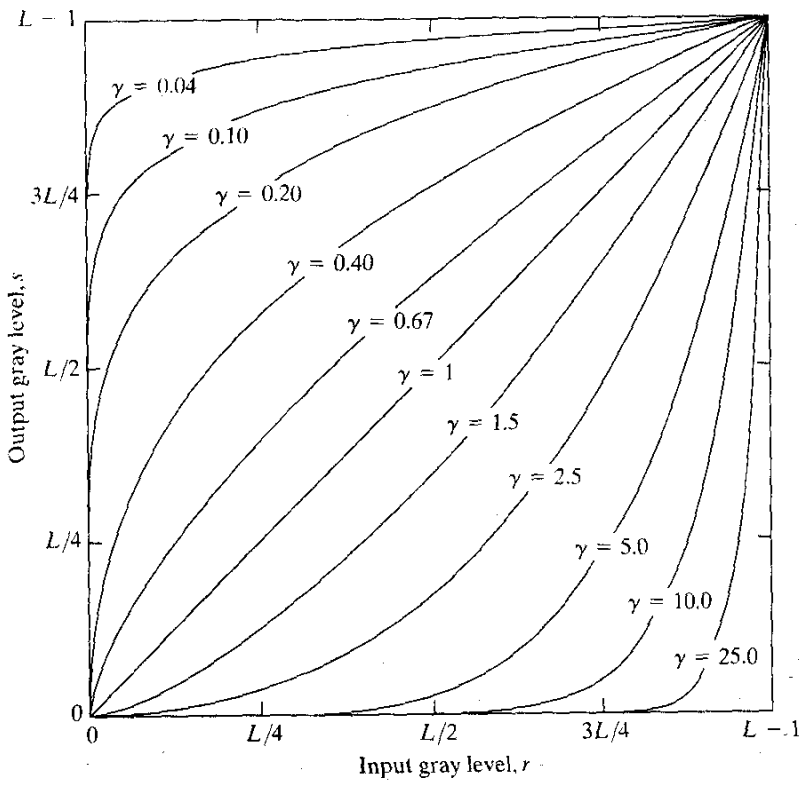

FIGURE 3.6 Plots of the equation $s = cr^{\gamma}$ for various values of γ ($c = 1$ in all cases).

er values of input levels. Unlike the log function, however, we notice here a family of possible transformation curves obtained simply by varying γ. As expected, we see in Fig. 3.6 that curves generated with values of $\gamma > 1$ have exactly the opposite effect as those generated with values of $\gamma < 1$. Finally, we note that Eq. (3.2-3) reduces to the identity transformation when $c = \gamma = 1$.

A variety of devices used for image capture, printing, and display respond according to a power law. By convention, the exponent in the power-law equation is referred to as *gamma* [hence our use of this symbol in Eq. (3.2-3)]. The process used to correct this power-law response phenomena is called *gamma correction*. For example, cathode ray tube (CRT) devices have an intensity-to-voltage response that is a power function, with exponents varying from approximately 1.8 to 2.5. With reference to the curve for $\gamma = 2.5$ in Fig. 3.6, we see that such display systems would tend to produce images that are darker than intended. This effect is illustrated in Fig. 3.7. Figure 3.7(a) shows a simple gray-scale linear wedge input into a CRT monitor. As expected, the output of the monitor appears darker than the input, as shown in Fig. 3.7(b). Gamma correction in this case is straightforward. All we need to do is preprocess the input image before inputting it into the monitor by performing the transformation $s = r^{1/2.5} = r^{0.4}$. The result is shown in Fig. 3.7(c). When input into the same monitor, this gamma-corrected input produces an output that is close in appearance to the original image, as shown in Fig. 3.7(d). A similar analysis would

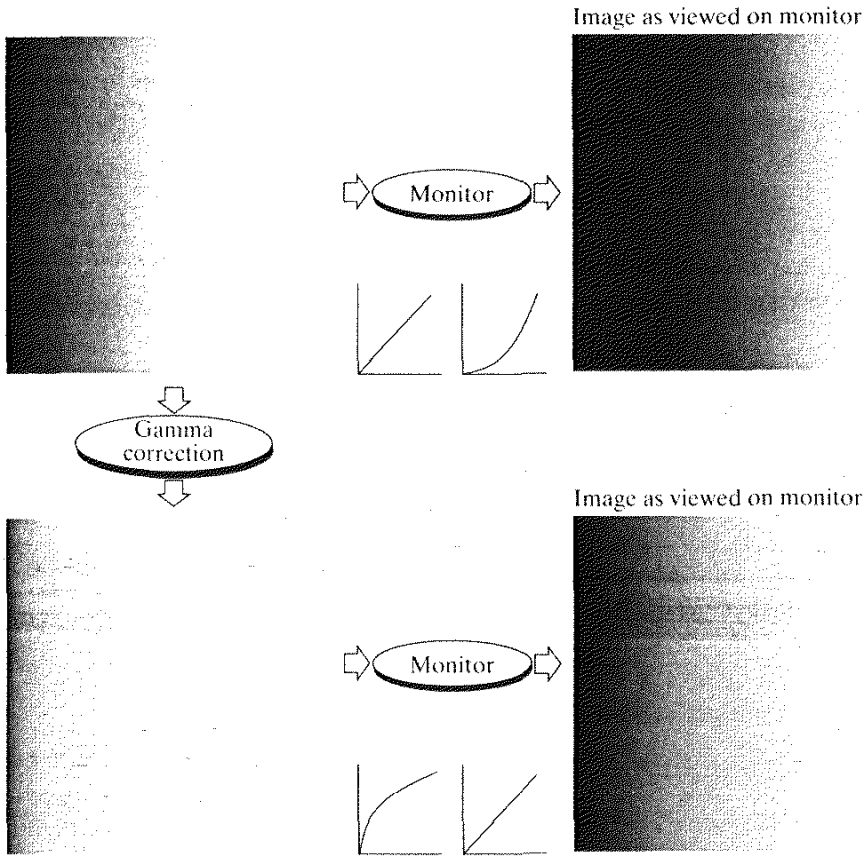

a b
c d

FIGURE 3.7
(a) Linear-wedge gray-scale image. (b) Response of monitor to linear wedge. (c) Gamma-corrected wedge. (d) Output of monitor.

apply to other imaging devices such as scanners and printers. The only difference would be the device-dependent value of gamma (Poynton [1996]).

Gamma correction is important if displaying an image accurately on a computer screen is of concern. Images that are not corrected properly can look either bleached out, or, what is more likely, too dark. Trying to reproduce colors accurately also requires some knowledge of gamma correction because varying the value of gamma correction changes not only the brightness, but also the ratios of red to green to blue. Gamma correction has become increasingly important in the past few years, as use of digital images for commercial purposes over the Internet has increased. It is not unusual that images created for a popular Web site will be viewed by millions of people, the majority of whom will have different monitors and/or monitor settings. Some computer systems even have partial gamma correction built in. Also, current image standards do not contain the value of gamma with which an image was created, thus complicating the issue further. Given these constraints, a reasonable approach when storing images in a Web site is to preprocess the images with a gamma that represents an "average" of the types of monitors and computer systems that one expects in the open market at any given point in time.

EXAMPLE 3.1: Contrast enhancement using power-law transformations.

In addition to gamma correction, power-law transformations are useful for general-purpose contrast manipulation. Figure 3.8(a) shows a magnetic resonance (MR) image of an upper thoracic human spine with a fracture dislocation

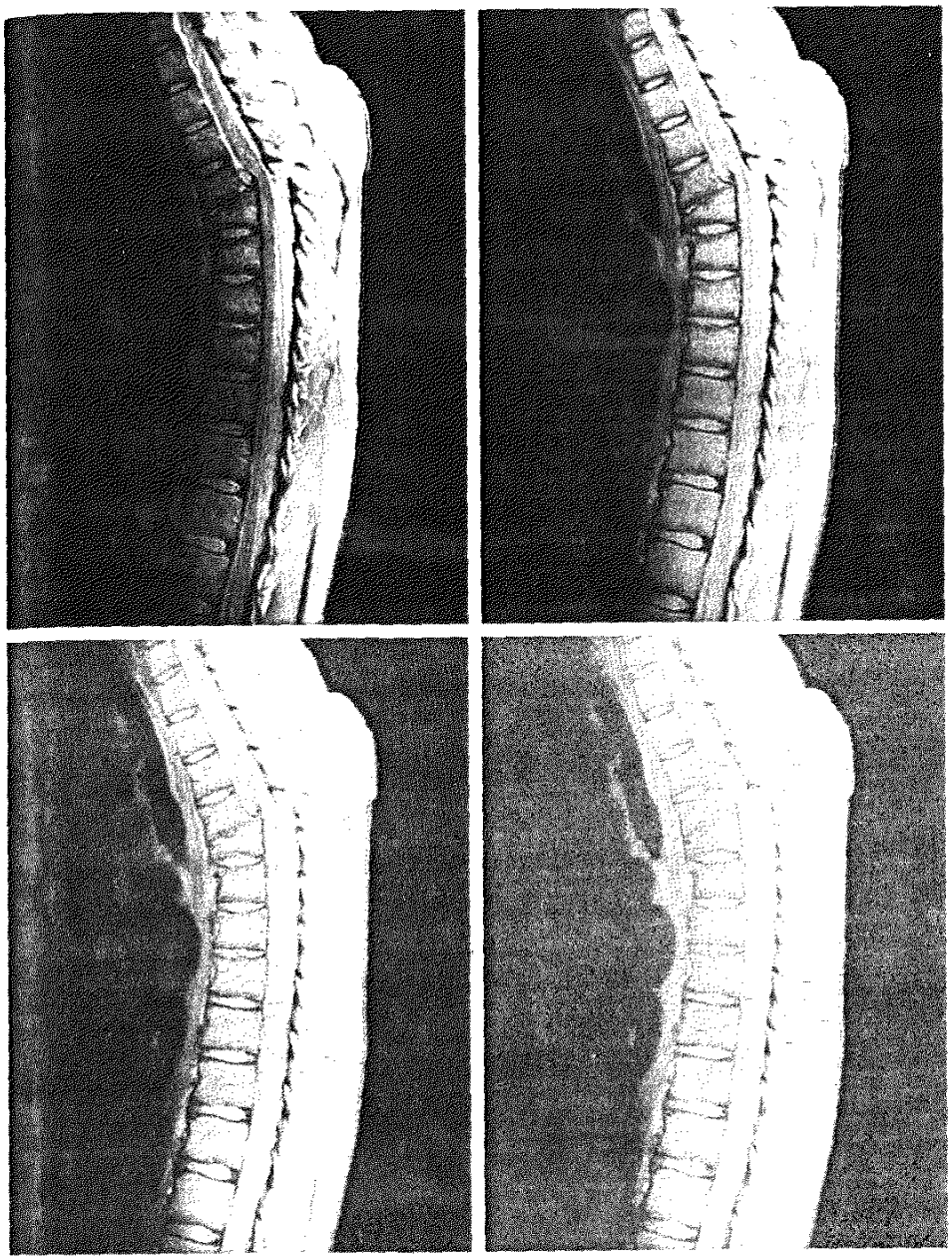

a b
c d

FIGURE 3.8
(a) Magnetic resonance (MR) image of a fractured human spine.
(b)–(d) Results of applying the transformation in Eq. (3.2-3) with $c = 1$ and $\gamma = 0.6, 0.4$, and 0.3, respectively. (Original image for this example courtesy of Dr. David R. Pickens, Department of Radiology and Radiological Sciences, Vanderbilt University Medical Center.)

and spinal cord impingement. The fracture is visible near the vertical center of the spine, approximately one-fourth of the way down from the top of the picture. Since the given image is predominantly dark, an expansion of gray levels are desirable. This can be accomplished with a power-law transformation with a fractional exponent. The other images shown in the figure were obtained by processing Fig. 3.8(a) with the power-law transformation function of Eq. (3.2-3). The values of gamma corresponding to images (b) through (d) are 0.6, 0.4, and 0.3, respectively (the value of c was 1 in all cases). We note that, as gamma decreased from 0.6 to 0.4, more detail became visible. A further decrease of gamma

to 0.3 enhanced a little more detail in the background, but began to reduce contrast to the point where the image started to have a very slight "washed-out" look, especially in the background. By comparing all results, we see that the best enhancement in terms of contrast and discernable detail was obtained with $\gamma = 0.4$. A value of $\gamma = 0.3$ is an approximate limit below which contrast in this particular image would be reduced to an unacceptable level.

EXAMPLE 3.2: Another illustration of power-law transformations.

Figure 3.9(a) shows the opposite problem of Fig. 3.8(a). The image to be enhanced now has a washed-out appearance, indicating that a compression of gray levels is desirable. This can be accomplished with Eq. (3.2-3) using values of γ greater than 1. The results of processing Fig. 3.9(a) with $\gamma = 3.0$, 4.0, and 5.0 are shown in Figs. 3.9(b) through (d). Suitable results were obtained with gamma values of 3.0 and 4.0, the latter having a slightly more appealing appearance because it has higher contrast. The result obtained with $\gamma = 5.0$ has areas that are too dark, in which some detail is lost. The dark region to the left of the main road in the upper left quadrant is an example of such an area.

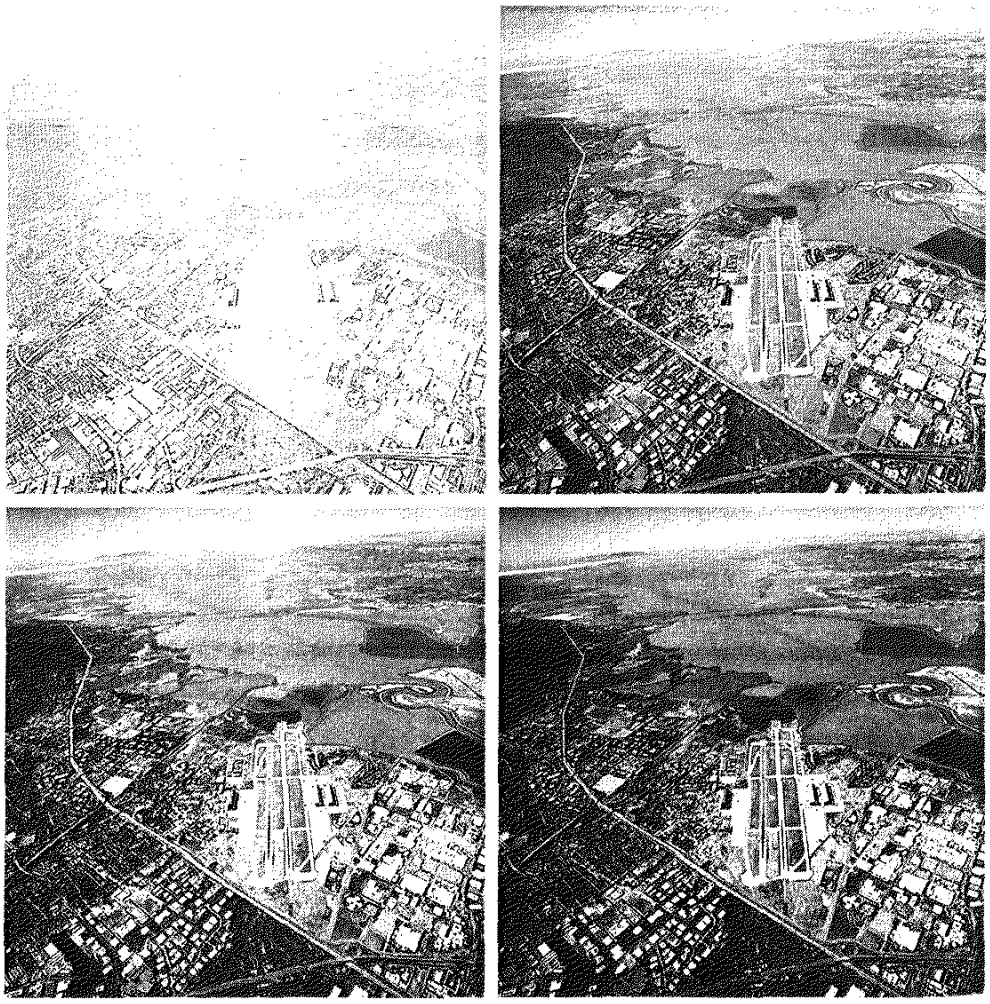

a b
c d

FIGURE 3.9
(a) Aerial image. (b)–(d) Results of applying the transformation in Eq. (3.2-3) with $c = 1$ and $\gamma = 3.0$, 4.0, and 5.0, respectively. (Original image for this example courtesy of NASA.)

Piecewise-Linear Transformation Functions

A complementary approach to the methods discussed in the previous three sections is to use piecewise linear functions. The principal advantage of piecewise linear functions over the types of functions we have discussed thus far is that the form of piecewise functions can be arbitrarily complex. In fact, as we will see shortly, a practical implementation of some important transformations can be formulated only as piecewise functions. The principal disadvantage of piecewise functions is that their specification requires considerably more user input.

Contrast stretching

One of the simplest piecewise linear functions is a contrast-stretching transformation. Low-contrast images can result from poor illumination, lack of dynamic range in the imaging sensor, or even wrong setting of a lens aperture during image acquisition. The idea behind contrast stretching is to increase the dynamic range of the gray levels in the image being processed.

Figure 3.10(a) shows a typical transformation used for contrast stretching. The locations of points (r_1, s_1) and (r_2, s_2) control the shape of the transformation

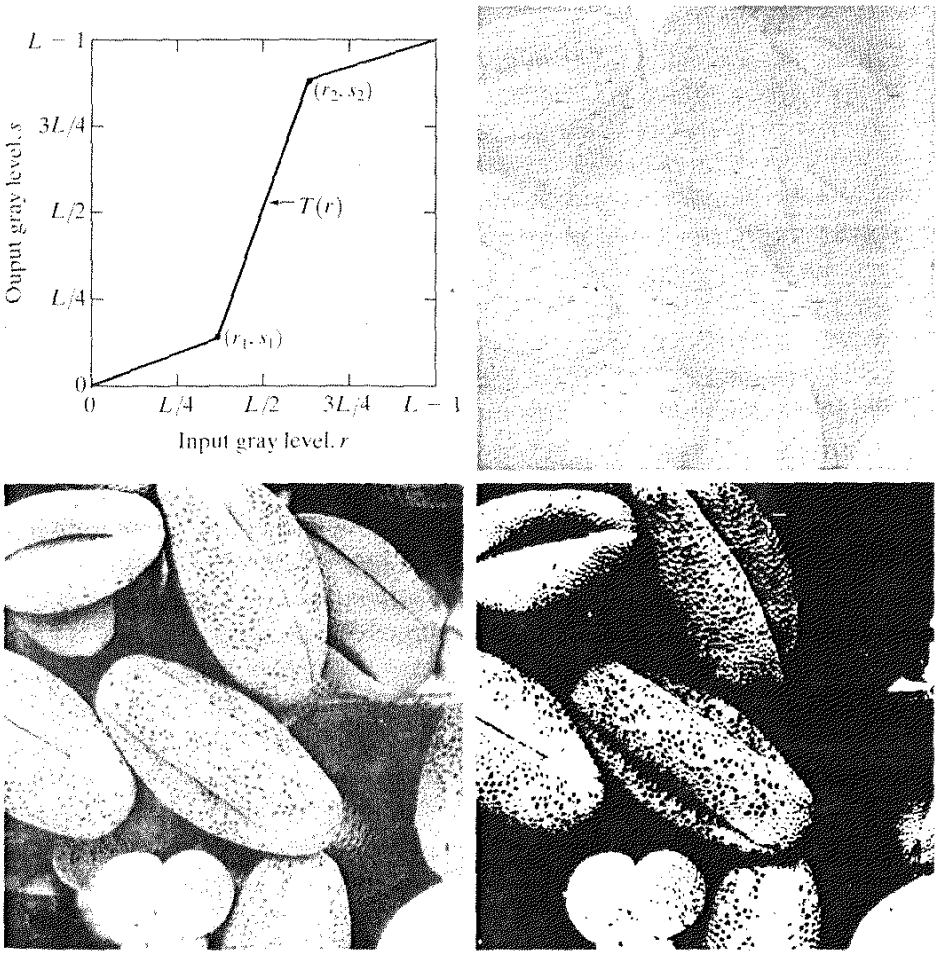

a b
c d

FIGURE 3.10 Contrast stretching. (a) Form of transformation function. (b) A low-contrast image. (c) Result of contrast stretching. (d) Result of thresholding. (Original image courtesy of Dr. Roger Heady, Research School of Biological Sciences, Australian National University, Canberra, Australia.)

function. If $r_1 = s_1$ and $r_2 = s_2$, the transformation is a linear function that produces no changes in gray levels. If $r_1 = r_2$, $s_1 = 0$ and $s_2 = L - 1$, the transformation becomes a *thresholding function* that creates a binary image, as illustrated in Fig. 3.2(b). Intermediate values of (r_1, s_1) and (r_2, s_2) produce various degrees of spread in the gray levels of the output image, thus affecting its contrast. In general, $r_1 \leq r_2$ and $s_1 \leq s_2$ is assumed so that the function is single valued and monotonically increasing. This condition preserves the order of gray levels, thus preventing the creation of intensity artifacts in the processed image.

Figure 3.10(b) shows an 8-bit image with low contrast. Fig. 3.10(c) shows the result of contrast stretching, obtained by setting $(r_1, s_1) = (r_{\min}, 0)$ and $(r_2, s_2) = (r_{\max}, L - 1)$ where $r_{\min}$ and $r_{\max}$ denote the minimum and maximum gray levels in the image, respectively. Thus, the transformation function stretched the levels linearly from their original range to the full range $[0, L - 1]$. Finally, Fig. 3.10(d) shows the result of using the thresholding function defined previously, with $r_1 = r_2 = m$, the mean gray level in the image. The original image on which these results are based is a scanning electron microscope image of pollen, magnified approximately 700 times.

Gray-level slicing

Highlighting a specific range of gray levels in an image often is desired. Applications include enhancing features such as masses of water in satellite imagery and enhancing flaws in X-ray images. There are several ways of doing level slicing, but most of them are variations of two basic themes. One approach is to display a high value for all gray levels in the range of interest and a low value for all other gray levels. This transformation, shown in Fig. 3.11(a), produces a binary image. The second approach, based on the transformation shown in Fig. 3.11(b), brightens the desired range of gray levels but preserves the background and gray-level tonalities in the image. Figure 3.11(c) shows a gray-scale image, and Fig. 3.11(d) shows the result of using the transformation in Fig. 3.11(a). Variations of the two transformations shown in Fig. 3.11 are easy to formulate.

Bit-plane slicing

Instead of highlighting gray-level ranges, highlighting the contribution made to total image appearance by specific bits might be desired. Suppose that each pixel in an image is represented by 8 bits. Imagine that the image is composed of eight 1-bit planes, ranging from bit-plane 0 for the least significant bit to bit-plane 7 for the most significant bit. In terms of 8-bit bytes, plane 0 contains all the lowest order bits in the bytes comprising the pixels in the image and plane 7 contains all the high-order bits. Figure 3.12 illustrates these ideas, and Fig. 3.14 shows the various bit planes for the image shown in Fig. 3.13. Note that the higher-order bits (especially the top four) contain the majority of the visually significant data. The other bit planes contribute to more subtle details in the image. Separating a digital image into its bit planes is useful for analyzing the relative importance played by each bit of the image, a process that aids in determining the adequacy of the number of bits used to quantize each pixel. Also, this type of decomposition is useful for image compression, as discussed in Chapter 8.

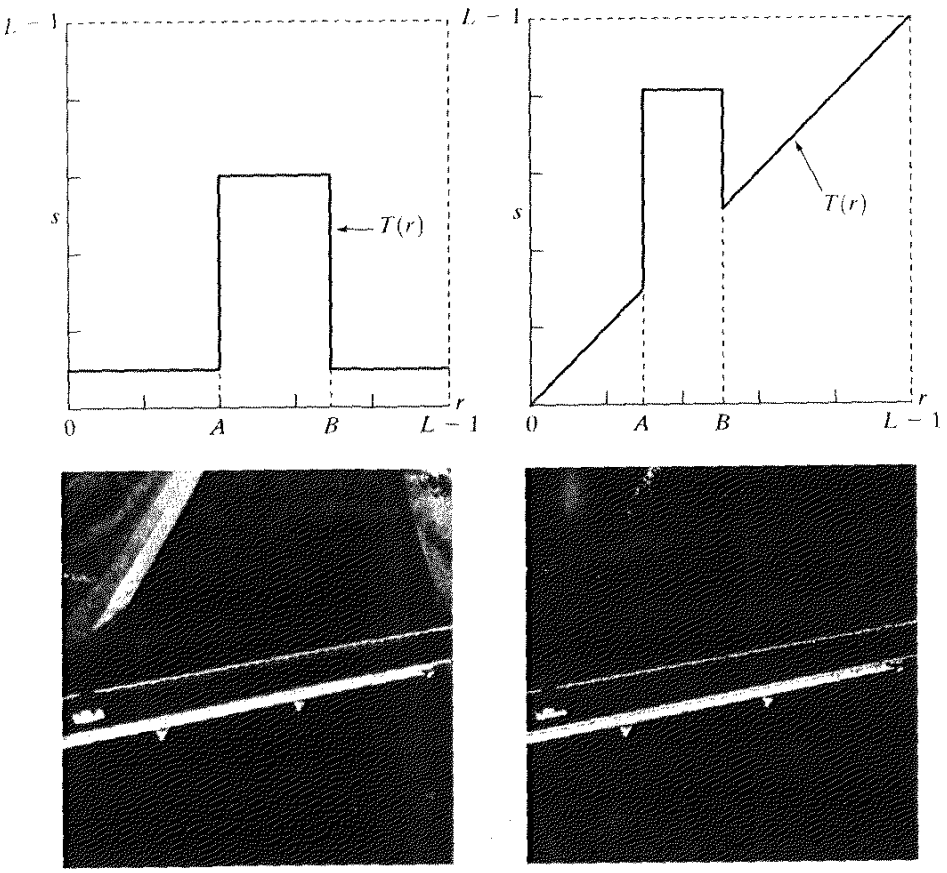

a b
c d

FIGURE 3.11
(a) This transformation highlights range $[A, B]$ of gray levels and reduces all others to a constant level. (b) This transformation highlights range $[A, B]$ but preserves all other levels. (c) An image. (d) Result of using the transformation in (a).

In terms of bit-plane extraction for an 8-bit image, it is not difficult to show that the (binary) image for bit-plane 7 can be obtained by processing the input image with a thresholding gray-level transformation function that (1) maps all levels in the image between 0 and 127 to one level (for example, 0); and (2) maps all levels between 129 and 255 to another (for example, 255). The binary image for bit-plane 7 in Fig. 3.14 was obtained in just this manner. It is left as an exercise (Problem 3.3) to obtain the gray-level transformation functions that would yield the other bit planes.

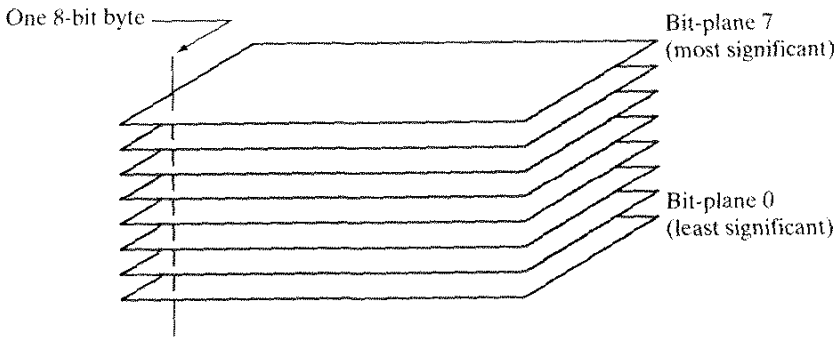

FIGURE 3.12
Bit-plane representation of an 8-bit image.

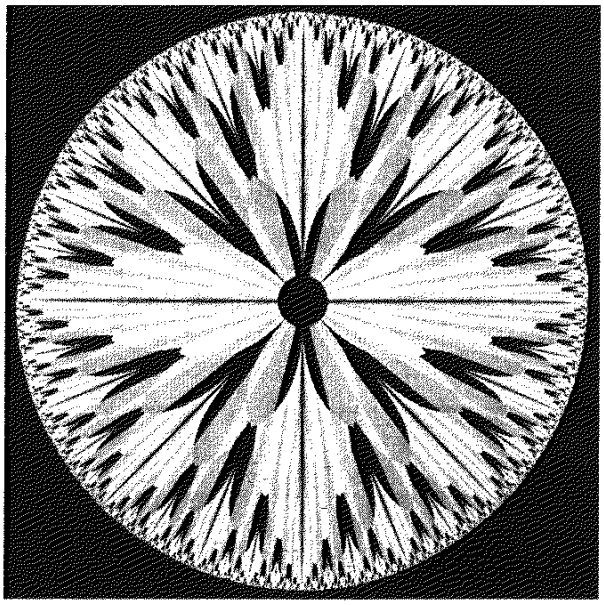

FIGURE 3.13 An 8-bit fractal image. (A fractal is an image generated from mathematical expressions). (Courtesy of Ms. Melissa D. Binde, Swarthmore College, Swarthmore, PA.)

See inside front cover
Consult the book web site for a review of basic probability theory.

3.3 Histogram Processing

The histogram of a digital image with gray levels in the range $[0, L-1]$ is a discrete function $h(r_k) = n_k$, where r_k is the kth gray level and n_k is the number of pixels in the image having gray level r_k. It is common practice to normalize a histogram by dividing each of its values by the total number of pixels in the image, denoted by n. Thus, a normalized histogram is given by $p(r_k) = n_k/n$, for $k = 0, 1, \ldots, L-1$. Loosely speaking, $p(r_k)$ gives an estimate of the probability of occurrence of gray level r_k. Note that the sum of all components of a normalized histogram is equal to 1.

Histograms are the basis for numerous spatial domain processing techniques. Histogram manipulation can be used effectively for image enhancement, as shown in this section. In addition to providing useful image statistics, we shall see in subsequent chapters that the information inherent in histograms also is quite useful in other image processing applications, such as image compression and segmentation. Histograms are simple to calculate in software and also lend themselves to economic hardware implementations, thus making them a popular tool for real-time image processing.

As an introduction to the role of histogram processing in image enhancement, consider Fig. 3.15, which is the pollen image of Fig. 3.10 shown in four basic gray-level characteristics: dark, light, low contrast, and high contrast. The right side of the figure shows the histograms corresponding to these images. The horizontal axis of each histogram plot corresponds to gray level values, r_k. The vertical axis corresponds to values of $h(r_k) = n_k$ or $p(r_k) = n_k/n$ if the values are normalized. Thus, as indicated previously, these histogram plots are simply plots of $h(r_k) = n_k$ versus r_k or $p(r_k) = n_k/n$ versus r_k.

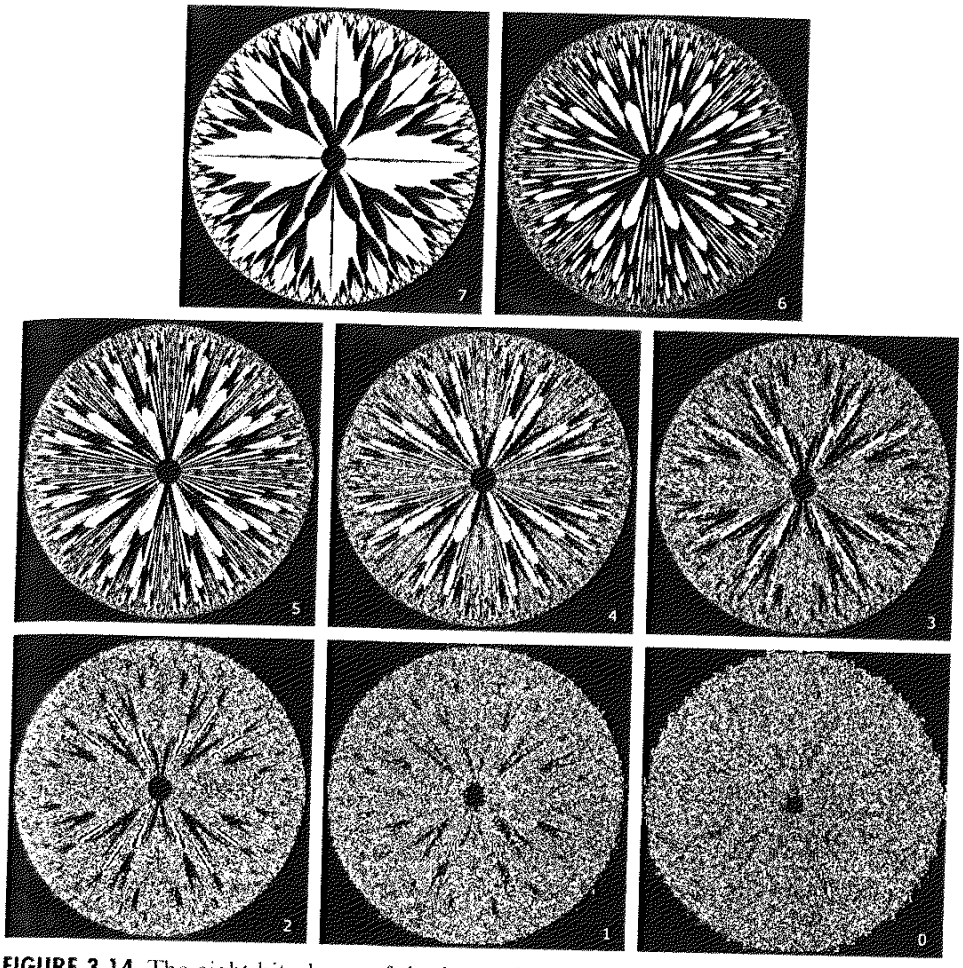

FIGURE 3.14 The eight bit planes of the image in Fig. 3.13. The number at the bottom, right of each image identifies the bit plane.

We note in the dark image that the components of the histogram are concentrated on the low (dark) side of the gray scale. Similarly, the components of the histogram of the bright image are biased toward the high side of the gray scale. An image with low contrast has a histogram that will be narrow and will be centered toward the middle of the gray scale. For a monochrome image this implies a dull, washed-out gray look. Finally, we see that the components of the histogram in the high-contrast image cover a broad range of the gray scale and, further, that the distribution of pixels is not too far from uniform, with very few vertical lines being much higher than the others. Intuitively, it is reasonable to conclude that an image whose pixels tend to occupy the entire range of possible gray levels and, in addition, tend to be distributed uniformly, will have an appearance of high contrast and will exhibit a large variety of gray tones. The net effect will be an image that shows a great deal of gray-level detail and has high dynamic range. It will be shown shortly that it is possible to develop a transformation function that can automatically achieve this effect, based only on information available in the histogram of the input image.

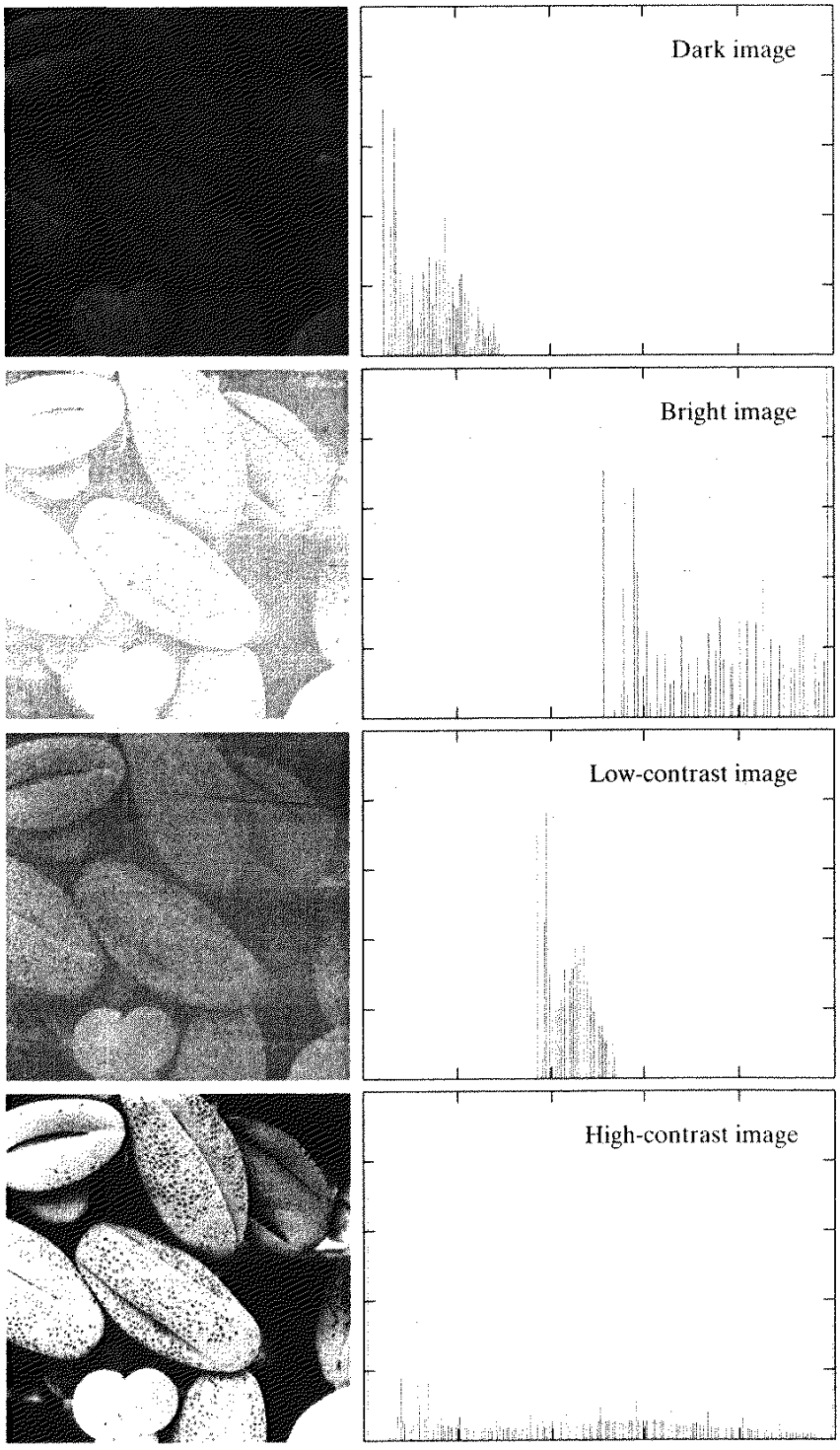

a b

FIGURE 3.15 Four basic image types: dark, light, low contrast, high contrast, and their cor responding histograms. (Original image courtesy of Dr. Roger Heady, Research Schoc of Biological Sciences, Australian National University, Canberra, Australia.)

Histogram Equalization

Consider for a moment continuous functions, and let the variable r represent the gray levels of the image to be enhanced. In the initial part of our discussion we assume that r has been normalized to the interval $[0, 1]$, with $r = 0$ representing black and $r = 1$ representing white. Later, we consider a discrete formulation and allow pixel values to be in the interval $[0, L - 1]$.

For any r satisfying the aforementioned conditions, we focus attention on transformations of the form

$$s = T(r) \qquad 0 \leq r \leq 1 \tag{3.3-1}$$

that produce a level s for every pixel value r in the original image. For reasons that will become obvious shortly, we assume that the transformation function $T(r)$ satisfies the following conditions:

(a) $T(r)$ is single-valued and monotonically increasing in the interval $0 \leq r \leq 1$; and

(b) $0 \leq T(r) \leq 1$ for $0 \leq r \leq 1$.

The requirement in (a) that $T(r)$ be single valued is needed to guarantee that the inverse transformation will exist, and the monotonicity condition preserves the increasing order from black to white in the output image. A transformation function that is not monotonically increasing could result in at least a section of the intensity range being inverted, thus producing some inverted gray levels in the output image. While this may be a desirable effect in some cases, that is not what we are after in the present discussion. Finally, condition (b) guarantees that the output gray levels will be in the same range as the input levels. Figure 3.16 gives an example of a transformation function that satisfies these two conditions. The inverse transformation from s back to r is denoted

$$r = T^{-1}(s) \qquad 0 \leq s \leq 1. \tag{3.3-2}$$

It can be shown by example (Problem 3.8) that even if $T(r)$ satisfies conditions (a) and (b), it is possible that the corresponding inverse $T^{-1}(s)$ may fail to be single valued.

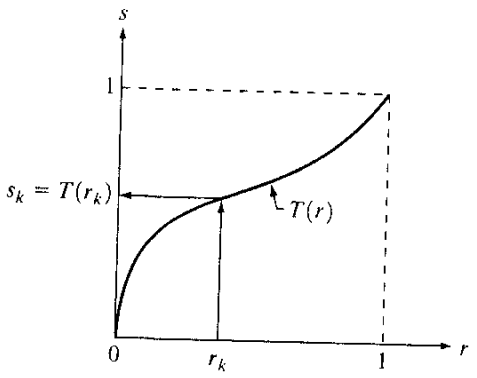

FIGURE 3.16 A gray-level transformation function that is both single valued and monotonically increasing.

The gray levels in an image may be viewed as random variables in the interval [0, 1]. One of the most fundamental descriptors of a random variable is its probability density function (PDF). Let $p_r(r)$ and $p_s(s)$ denote the probability density functions of random variables r and s, respectively, where the subscripts on p are used to denote that p_r and p_s are different functions. A basic result from an elementary probability theory is that, if $p_r(r)$ and $T(r)$ are known and $T^{-1}(s)$ satisfies condition (a), then the probability density function $p_s(s)$ of the transformed variable s can be obtained using a rather simple formula:

$$p_s(s) = p_r(r)\left|\frac{dr}{ds}\right|. \tag{3.3-3}$$

Thus, the probability density function of the transformed variable, s, is determined by the gray-level PDF of the input image and by the chosen transformation function.

A transformation function of particular importance in image processing has the form

$$s = T(r) = \int_0^r p_r(w)\,dw \tag{3.3-4}$$

where w is a dummy variable of integration. The right side of Eq. (3.3-4) is recognized as the cumulative distribution function (CDF) of random variable r. Since probability density functions are always positive, and recalling that the integral of a function is the area under the function, it follows that this transformation function is single valued and monotonically increasing, and, therefore, satisfies condition (a). Similarly, the integral of a probability density function for variables in the range [0, 1] also is in the range [0, 1], so condition (b) is satisfied as well.

Given transformation function $T(r)$, we find $p_s(s)$ by applying Eq. (3.3-3). We know from basic calculus (Leibniz's rule) that the derivative of a definite integral with respect to its upper limit is simply the integrand evaluated at that limit. In other words,

$$\begin{aligned}\frac{ds}{dr} &= \frac{dT(r)}{dr} \\ &= \frac{d}{dr}\left[\int_0^r p_r(w)\,dw\right] \\ &= p_r(r).\end{aligned} \tag{3.3-5}$$

Substituting this result for dr/ds into Eq. (3.3-3), and keeping in mind that all probability values are positive, yields

$$\begin{aligned}p_s(s) &= p_r(r)\left|\frac{dr}{ds}\right| \\ &= p_r(r)\left|\frac{1}{p_r(r)}\right| \\ &= 1 \qquad 0 \le s \le 1.\end{aligned} \tag{3.3-6}$$

Because $p_s(s)$ is a probability density function, it follows that it must be zero outside the interval [0, 1] in this case because its integral over all values of s must equal 1. We recognize the form of $p_s(s)$ given in Eq. (3.3-6) as a *uniform* probability density function. Simply stated, we have demonstrated that performing the transformation function given in Eq. (3.3-4) yields a random variable s characterized by a uniform probability density function. It is important to note from Eq. (3.3-4) that $T(r)$ depends on $p_r(r)$, but, as indicated by Eq. (3.3-6), the resulting $p_s(s)$ *always* is uniform, *independent* of the form of $p_r(r)$.

For discrete values we deal with probabilities and summations instead of probability density functions and integrals. The probability of occurrence of gray level r_k in an image is approximated by

$$p_r(r_k) = \frac{n_k}{n} \qquad k = 0, 1, 2, \ldots, L - 1 \tag{3.3-7}$$

where, as noted at the beginning of this section, n is the total number of pixels in the image, n_k is the number of pixels that have gray level r_k, and L is the total number of possible gray levels in the image. The discrete version of the transformation function given in Eq. (3.3-4) is

$$\begin{aligned} s_k = T(r_k) &= \sum_{j=0}^{k} p_r(r_j) \\ &= \sum_{j=0}^{k} \frac{n_j}{n} \qquad k = 0, 1, 2, \ldots, L - 1. \end{aligned} \tag{3.3-8}$$

Thus, a processed (output) image is obtained by mapping each pixel with level r_k in the input image into a corresponding pixel with level s_k in the output image via Eq. (3.3-8). As indicated earlier, a plot of $p_r(r_k)$ versus r_k is called a *histogram*. The transformation (mapping) given in Eq. (3.3-8) is called *histogram equalization* or *histogram linearization*. It is not difficult to show (Problem 3.9) that the transformation in Eq. (3.3-8) satisfies conditions (a) and (b) stated previously in this section.

Unlike its continuous counterpart, it cannot be proved in general that this discrete transformation will produce the discrete equivalent of a uniform probability density function, which would be a uniform histogram. However, as will be seen shortly, use of Eq. (3.3-8) does have the general tendency of spreading the histogram of the input image so that the levels of the histogram-equalized image will span a fuller range of the gray scale.

We discussed earlier in this section the many advantages of having gray-level values that cover the entire gray scale. In addition to producing gray levels that have this tendency, the method just derived has the additional advantage that it is fully "automatic." In other words, given an image, the process of histogram equalization consists simply of implementing Eq. (3.3-8), which is based on information that can be extracted directly from the given image, without the need for further parameter specifications. We note also the simplicity of the computations that would be required to implement the technique.

The inverse transformation from s back to r is denoted by

$$r_k = T^{-1}(s_k) \qquad k = 0, 1, 2, \ldots, L - 1 \tag{3.3-9}$$

It can be shown (Problem 3.9) that the inverse transformation in Eq. (3.3-9) satisfies conditions (a) and (b) stated previously in this section only if none of the levels, $r_k, k = 0, 1, 2, \ldots, L - 1$, are missing from the input image. Although the inverse transformation is not used in histogram equalization, it plays a central role in the histogram-matching scheme developed in the next section. We also discuss in that section details of how to implement histogram processing techniques.

EXAMPLE 3.3: Histogram equalization.

■ Figure 3.17(a) shows the four images from Fig. 3.15, and Fig. 3.17(b) shows the result of performing histogram equalization on each of these images. The first three results (top to bottom) show significant improvement. As expected, histogram equalization did not produce a significant visual difference in the fourth image because the histogram of this image already spans the full spectrum of the gray scale. The transformation functions used to generate the images in Fig. 3.17(b) are shown in Fig. 3.18. These functions were generated from the histograms of the original images [see Fig. 3.15(b)] using Eq. (3.3-8). Note that transformation (4) has a basic linear shape, again indicating that the gray levels in the fourth input image are nearly uniformly distributed. As was just noted, we would expect histogram equalization in this case to have negligible effect on the appearance of the image.

The histograms of the equalized images are shown in Fig. 3.17(c). It is of interest to note that, while all these histograms are different, the histogram-equalized images themselves are visually very similar. This is not unexpected because the difference between the images in the left column is simply one of contrast, not of content. In other words, since the images have the same content, the increase in contrast resulting from histogram equalization was enough to render any gray-level differences in the resulting images visually indistinguishable. Given the significant contrast differences of the images in the left column, this example illustrates the power of histogram equalization as an adaptive enhancement tool.

3.3.2 Histogram Matching (Specification)

As indicated in the preceding discussion, histogram equalization automatically determines a transformation function that seeks to produce an output image that has a uniform histogram. When automatic enhancement is desired, this is a good approach because the results from this technique are predictable and the method is simple to implement. We show in this section that there are applications in which attempting to base enhancement on a uniform histogram is not the best approach. In particular, it is useful sometimes to be able to specify the shape of the histogram that we wish the processed image to have. The method used to generate a processed image that has a specified histogram is called *histogram matching* or *histogram specification*.

Development of the method

Let us return for a moment to continuous gray levels r and z (considered continuous random variables), and let $p_r(r)$ and $p_z(z)$ denote their corresponding continuous probability density functions. In this notation, r and z denote

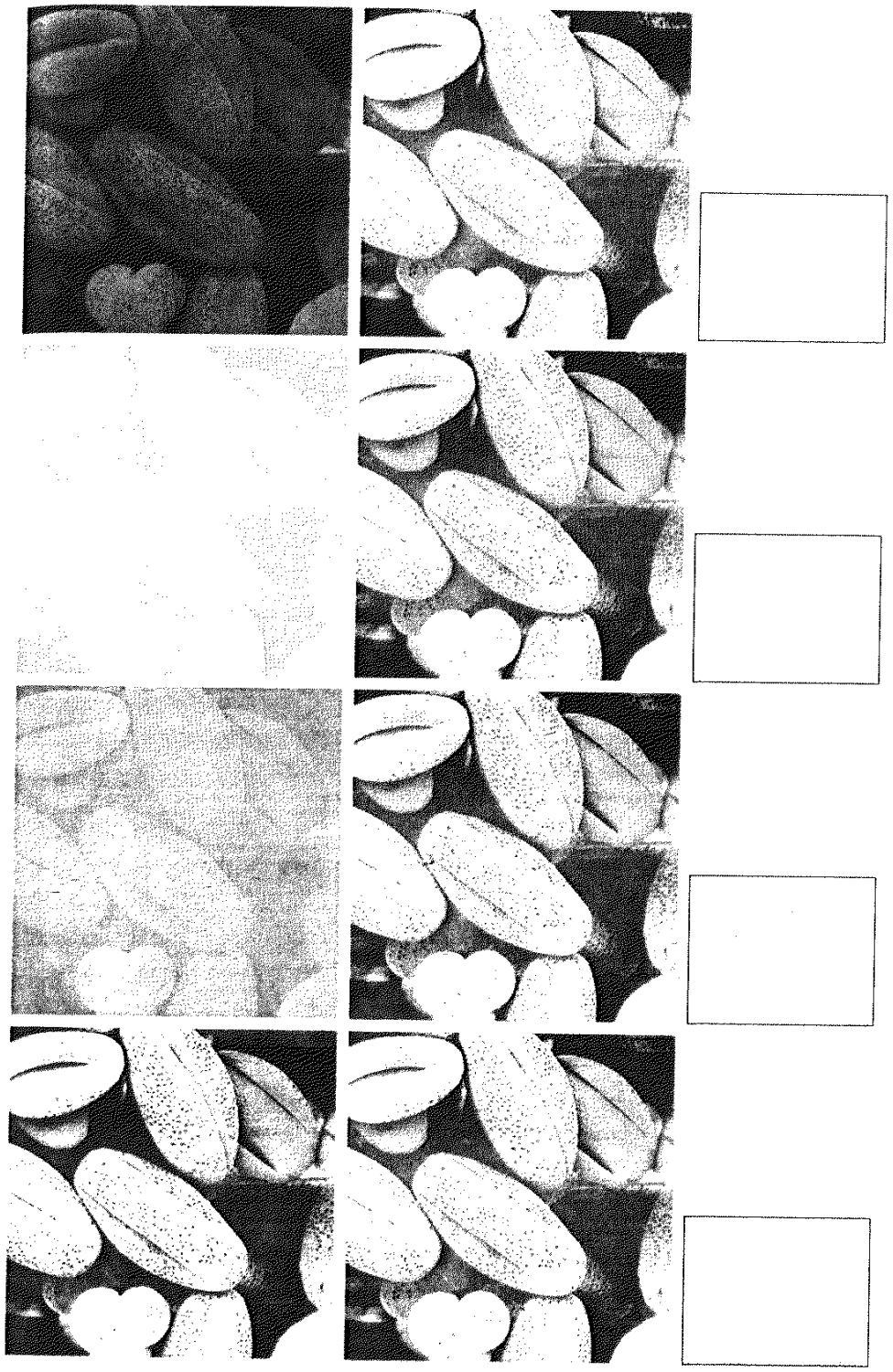

a b c

FIGURE 3.17 (a) Images from Fig. 3.15. (b) Results of histogram equalization. (c) Corresponding histograms.

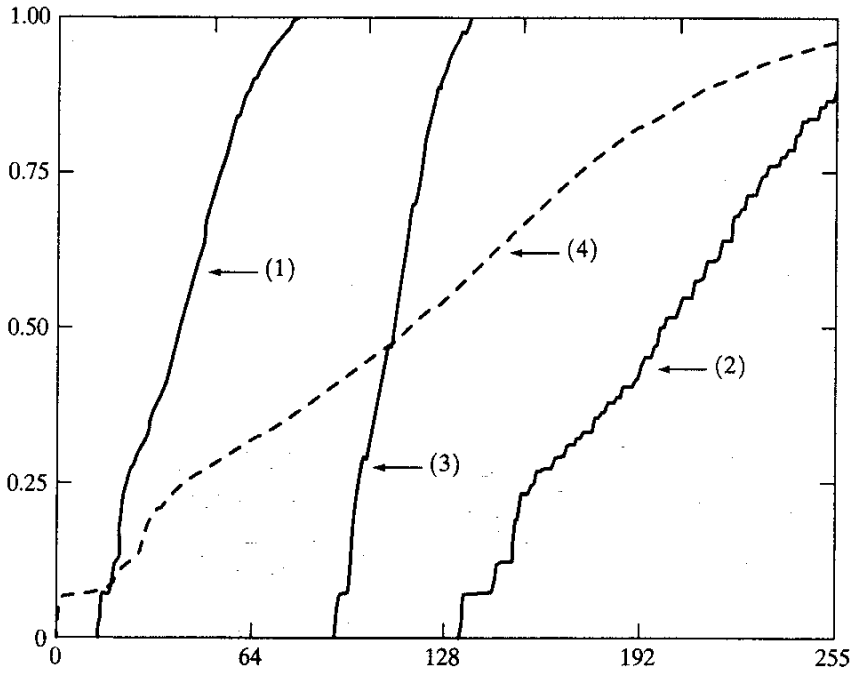

FIGURE 3.18 Transformation functions (1) through (4) were obtained from the histograms of the images in Fig.3.17(a), using Eq. (3.3-8).

the gray levels of the input and output (processed) images, respectively. We can estimate $p_r(r)$ from the given input image, while $p_z(z)$ is the *specified* probability density function that we wish the output image to have.

Let s be a random variable with the property

$$s = T(r) = \int_0^r p_r(w)\, dw \tag{3.3-10}$$

where w is a dummy variable of integration. We recognize this expression as the continuos version of histogram equalization given in Eq. (3.3-4). Suppose next that we define a random variable z with the property

$$G(z) = \int_0^z p_z(t)\, dt = s \tag{3.3-11}$$

where t is a dummy variable of integration. It then follows from these two equations that $G(z) = T(r)$ and, therefore, that z must satisfy the condition

$$z = G^{-1}(s) = G^{-1}[T(r)]. \tag{3.3-12}$$

The transformation $T(r)$ can be obtained from Eq. (3.3-10) once $p_r(r)$ has been estimated from the input image. Similarly, the transformation function $G(z)$ can be obtained using Eq. (3.3-11) because $p_z(z)$ is given.

Assuming that G^{-1} exists and that it satisfies conditions (a) and (b) in the previous section, Eqs. (3.3-10) through (3.3-12) show that an image with a specified probability density function can be obtained from an input image by using the following procedure: (1) Obtain the transformation function $T(r)$ using Eq. (3.3-10). (2) Use Eq. (3.3-11) to obtain the transformation function $G(z)$. (3) Obtain the inverse transformation function G^{-1}. (4) Obtain the output image

by applying Eq. (3.3-12) to all the pixels in the input image. The result of this procedure will be an image whose gray levels, z, have the specified probability density function $p_z(z)$.

Although the procedure just described is straightforward in principle, it is seldom possible in practice to obtain analytical expressions for $T(r)$ and for G^{-1}. Fortunately, this problem is simplified considerably in the case of discrete values. The price we pay is the same as in histogram equalization, where only an approximation to the desired histogram is achievable. In spite of this, however, some very useful results can be obtained even with crude approximations.

The discrete formulation of Eq. (3.3-10) is given by Eq. (3.3-8), which we repeat here for convenience:

$$\begin{aligned} s_k = T(r_k) &= \sum_{j=0}^{k} p_r(r_j) \\ &= \sum_{j=0}^{k} \frac{n_j}{n} \qquad k = 0, 1, 2, \ldots, L-1 \end{aligned} \tag{3.3-13}$$

where n is the total number of pixels in the image, n_j is the number of pixels with gray level r_j, and L is the number of discrete gray levels. Similarly, the discrete formulation of Eq. (3.3-11) is obtained from the given histogram $p_z(z_i), i = 0, 1, 2, \ldots, L-1$, and has the form

$$v_k = G(z_k) = \sum_{i=0}^{k} p_z(z_i) = s_k \qquad k = 0, 1, 2, \ldots, L-1. \tag{3.3-14}$$

As in the continuous case, we are seeking values of z that satisfy this equation. The variable v_k was added here for clarity in the discussion that follows. Finally, the discrete version of Eq. (3.3-12) is given by

$$z_k = G^{-1}[T(r_k)] \qquad k = 0, 1, 2, \ldots, L-1 \tag{3.3-15}$$

or, from Eq. (3.3-13),

$$z_k = G^{-1}(s_k) \qquad k = 0, 1, 2, \ldots, L-1. \tag{3.3-16}$$

Equations (3.3-13) through (3.3-16) are the foundation for implementing histogram matching for digital images. Equation (3.3-13) is a mapping from the levels in the original image into corresponding levels s_k based on the histogram of the original image, which we compute from the pixels in the image. Equation (3.3-14) computes a transformation function G from the given histogram $p_z(z)$. Finally, Eq. (3.3-15) or its equivalent, Eq. (3.3-16), gives us (an approximation of) the desired levels of the image with that histogram. The first two equations can be implemented easily because all the quantities are known. Implementation of Eq. (3.3-16) is straightforward, but requires additional explanation.

Implementation

We start by noting the following: (1) Each set of gray levels $\{r_j\}$, $\{s_j\}$, and $\{z_j\}$, $j = 0, 1, 2, \ldots, L-1$, is a one-dimensional array of dimension $L \times 1$. (2) All mappings from r to s and from s to z are simple table lookups between a given

pixel value and these arrays. (3) Each of the elements of these arrays, for example, s_k, contains two important pieces of information: The subscript k denotes the location of the element in the array, and s denotes the value at that location. (4) We need to be concerned only with integer pixel values. For example, in the case of an 8-bit image, $L = 256$ and the elements of each of the arrays just mentioned are integers between 0 and 255. This implies that we now work with gray level values in the interval $[0, L - 1]$ instead of the normalized interval $[0, 1]$ that we used before to simplify the development of histogram processing techniques.

In order to see how histogram matching actually can be implemented, consider Fig. 3.19(a), ignoring for a moment the connection shown between this figure and Fig. 3.19(c). Figure 3.19(a) shows a hypothetical discrete transformation function $s = T(r)$ obtained from a given image. The first gray level in the image, r_1, maps to s_1; the second gray level, r_2, maps to s_2; the kth level r_k maps to s_k; and so on (the important point here is the *ordered* correspondence between these values). Each value s_j in the array is precomputed using Eq. (3.3-13), so the process of mapping simply uses the actual value of a pixel as an index in an array to determine the corresponding value of s. This process is particularly easy because we are dealing with integers. For example, the s mapping for an 8-bit pixel with value 127 would be found in the 128th position in array $\{s_j\}$ (recall that we start at 0) out of the possible 256 positions. If we stopped here and mapped the value of each pixel of an input image by the

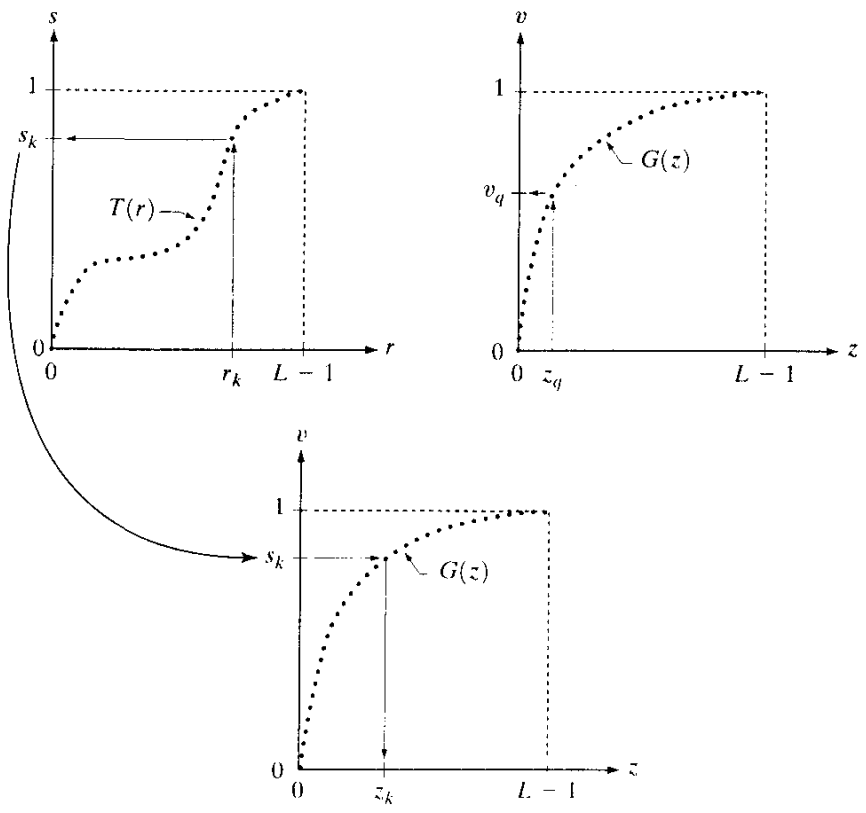

a b
c

FIGURE 3.19
(a) Graphical interpretation of mapping from r_k to s_k via $T(r)$. (b) Mapping of z_q to its corresponding value v_q via $G(z)$. (c) Inverse mapping from s_k to its corresponding value of z_k.

method just described, the output would be a histogram-equalized image, according to Eq. (3.3-8).

In order to implement histogram matching we have to go one step further. Figure 3.19(b) is a hypothetical transformation function G obtained from a given histogram $p_z(z)$ by using Eq. (3.3-14). For any z_q, this transformation function yields a corresponding value v_q. This mapping is shown by the arrows in Fig. 3.19(b). Conversely, given any value v_q, we would find the corresponding value z_q from G^{-1}. In terms of the figure, all this means graphically is that we would reverse the direction of the arrows to map v_q into its corresponding z_q. However, we know from the definition in Eq. (3.3-14) that $v = s$ for corresponding subscripts, so we can use exactly this process to find the z_k corresponding to any value s_k that we computed previously from the equation $s_k = T(r_k)$. This idea is shown in Fig. 3.19(c).

Since we really do not have the z's (recall that finding these values is precisely the objective of histogram matching), we must resort to some sort of iterative scheme to find z from s. The fact that we are dealing with integers makes this a particularly simple process. Basically, because $v_k = s_k$, we have from Eq. (3.3-14) that the z's for which we are looking must satisfy the equation $G(z_k) = s_k$, or $(G(z_k) - s_k) = 0$. Thus, all we have to do to find the value of z_k corresponding to s_k is to iterate on values of z such that this equation is satisfied for $k = 0, 1, 2, \ldots, L - 1$. This is the same thing as Eq. (3.3-16), except that we do not have to find the inverse of G because we are going to iterate on z. Since we are dealing with integers, the closest we can get to satisfying the equation $(G(z_k) - s_k) = 0$ is to let $z_k = \hat{z}$ for each value of k, where $\hat{z}$ is the *smallest* integer in the interval $[0, L - 1]$ such that

$$(G(\hat{z}) - s_k) \geq 0 \qquad k = 0, 1, 2, \ldots, L - 1. \tag{3.3-17}$$

Given a value s_k, all this means conceptually in terms of Fig. 3.19(c) is that we would start with $\hat{z} = 0$ and increase it in integer steps until Eq. (3.3-17) is satisfied, at which point we let $z_k = \hat{z}$. Repeating this process for all values of k would yield all the required mappings from s to z, which constitutes the implementation of Eq. (3.3-16). In practice, we would not have to start with $\hat{z} = 0$ each time because the values of s_k are known to increase monotonically. Thus, for $k = k + 1$, we would start with $\hat{z} = z_k$ and increment in integer values from there.

The procedure we have just developed for histogram matching may be summarized as follows:

1. Obtain the histogram of the given image.
2. Use Eq. (3.3-13) to precompute a mapped level s_k for each level r_k.
3. Obtain the transformation function G from the given $p_z(z)$ using Eq. (3.3-14).
4. Precompute z_k for each value of s_k using the iterative scheme defined in connection with Eq. (3.3-17).
5. For each pixel in the original image, if the value of that pixel is r_k, map this value to its corresponding level s_k; then map level s_k into the final level z_k. Use the precomputed values from Steps (2) and (4) for these mappings.

Note that Step (5) implements two mappings for each pixel in the image being processed. The first mapping is nothing more than histogram equalization. If the histogram-equalized image is not required, it obviously would be beneficial to combine both transformations into one in order to save an intermediate step.

Finally, we note that, even in the discrete case, we need to be concerned about G^{-1} satisfying conditions (a) and (b) of the previous section. It is not difficult to show (Problem 3.9) that the only way to guarantee that G^{-1} be single valued and monotonic is to require that G be strictly monotonic (i.e., always increasing), which means simply that none of the values of the specified histogram $p_z(z_i)$ in Eq. (3.3-14) can be zero.

EXAMPLE 3.4: Comparison between histogram equalization and histogram matching.

■ Figure 3.20(a) shows an image of the Mars moon, Phobos, taken by NASA's *Mars Global Surveyor*. Figure 3.20(b) shows the histogram of Fig. 3.20(a). The image is dominated by large, dark areas, resulting in a histogram characterized by a large concentration of pixels in the dark end of the gray scale. At first glance, one might conclude that histogram equalization would be a good approach to enhance this image, so that details in the dark areas become more visible. It is demonstrated in the following discussion that this is not so.

Figure 3.21(a) shows the histogram equalization transformation [Eq. (3.3-8) or (3.3-13)] obtained from the histogram shown in Fig. 3.20(b). The most relevant characteristic of this transformation function is how fast it rises from gray level 0 to a level near 190. This is caused by the large concentration of pixels in the input histogram having levels very near 0. When this transformation is applied to the levels of the input image to obtain a histogram-equalized result, the net effect is to map a very narrow interval of dark pixels into the upper end of the gray scale of the output image. Because numerous pixels in the input image have levels precisely in this interval, we would expect the result to be an

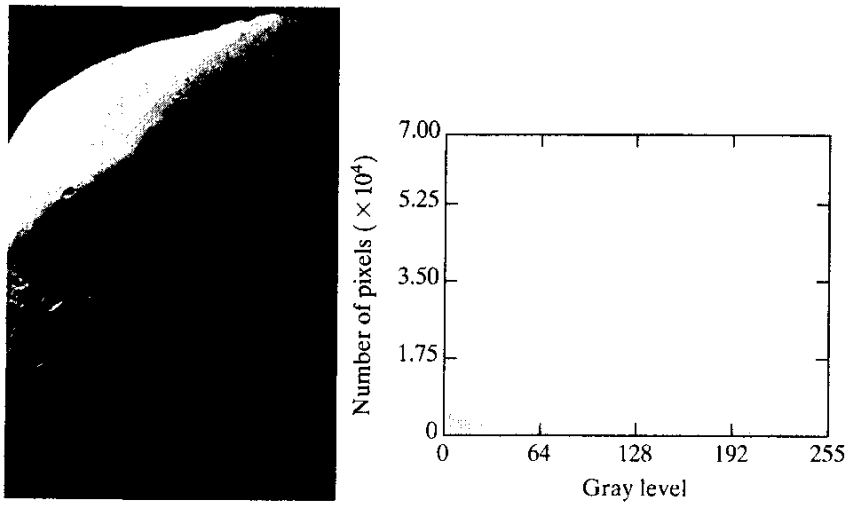

a b

FIGURE 3.20 (a) Image of the Mars moon Phobos taken by NASA's *Mars Global Surveyor*. (b) Histogram. (Original image courtesy of NASA.)

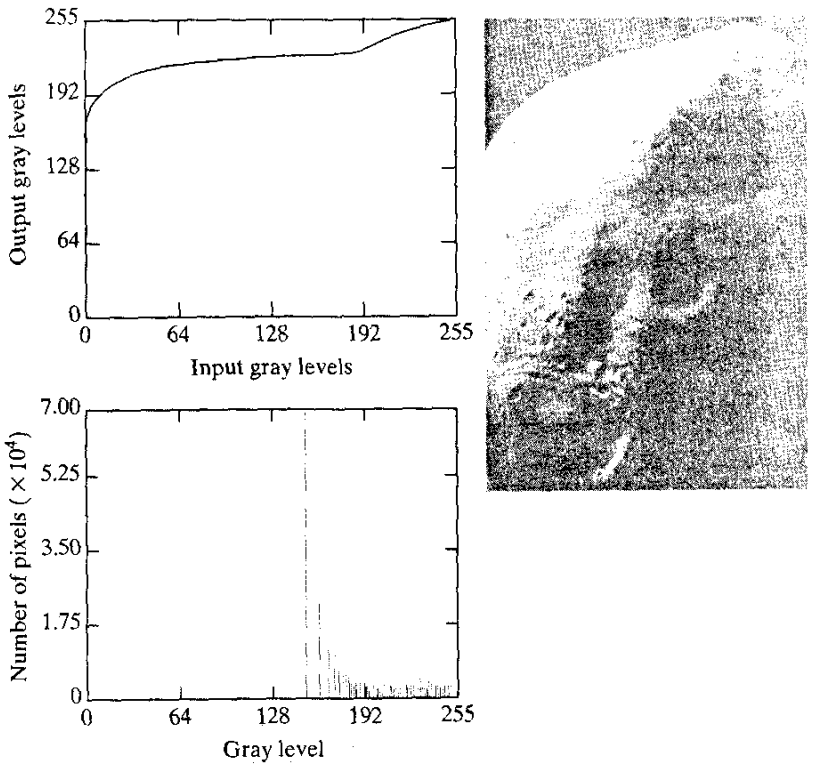

a b
c

FIGURE 3.21
(a) Transformation function for histogram equalization. (b) Histogram-equalized image (note the washed-out appearance). (c) Histogram of (b).

image with a light, washed-out appearance. As shown in Fig. 3.21(b), this is indeed the case. The histogram of this image is shown in Fig. 3.21(c). Note how all the gray levels are biased toward the upper one-half of the gray scale.

Since the problem with the transformation function in Fig. 3.21(a) was caused by a large concentration of pixels in the original image with levels near 0, a reasonable approach is to modify the histogram of that image so that it does not have this property. Figure 3.22(a) shows a *manually specified* function that preserves the general shape of the original histogram, but has a smoother transition of levels in the dark region of the gray scale. Sampling this function into 256 equally spaced discrete values produced the desired specified histogram. The transformation function $G(z)$ obtained from this histogram using Eq. (3.3-14) is labeled transformation (1) in Fig. 3.22(b). Similarly, the inverse transformation $G^{-1}(s)$ from Eq. (3.3-16) [obtained using the iterative technique discussed in connection with Eq. (3.3-17)] is labeled transformation (2) in Fig. 3.22(b). The enhanced image in Fig. 3.22(c) was obtained by applying transformation (2) to the pixels of the histogram-equalized image in Fig. 3.21(b). The improvement of the histogram-specified image over the result obtained by histogram equalization is evident by comparing these two images. It is of interest to note that a rather modest change in the original histogram was all that was required to obtain a significant improvement in enhancement. The histogram of Fig. 3.22(c) is shown in Fig. 3.22(d). The most distinguishing feature of this histogram is how its low end has shifted right toward the lighter region of the gray scale, as desired. ■

a c
b
d

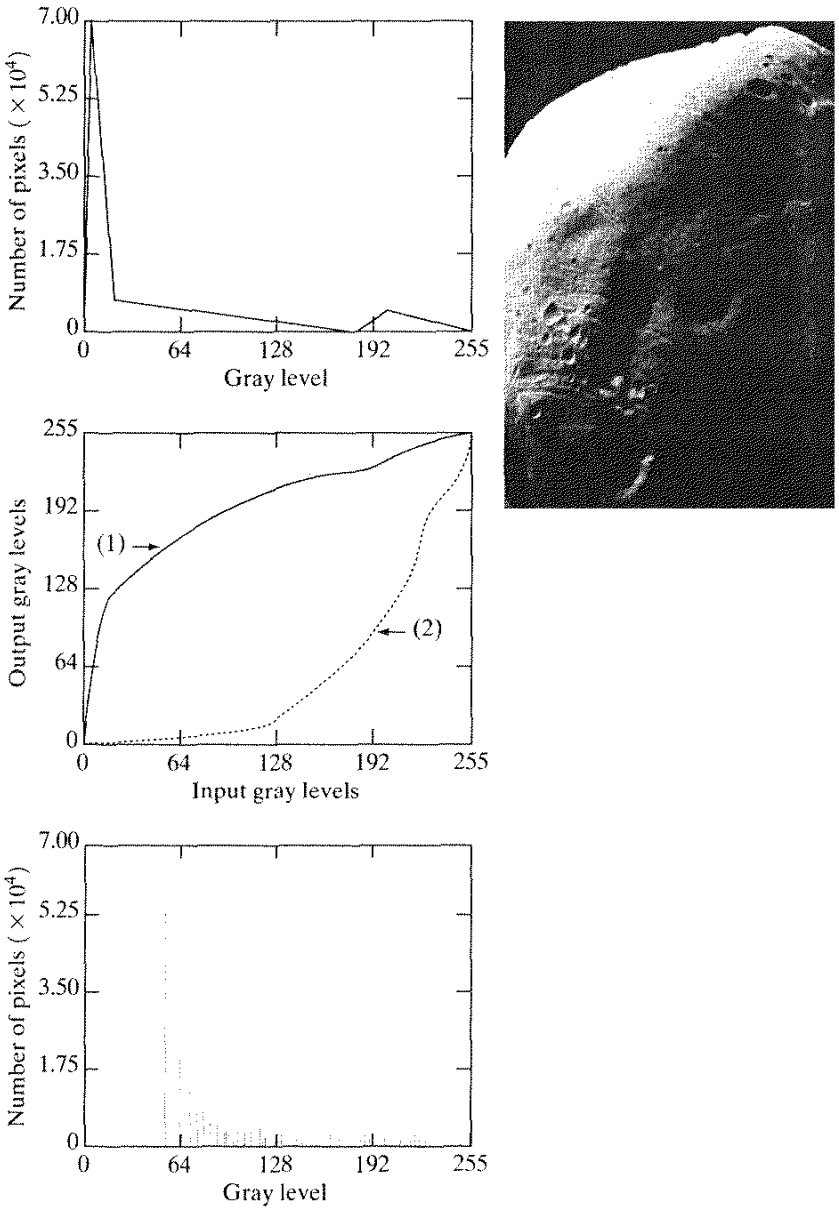

FIGURE 3.22
(a) Specified histogram.
(b) Curve (1) is from Eq. (3.3-14), using the histogram in (a); curve (2) was obtained using the iterative procedure in Eq. (3.3-17).
(c) Enhanced image using mappings from curve (2).
(d) Histogram of (c).

Although it probably is obvious by now, we emphasize before leaving this section that histogram specification is, for the most part, a trial-and-error process. One can use guidelines learned from the problem at hand, just as we did in the preceding example. At times, there may be cases in which it is possible to formulate what an "average" histogram should look like and use that as the specified histogram. In cases such as these, histogram specification becomes a straightforward process. In general, however, there are no rules for specifying histograms, and one must resort to analysis on a case-by-case basis for any given enhancement task.

Local Enhancement

The histogram processing methods discussed in the previous two sections are *global*, in the sense that pixels are modified by a transformation function based on the gray-level content of an entire image. Although this global approach is suitable for overall enhancement, there are cases in which it is necessary to enhance details over small areas in an image. The number of pixels in these areas may have negligible influence on the computation of a global transformation whose shape does not necessarily guarantee the desired local enhancement. The solution is to devise transformation functions based on the gray-level distribution—or other properties—in the neighborhood of every pixel in the image. Although processing methods based on neighborhoods are the topic of Section 3.5, we discuss local histogram processing here for the sake of clarity and continuity. The reader will have no difficulty in following the discussion.

The histogram processing techniques previously described are easily adaptable to local enhancement. The procedure is to define a square or rectangular neighborhood and move the center of this area from pixel to pixel. At each location, the histogram of the points in the neighborhood is computed and either a histogram equalization or histogram specification transformation function is obtained. This function is finally used to map the gray level of the pixel centered in the neighborhood. The center of the neighborhood region is then moved to an adjacent pixel location and the procedure is repeated. Since only one new row or column of the neighborhood changes during a pixel-to-pixel translation of the region, updating the histogram obtained in the previous location with the new data introduced at each motion step is possible (Problem 3.11). This approach has obvious advantages over repeatedly computing the histogram over all pixels in the neighborhood region each time the region is moved one pixel location. Another approach used some times to reduce computation is to utilize nonoverlapping regions, but this method usually produces an undesirable checkerboard effect.

EXAMPLE 3.5: Enhancement using local histograms.

Figure 3.23(a) shows an image that has been slightly blurred to reduce its noise content (see Section 3.6.1 regarding blurring). Figure 3.23(b) shows the result of global histogram equalization. As is often the case when this technique is applied to smooth, noisy areas, Fig. 3.23(b) shows considerable enhancement of the noise, with a slight increase in contrast. Note that no new structural details were brought out by this method. However, local histogram equalization using a 7×7 neighborhood revealed the presence of small squares inside the larger dark squares. The small squares were too close in gray level to the larger ones, and their sizes were too small to influence global histogram equalization significantly. Note also the finer noise texture in Fig. 3.23(c), a result of local processing using relatively small neighborhoods.

Use of Histogram Statistics for Image Enhancement

Instead of using the image histogram directly for enhancement, we can use instead some statistical parameters obtainable directly from the histogram. Let r denote a discrete random variable representing discrete gray-levels in the range

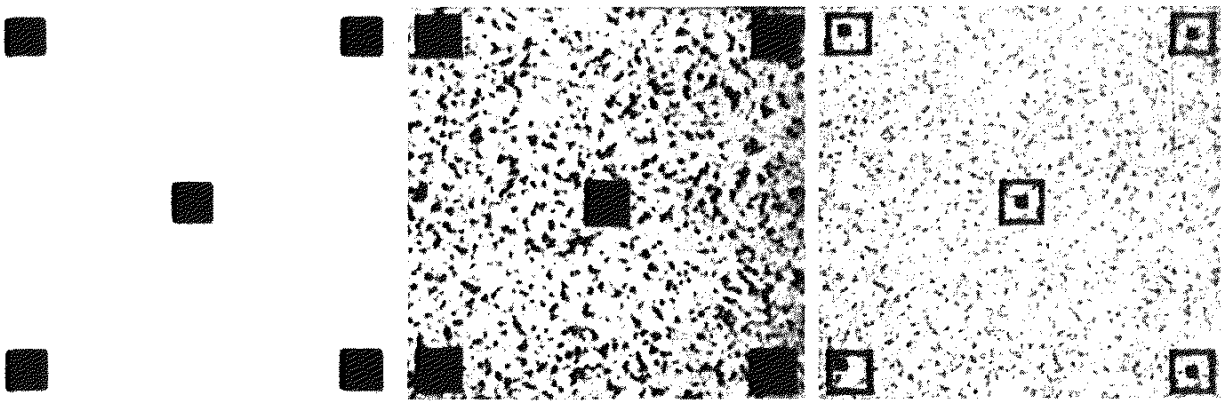

a b c

FIGURE 3.23 (a) Original image. (b) Result of global histogram equalization. (c) Result of local histogram equalization using a 7 × 7 neighborhood about each pixel.

$[0, L-1]$, and let $p(r_i)$ denote the normalized histogram component corresponding to the ith value of r. As indicated previously in this section, we may view $p(r_i)$ as an estimate of the probability of occurrence of gray level r_i. The nth moment of r about its mean is defined as

$$\mu_n(r) = \sum_{i=0}^{L-1} (r_i - m)^n p(r_i) \tag{3.3-18}$$

where m is the mean value of r (its average gray level):

$$m = \sum_{i=0}^{L-1} r_i p(r_i). \tag{3.3-19}$$

It follows from Eqs. (3.3-18) and (3.3-19) that $\mu_0 = 1$ and $\mu_1 = 0$. The second moment is given by

$$\mu_2(r) = \sum_{i=0}^{L-1} (r_i - m)^2 p(r_i). \tag{3.3-20}$$

We recognize this expression as the variance of r, which is denoted conventionally by $\sigma^2(r)$. The standard deviation is defined simply as the square root of the variance. We will revisit moments in Chapter 11 in connection with image description. In terms of enhancement, however, we are interested primarily in the mean, which is a measure of average gray level in an image, and the variance (or standard deviation), which is a measure of average contrast.

We consider two uses of the mean and variance for enhancement purposes. The *global* mean and variance are measured over an entire image and are useful primarily for gross adjustments of overall intensity and contrast. A much more powerful use of these two measures is in local enhancement, where the *local* mean and variance are used as the basis for making changes that depend on image characteristics in a predefined region about each pixel in the image.

Let (x, y) be the coordinates of a pixel in an image, and let S_{xy} denote a neighborhood (subimage) of specified size, centered at (x, y). From Eq. (3.3-19) the mean value $m_{S_{xy}}$ of the pixels in S_{xy} can be computed using the expression

$$m_{S_{xy}} = \sum_{(s,t)\in S_{xy}} r_{s,t} p(r_{s,t}) \tag{3.3-21}$$

where $r_{s,t}$ is the gray level at coordinates (s, t) in the neighborhood, and $p(r_{s,t})$ is the neighborhood normalized histogram component corresponding to that value of gray level. Similarly, from Eq. (3.3-20), the gray-level variance of the pixels in region S_{xy} is given by

$$\sigma^2_{S_{xy}} = \sum_{(s,t)\in S_{xy}} [r_{s,t} - m_{S_{xy}}]^2 p(r_{s,t}). \tag{3.3-22}$$

The local mean is a measure of average gray level in neighborhood S_{xy}, and the variance (or standard deviation) is a measure of contrast in that neighborhood.

An important aspect of image processing using the local mean and variance is the flexibility they afford in developing simple, yet powerful enhancement techniques based on statistical measures that have a close, predictable correspondence with image appearance. We illustrate these characteristics by means of an example.

EXAMPLE 3.6: Enhancement based on local statistics.

Figure 3.24 shows an SEM (scanning electron microscope) image of a tungsten filament wrapped around a support. The filament in the center of the image and its support are quite clear and easy to study. There is another filament structure on the right side of the image, but it is much darker and its size and other features are not as easily discernable. Local enhancement by contrast manipulation is an ideal approach to try on problems such as this, where part of the image is acceptable, but other parts may contain hidden features of interest.

In this particular case, the problem is to enhance dark areas while leaving the light area as unchanged as possible since it does note require enhancement. We can use the concepts presented in this section to formulate an enhancement method that can tell the difference between dark and light and, at the same time, is capable of enhancing only the dark areas. A measure of whether an area is relatively light or dark at a point (x, y) is to compare the local average gray level $m_{S_{xy}}$ to the average image gray level, called the global mean and denoted M_G. This latter quantity is obtained by letting S encompass the entire image. Thus, we have the first element of our enhancement scheme: We will consider the pixel at a point (x, y) as a candidate for processing if $m_{S_{xy}} \leq k_0 M_G$, where k_0 is a positive constant with value less than 1.0. Since we are interested in enhancing areas that have low contrast, we also need a measure to determine whether the contrast of an area makes it a candidate for enhancement. Thus, we will consider the pixel at a point (x, y) as a candidate for enhancement if $\sigma_{S_{xy}} \leq k_2 D_G$, where D_G is the global standard deviation and k_2 is a positive constant. The value of this constant will be greater than 1.0 if we are interested in enhancing light areas and less than 1.0 for dark areas. Finally, we need to restrict

the lowest values of contrast we are willing to accept, otherwise the procedure would attempt to enhance even constant areas, whose standard deviation is zero. Thus, we also set a lower limit on the local standard deviation by requiring that $k_1 D_G \leq \sigma_{S_{xy}}$, with $k_1 < k_2$. A pixel at (x, y) that meets all the conditions for local enhancement is processed simply by multiplying it by a specified constant, E, to increase (or decrease) the value of its gray level relative to the rest of the image. The values of pixels that do not meet the enhancement conditions are left unchanged.

A summary of the enhancement method is as follows. Let $f(x, y)$ represent the value of an image pixel at any image coordinates (x, y), and let $g(x, y)$ represent the corresponding enhanced pixel at those coordinates. Then

$$g(x, y) = \begin{cases} E \cdot f(x, y) & \text{if } m_{S_{xy}} \leq k_0 M_G \quad \text{AND} \quad k_1 D_G \leq \sigma_{S_{xy}} \leq k_2 D_G \\ f(x, y) & \text{otherwise} \end{cases}$$

where, as indicated previously, E, k_0, k_1, and k_2 are specified parameters; M_G is the global mean of the input image; and D_G is its global standard deviation.

Normally, making a successful selection of parameters requires a bit of experimentation to gain familiarity with a given image or class of images. In this case, the following values were selected: $E = 4.0$, $k_0 = 0.4$, $k_1 = 0.02$, and $k_2 = 0.4$. The relatively low value of 4.0 for E was chosen so that, when it was multiplied by the levels in the areas being enhanced (which are dark), the result would still tend toward the dark end of the scale, and thus preserve the general visual balance of the image. The value of k_0 was chosen as somewhat less than half the global mean since it is obvious by looking at the image that the areas that require enhancement definitely are dark enough to be below half the global mean. A similar analysis led to the choice of values for k_1 and k_2. Choosing these constants is not a difficult task in general, but their choice

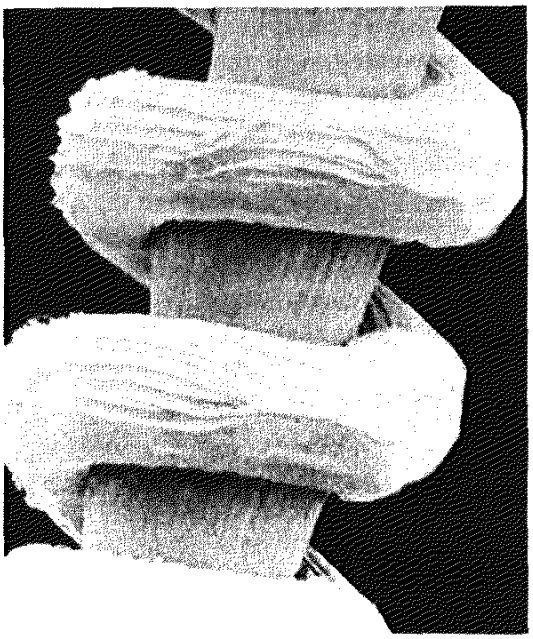

FIGURE 3.24 SEM image of a tungsten filament and support, magnified approximately 130×. (Original image courtesy of Mr. Michael Shaffer, Department of Geological Sciences, University of Oregon, Eugene).

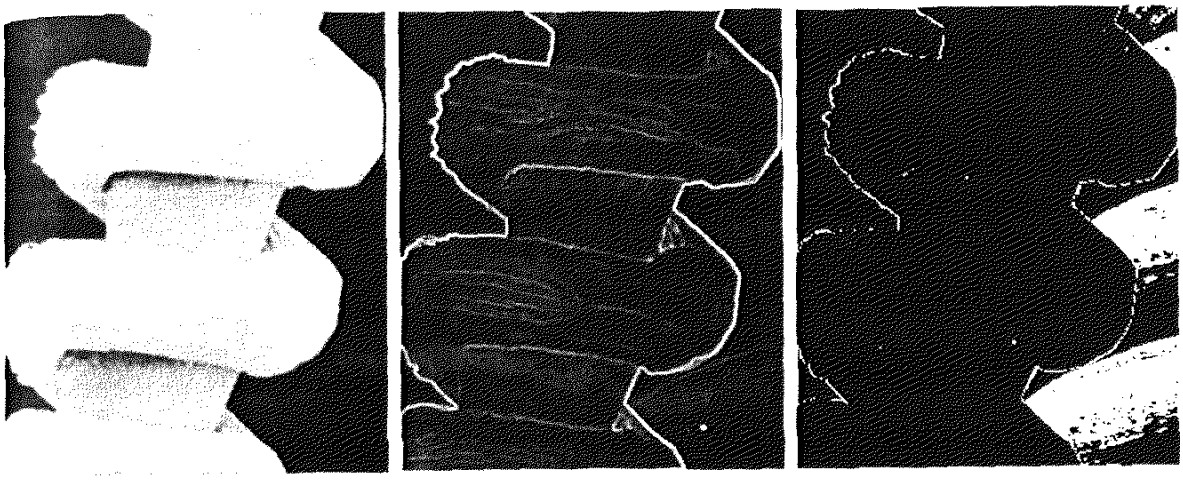

a b c

FIGURE 3.25 (a) Image formed from all local means obtained from Fig. 3.24 using Eq. (3.3-21). (b) Image formed from all local standard deviations obtained from Fig. 3.24 using Eq. (3.3-22). (c) Image formed from all multiplication constants used to produce the enhanced image shown in Fig. 3.26.

definitely must be guided by a logical analysis of the enhancement problem at hand. Finally, the choice of size for the local area should be as small as possible in order to preserve detail and keep the computational burden as low as possible. We chose a small (3×3) local region.

Figure 3.25(a) shows the values of $m_{S_{xy}}$ for all values of (x, y). Since the value of $m_{S_{xy}}$ for each (x, y) is the average of the neighboring pixels in a 3×3 area centered at (x, y), we expect the result to be similar to the original image, but

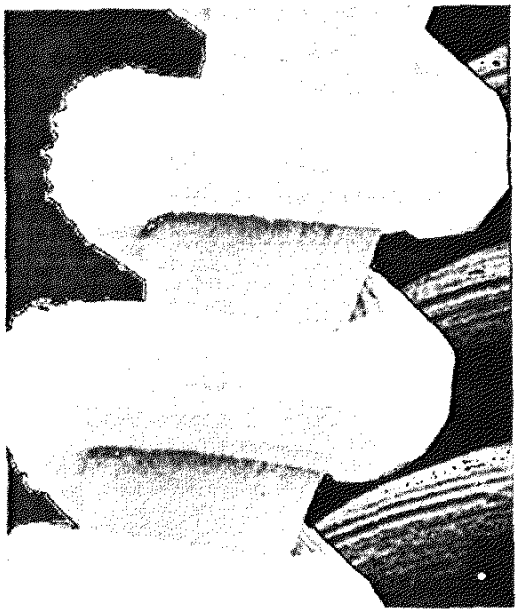

FIGURE 3.26 Enhanced SEM image. Compare with Fig. 3.24. Note in particular the enhanced area on the right side of the image.

slightly blurred. This indeed is the case in Fig. 3.25(a). Figure 3.25(b) shows in image formed using all the values of $\sigma_{S_{xy}}$. Similarly, we can construct an image out the values that multiply $f(x, y)$ at each coordinate pair (x, y) to form $g(x, y)$. Since the values are either 1 or E, the image is binary, as shown in Fig. 3.25(c). The dark areas correspond to 1 and the light areas to E. Thus, any light point in Fig. 3.25(c) signifies a coordinate pair (x, y) at which the enhancement procedure multiplied $f(x, y)$ by E to produce an enhanced pixel. The dark points represent coordinates at which the procedure did not to modify the pixel values.

The enhanced image obtained with the method just described is shown in Fig. 3.26. In comparing this image with the original in Fig. 3.24, we note the obvious detail that has been brought out on the right side of the enhanced image. It is worthwhile to point out that the unenhanced portions of the image (the light areas) were left intact for the most part. We do note the appearance of some small bright dots in the shadow areas where the coil meets the support stem, and around some of the borders between the filament and the background. These are undesirable artifacts created by the enhancement technique. In other words, the points appearing as light dots met the criteria for enhancement and their values were amplified by factor E. Introduction of artifacts is a definite drawback of a method such as the one just described because of the nonlinear way in which they process an image. The key point here, however, is that the image was enhanced in a most satisfactory way as far as bringing out the desired detail. ■

It is not difficult to imagine the numerous ways in which the example just given could be adapted or extended to other situations in which local enhancement is applicable.

3.4 Enhancement Using Arithmetic/Logic Operations

Arithmetic/logic operations involving images are performed on a pixel-by-pixel basis between two or more images (this excludes the logic operation NOT, which is performed on a single image). As an example, subtraction of two images results in a new image whose pixel at coordinates (x, y) is the difference between the pixels in that same location in the two images being subtracted. Depending on the hardware and/or software being used, the actual mechanics of implementing arithmetic/logic operations can be done sequentially, one pixel at a time, or in parallel, where all operations are performed simultaneously.

Logic operations similarly operate on a pixel-by-pixel basis[†]. We need only be concerned with the ability to implement the AND, OR, and NOT logic operators because these three operators are *functionally complete*. In other words, any other logic operator can be implemented by using only these three basic functions. When dealing with logic operations on gray-scale images, pixel values are processed as strings of binary numbers. For example, performing the NOT operation on a black, 8-bit pixel (a string of eight 0's) produces a white pixel

[†] Recall that, for two binary variables a and b: aANDb yields 1 only when both a and b are 1; otherwise the result is 0. Similarly, aORb is 0 when both variables are 0; otherwise the result is 1. Finally, if a is 1, NOT (a) is 0, and vice versa.

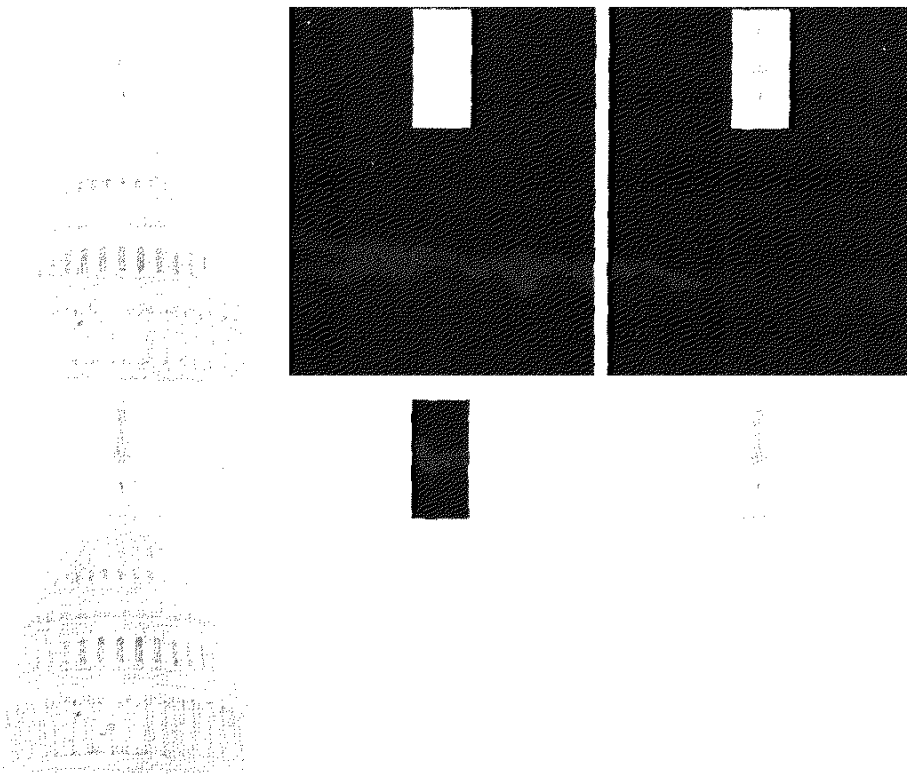

a b c
d e f

FIGURE 3.27
(a) Original image. (b) AND image mask. (c) Result of the AND operation on images (a) and (b). (d) Original image. (e) OR image mask. (f) Result of operation OR on images (d) and (e).

(a string of eight 1's). Intermediate values are processed the same way, changing all 1's to 0's and vice versa. Thus, the NOT logic operator performs the same function as the negative transformation of Eq. (3.2-1). The AND and OR operations are used for *masking*; that is, for selecting subimages in an image, as illustrated in Fig. 3.27. In the AND and OR image masks, light represents a binary 1 and dark represents a binary 0. Masking sometimes is referred to as *region of interest* (ROI) processing. In terms of enhancement, masking is used primarily to isolate an area for processing. This is done to highlight that area and differentiate it from the rest of the image. Logic operations also are used frequently in conjunction with morphological operations, as discussed in Chapter 9.

Of the four arithmetic operations, subtraction and addition (in that order) are the most useful for image enhancement. We consider division of two images simply as multiplication of one image by the reciprocal of the other. Aside from the obvious operation of multiplying an image by a constant to increase its average gray level, image multiplication finds use in enhancement primarily as a masking operation that is more general than the logical masks discussed in the previous paragraph. In other words, multiplication of one image by another can be used to implement gray-level, rather than binary, masks. We give an example in Section 3.8 of how such a masking operation can be a useful tool. In the remainder of this section, we develop and illustrate methods based on subtraction and addition for image enhancement. Other uses of image multiplication are discussed in Chapter 5, in the context of image restoration.

3.4.1 Image Subtraction

The difference between two images $f(x, y)$ and $h(x, y)$, expressed as

$$g(x, y) = f(x, y) - h(x, y), \tag{3.4-1}$$

is obtained by computing the difference between all pairs of corresponding pixels from f and h. The key usefulness of subtraction is the enhancement of *differences* between images. We illustrate this concept by returning briefly to the discussion in Section 3.2.4, where we showed that the higher-order bit planes of an image carry a significant amount of visually relevant detail, while the lower planes contribute more to fine (often imperceptible) detail. Figure 3.28(a) shows the fractal image used earlier to illustrate the concept of bit planes. Figure 3.28(b) shows the result of discarding (setting to zero) the four least significant bit planes of the original image. The images are nearly identical visually, with the exception of a very slight drop in overall contrast due to less variability of the gray-level values in the image of Fig. 3.28(b). The pixel-by-pixel difference between these two images is shown in Fig. 3.28(c). The differences in pixel values are so small that the difference image appears nearly black when displayed on an 8-bit

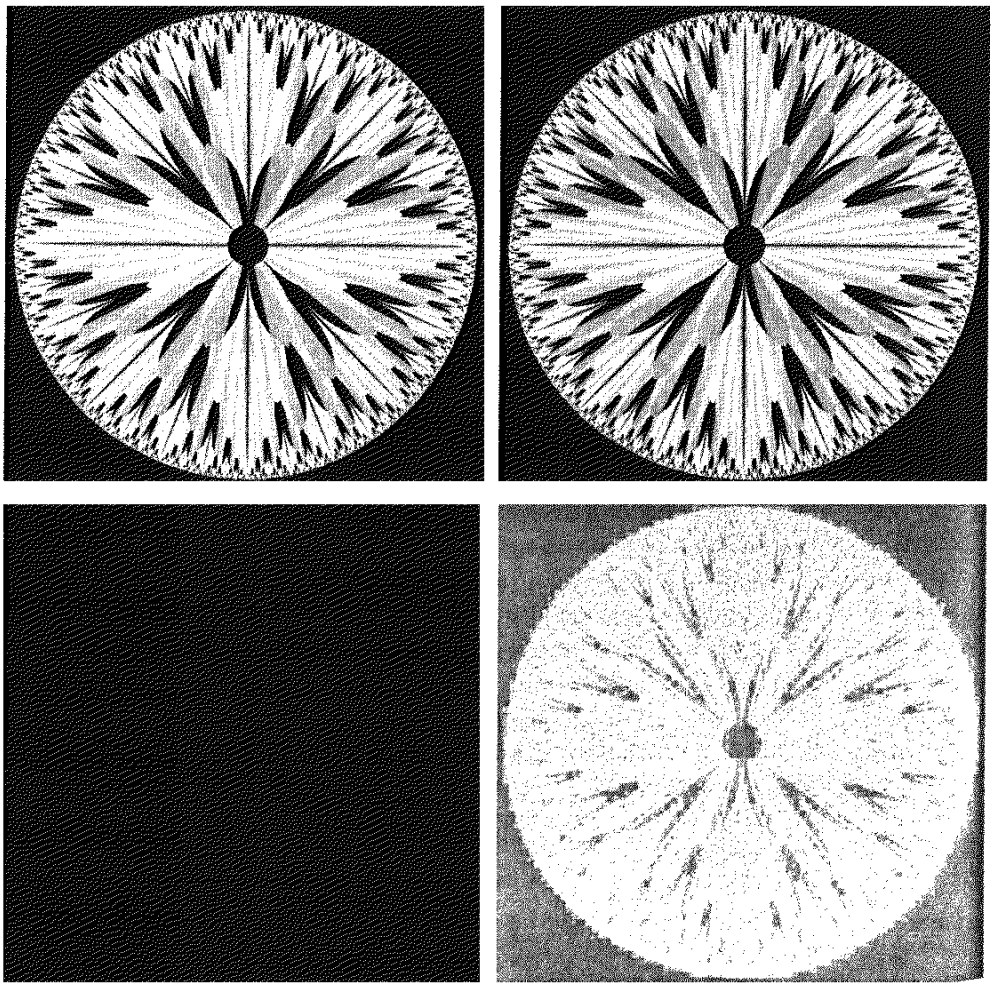

a b
c d

FIGURE 3.28
(a) Original fractal image. (b) Result of setting the four lower-order bit planes to zero. (c) Difference between (a) and (b). (d) Histogram-equalized difference image. (Original image courtesy of Ms. Melissa D. Binde, Swarthmore College, Swarthmore, PA).

display. In order to bring out more detail, we can perform a contrast stretching transformation, such as those discussed in Sections 3.2 or 3.3. We chose histogram equalization, but an appropriate power-law transformation would have done the job also. The result is shown in Fig. 3.28(d). This is a very useful image for evaluating the effect of setting to zero the lower-order planes.

EXAMPLE 3.7: Use of image subtraction in mask mode radiography.

One of the most commercially successful and beneficial uses of image subtraction is in the area of medical imaging called *mask mode radiography*. In this case $h(x, y)$, the *mask*, is an X-ray image of a region of a patient's body captured by an intensified TV camera (instead of traditional X-ray film) located opposite an X-ray source. The procedure consists of injecting a contrast medium into the patient's bloodstream, taking a series of images of the same anatomical region as $h(x, y)$, and subtracting this mask from the series of incoming images after injection of the contrast medium. The net effect of subtracting the mask from each sample in the incoming stream of TV images is that the areas that are different between $f(x, y)$ and $h(x, y)$ appear in the output image as enhanced detail. Because images can be captured at TV rates, this procedure in essence gives a movie showing how the contrast medium propagates through the various arteries in the area being observed.

Figure 3.29(a) shows an X-ray image of the top of a patient's head prior to injection of an iodine medium into the bloodstream. The camera yielding this image was positioned above the patient's head, looking down. As a reference point, the bright spot in the lower one-third of the image is the core of the spinal column. Figure 3.29(b) shows the difference between the mask (Fig. 3.29a) and an image taken some time after the medium was introduced into the bloodstream. The bright arterial paths carrying the medium are unmistakably enhanced in Fig. 3.29(b). These arteries appear quite bright because they are not subtracted out (that is, they are not part of the mask image). The overall background is much darker than that in Fig. 3.29(a) because differences between areas of little change yield low values, which in turn appear as dark shades of gray in the difference image. Note, for instance, that the spinal cord, which is bright in Fig. 3.29(a), appears quite dark in Fig. 3.29(b) as a result of subtraction. ∎

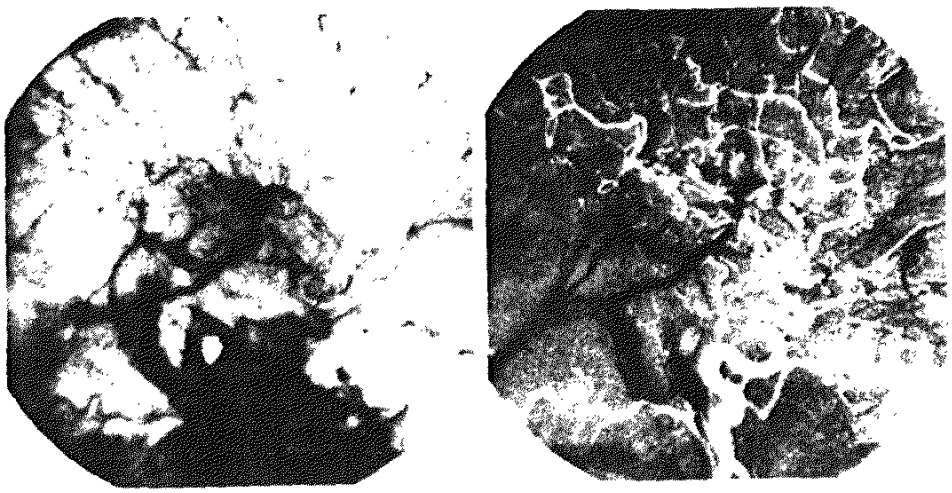

a b

FIGURE 3.29 Enhancement by image subtraction. (a) Mask image. (b) An image (taken after injection of a contrast medium into the bloodstream) with mask subtracted out.

A few comments on implementation are an order before we leave this section. In practice, most images are displayed using 8 bits (even 24-bit color images consists of three separate 8-bit channels). Thus, we expect image values not to be outside the range from 0 to 255. The values in a difference image can range from a minimum of −255 to a maximum of 255, so some sort of scaling is required to display the results. There are two principal ways to scale a difference image. One method is to add 255 to every pixel and then divide by 2. It is not guaranteed that the values will cover the entire 8-bit range from 0 to 255, but all pixel values definitely will be within this range. This method is fast and simple to implement, but it has the limitations that the full range of the display may not be utilized and, potentially more serious, the truncation inherent in the division by 2 will generally cause loss in accuracy.

If more accuracy and full coverage of the 8-bit range are desired, then we can resort to another approach. First, the value of the minimum difference is obtained and its negative added to all the pixels in the difference image (this will create a modified difference image whose minimum values is 0). Then, all the pixels in the image are scaled to the interval [0, 255] by multiplying each pixel by the quantity 255/Max, where Max is the maximum pixel value in the modified difference image. It is evident that this approach is considerably more complex and difficult to implement.

Before leaving this section we note also that change detection via image subtraction finds another major application in the area of segmentation, which is the topic of Chapter 10. Basically, segmentation techniques attempt to subdivide an image into regions based on a specified criterion. Image subtraction for segmentation is used when the criterion is "changes." For instance, in tracking (segmenting) moving vehicles in a sequence of images, subtraction is used to remove all stationary components in an image. What is left should be the moving elements in the image, plus noise.

3.4.2 Image Averaging

Consider a noisy image $g(x, y)$ formed by the addition of noise $\eta(x, y)$ to an original image $f(x, y)$; that is,

$$g(x, y) = f(x, y) + \eta(x, y) \tag{3.4-2}$$

where the assumption is that at every pair of coordinates (x, y) the noise is uncorrelated[†] and has zero average value. The objective of the following procedure is to reduce the noise content by adding a set of noisy images, $\{g_i(x, y)\}$.

If the noise satisfies the constraints just stated, it can be shown (Problem 3.15) that if an image $\bar{g}(x, y)$ is formed by averaging K different noisy images,

$$\bar{g}(x, y) = \frac{1}{K} \sum_{i=1}^{K} g_i(x, y) \tag{3.4-3}$$

[†] Recall that the variance of a random variable x with mean m is defined as $E[(x - m)^2]$, where $E\{\cdot\}$ is the expected value of the argument. The covariance of two random variables x_i and x_j is defined as $E[(x_i - m_i)(x_j - m_j)]$. If the variables are *uncorrelated*, their covariance is 0.

then it follows that

$$E\{\bar{g}(x, y)\} = f(x, y) \tag{3.4-4}$$

and

$$\sigma^2_{\bar{g}(x,y)} = \frac{1}{K}\sigma^2_{\eta(x,y)} \tag{3.4-5}$$

where $E\{\bar{g}(x, y)\}$ is the expected value of $\bar{g}$, and $\sigma^2_{\bar{g}(x,y)}$ and $\sigma^2_{\bar{\eta}(x,y)}$ are the variances of $\bar{g}$ and η, all at coordinates (x, y). The standard deviation at any point in the average image is

$$\sigma_{\bar{g}(x,y)} = \frac{1}{\sqrt{K}}\sigma_{\eta(x,y)}. \tag{3.4-6}$$

As K increases, Eqs. (3.4-5) and (3.4-6) indicate that the variability (noise) of the pixel values at each location (x, y) decreases. Because $E\{\bar{g}(x, y)\} = f(x, y)$, this means that $\bar{g}(x, y)$ approaches $f(x, y)$ as the number of noisy images used in the averaging process increases. In practice, the images $g_i(x, y)$ must be registered (aligned) in order to avoid the introduction of blurring and other artifacts in the output image.

EXAMPLE 3.8: Noise reduction by image averaging.

■ An important application of image averaging is in the field of astronomy, where imaging with very low light levels is routine, causing sensor noise frequently to render single images virtually useless for analysis. Figure 3.30(a) shows an image of a galaxy pair called NGC 3314, taken by NASA's Hubble Space Telescope with a wide field planetary camera. NGC 3314 lies about 140 million light-years from Earth, in the direction of the southern-hemisphere constellation Hydra. The bright stars forming a pinwheel shape near the center of the front galaxy have formed recently from interstellar gas and dust. Figure 3.30(b) shows the same image, but corrupted by uncorrelated Gaussian noise with zero mean and a standard deviation of 64 gray levels. This image is useless for all practical purposes. Figures 3.30(c) through (f) show the results of averaging 8, 16, 64, and 128 images, respectively. We see that the result obtained with $K = 128$ is reasonably close to the original in visual appearance.

We can get a better appreciation from Fig. 3.31 for how reduction in the visual appearance of noise takes place as a function of increasing K. This figure shows the difference images between the original [Fig. 3.30(a)] and each of the averaged images in Figs. 3.30(c) through (f). The histograms corresponding to the difference images are also shown in the figure. As usual, the vertical scale in the histograms represents number of pixels and is in the range $[0, 2.6 \times 10^4]$. The horizontal scale represents gray level and is in the range $[0, 255]$. Notice in the histograms that the mean and standard deviation of the difference images decrease as K increases. This is as expected because, according to Eqs. (3.4-3) and (3.4-4), the average image should approach the original as K increases. We can also see the effect of a decreasing mean in the difference images on the left column of Fig. 3.31, which become darker as the K increases.

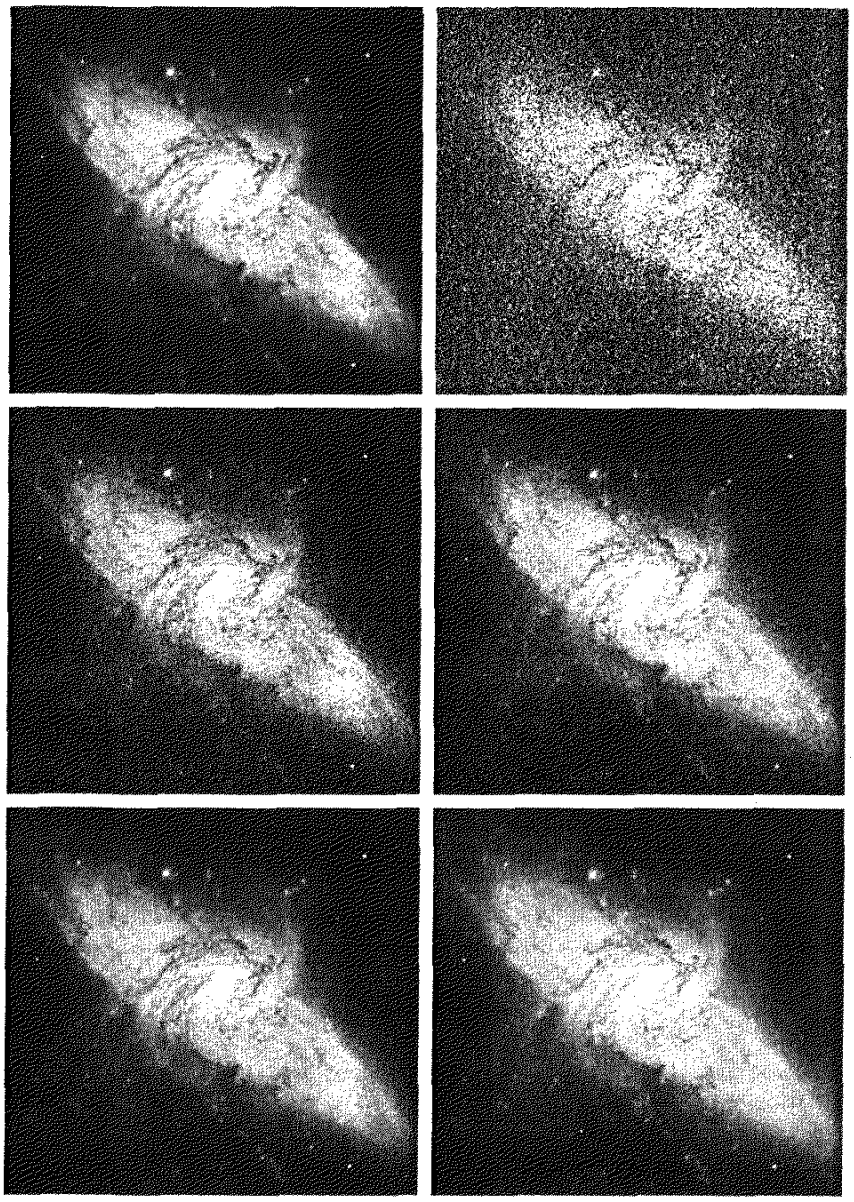

a b
c d
e f

FIGURE 3.30 (a) Image of Galaxy Pair NGC 3314. (b) Image corrupted by additive Gaussian noise with zero mean and a standard deviation of 64 gray levels. (c)–(f) Results of averaging $K = 8, 16, 64$, and 128 noisy images. (Original image courtesy of NASA.)

Addition is the discrete formulation of continuous integration. In astronomical observations, a process equivalent to the method just described is to use the integrating capabilities of CCD or similar sensors for noise reduction by observing the same scene over long periods of time. The net effect, however, is analogous to the procedure just discussed. Cooling the sensor further reduces its noise level.

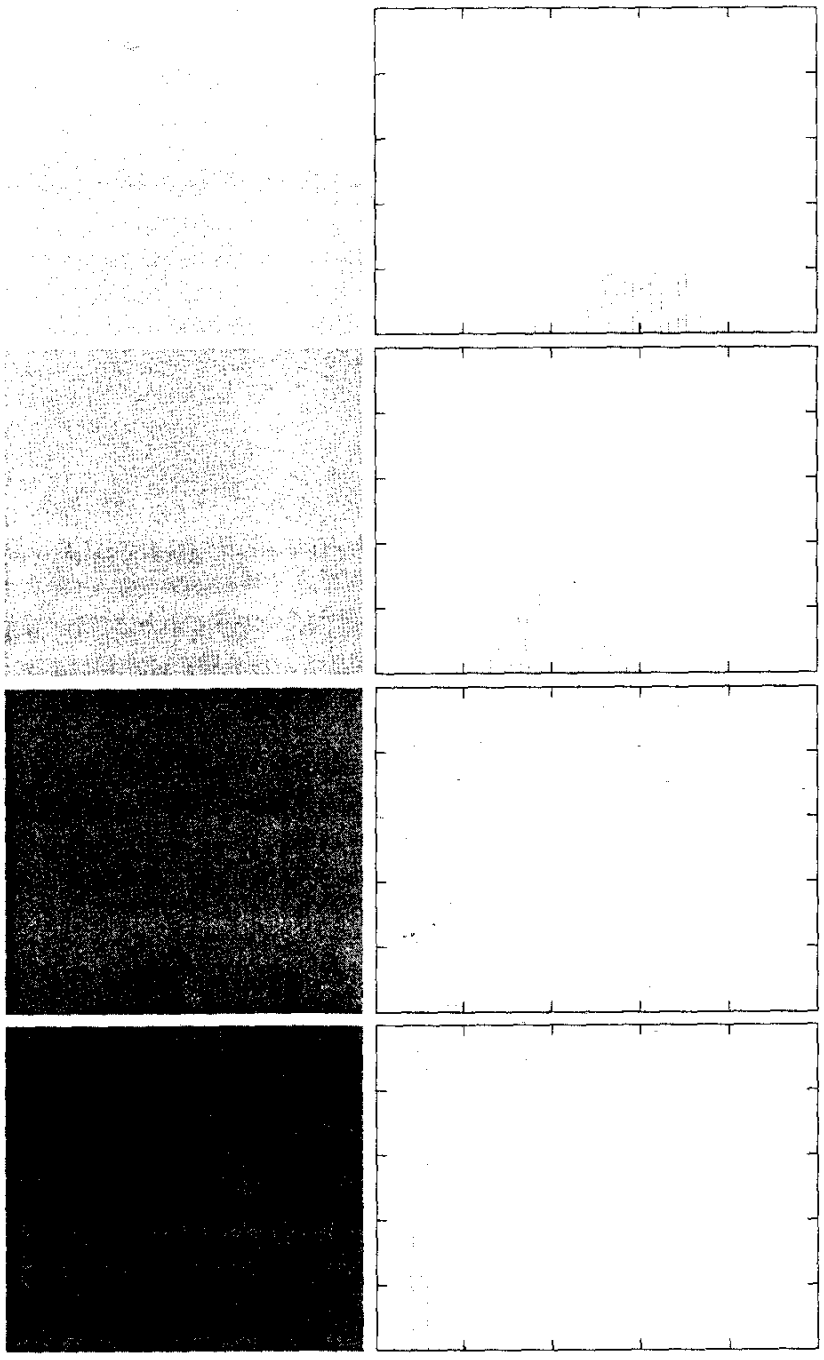

a b

FIGURE 3.31
(a) From top to bottom: Difference images between Fig. 3.30(a) and the four images in Figs. 3.30(c) through (f), respectively. (b) Corresponding histograms.

As in the case of image subtraction, adding two or more 8-bit images requires special care when it comes to displaying the result on an 8-bit display. The values in the sum of K, 8-bit images can range from 0 to $255 \times K$. Scaling back to 8 bits in this case consists simply of dividing the result by K. Naturally, some accuracy will be lost in the process, but this is unavoidable if the display has to be limited to 8 bits.

It is possible in some implementations of image averaging to have negative values when noise is added to an image. In fact, in the example just given, this was precisely the case because Gaussian random variables with zero mean and nonzero variance have negative as well as positive values. The images in the example were scaled using the second scaling method discussed at the end of the previous section. That is, the minimum value in a given average image was obtained and its negative was added to the image. Then all the pixels in the modified image were scaled to the range [0, 255] by multiplying each pixel in the modified image by the quantity 255/Max, where Max was the maximum pixel value in that image.

3.5 Basics of Spatial Filtering

As mentioned in Section 3.1, some neighborhood operations work with the values of the image pixels in the neighborhood *and* the corresponding values of a subimage that has the same dimensions as the neighborhood. The subimage is called a *filter, mask, kernel, template,* or *window*, with the first three terms being the most prevalent terminology. The values in a filter subimage are referred to as *coefficients*, rather than pixels.

The concept of filtering has its roots in the use of the Fourier transform for signal processing in the so-called *frequency domain*. This topic is discussed in more detail in Chapter 4. In the present chapter, we are interested in filtering operations that are performed directly on the pixels of an image. We use the term *spatial filtering* to differentiate this type of process from the more traditional frequency domain filtering.

The mechanics of spatial filtering are illustrated in Fig. 3.32. The process consists simply of moving the filter mask from point to point in an image. At each point (x, y), the *response* of the filter at that point is calculated using a predefined relationship. For *linear* spatial filtering (see Section 2.6 regarding linearity), the response is given by a sum of products of the filter coefficients and the corresponding image pixels in the area spanned by the filter mask. For the 3×3 mask shown in Fig. 3.32, the result (or response), R, of linear filtering with the filter mask at a point (x, y) in the image is

$$R = w(-1,-1)f(x-1, y-1) + w(-1,0)f(x-1, y) + \cdots + w(0,0)f(x, y) + \cdots + w(1,0)f(x+1, y) + w(1,1)f(x+1, y+1),$$

which we see is the sum of products of the mask coefficients with the corresponding pixels directly under the mask. Note in particular that the coefficient $w(0, 0)$ coincides with image value $f(x, y)$, indicating that the mask is centered at (x, y) when the computation of the sum of products takes place. For a mask of size $m \times n$, we assume that $m = 2a + 1$ and $n = 2b + 1$, where a and b are nonnegative integers. All this says is that our focus in the following discussion will be on masks of *odd* sizes, with the smallest meaningful size being 3×3 (we exclude from our discussion the trivial case of a 1×1 mask).